FBXL5: SENSOR AND REGULATOR OF MAMMALIAN IRON HOMEOSTASIS

APPROVED BY SUPERVISORY COMMITTEE

Richard Bruick, Ph.D.

Zhijian Chen, Ph.D.

Steven McKnight, Ph.D.

George DeMartino, Ph.D.

DEDICATION

To my parents, from whom I have learned countless lessons

FBXL5: SENSOR AND REGULATOR OF MAMMALIAN IRON HOMEOSTASIS

by

AMEEN ABDULLA SALAHUDEEN

DISSERTATION

Presented to the Faculty of the Graduate School of Biomedical Sciences

The University of Texas Southwestern Medical Center at Dallas

In Partial Fulfillment of the Requirements

For the Degree of

DOCTOR OF PHILOSOPHY

The University of Texas Southwestern Medical Center at Dallas

Dallas, Texas

August, 2009

ACKNOWLEDGEMENTS

My first experience as a UT Southwestern student was doing a laboratory rotation in the Biochemistry department. That summer I worked with Tim Rand, a student in Xiaodong Wang's laboratory, on mechanisms of RNA interference.

When I arrived for my first day of work, I wore a tie because I had to take a photo for my ID badge, and also because I had a formal engagement that evening. These reasons, however, were not obvious to the professor who then walked into the lab with a wide eyed graduate student in tow. He glanced in my direction and said, "Scientists don't wear ties," and then proceeded to completely ignore me and ask Tim about hydrophobic chromatography media. After he left, I asked Tim for this person's name and learned that it was Rick Bruick.

Clearly, Rick was a no-nonsense and to-the-point person. From talking to other people in the department, I learned that Rick took the same approach to his work, and that he had a high level of intensity and diligence in his science. Learning these things about Rick made it easy to choose his lab for my dissertation research. The three years I spent in Rick's lab taught me many aspects of making scientific discoveries, as well as how to maintain a high standard in conducting scientific research.

In addition to Rick's guidance, I received tremendous support from many people in the Biochemistry department. The first year of my dissertation research was mostly spent learning the tools of the biochemistry trade. The people who supported me in this endeavor were Abdullah Ozer, Lei Zhang, Lai Wang, Ayman Ismail, Jinsong Yang, Tim Rand, Fengue Du, Leeju Wu, Sean Petersen, Gabriel Pineda, Sunil Laxman, Arati Ramesh, Midhat Farooqi, Robert Li, Rodney Infante, Xinlin Du, Hewen Ma, and members of the McKnight lab, Tu lab, Brown and Goldstein lab, Gardner lab, Xiaodong Wang lab, Qinghua Liu lab, Roth lab, Lynch lab, Winkler lab, Structural Biology Lab, and High Throughput Screening Facility. These people didn't just teach me the fundamentals of common assays, they taught me how to do them efficiently and exceptionally well. I am honored to have had these people as colleagues, and to have them shape my thought process in the practical methods of performing experiments.

My second and third years in the laboratory were essentially the climax and conclusion of my dissertation research. The rapid pace of discovery and solving molecular mechanisms could not have been done without the work of my lab partners, Joel Thompson and Julio Ruiz. Our combined efforts under our Rick's guidance brought together a complete story of iron sensing and the regulation of iron homeostasis in mammals.

I would also like to thank my dissertation committee for their time spent evaluating my progress, and their helpful suggestions for this body of work.

FBXL5: SENSOR AND REGULATOR OF MAMMALIAN IRON HOMEOSTASIS

AMEEN ABDULLA SALAHUDEEN

The University of Texas Southwestern Medical Center at Dallas, 2009

RICHARD KEITH BRUICK, Ph.D.

While iron is an important cofactor for many proteins, the chemical properties of iron that favor its biological roles can lead to toxic side reactions that damage macromolecules. Cellular iron homeostasis is maintained by the coordinate posttranscriptional regulation of gene products responsible for iron uptake, release, utilization, and storage. This process is mediated by Iron Regulatory Proteins (IRPs) that bind to Iron Responsive Elements (IREs) in the mRNAs of these genes. When iron bioavailability is low IRPs bind IREs within these mRNAs, affecting their subsequent translation or stability. When cellular free

iron availability is high, IRPs are preferentially degraded by the proteasome. An SCF E3 ubiquitin ligase complex containing the FBXL5 protein regulates this process as a function of cellular iron and oxygen concentrations. This process occurs through the stability of FBXL5, which accumulates under iron and oxygen replete conditions and is targeted for degradation upon iron depletion. FBXL5 contains an iron- and oxygen-sensing hemerythrin domain that acts as a ligand-binding regulatory switch mediating its stability. As a result, FBXL5 directly senses iron and oxygen levels to serve as a regulator of cellular iron homeostasis.

TABLE OF CONTENTS

PRIOR PUBLICATIONS

1. **Salahudeen AA** and Bruick RK. Maintaining Mammalian Iron and Oxygen Homeostasis: Sensors, Regulation, and Crosstalk. Ann NY Acad Sci. In Press.

2. **Salahudeen AA**, Thompson JW, Ruiz JC, Ma H, Li Q, Kinch LN, Grishin NV, and Bruick RK. An E3 Ligase Possessing an Iron Responsive Hemerythrin Domain is a Regulator of Iron Homeostasis. Science. In Press. PMID: 19762597

3. **Salahudeen AA**, Jenkins JK, Huang H, Ndebele K, Salahudeen AK. (2001). Overexpression of heme oxygenase protects renal tubular cells against cold storage injury: studies using hemin induction and HO-1 gene transfer. Transplantation. *72*, 1498-504.

LIST OF FIGURES

LIST OF DEFINITIONS

ATP - adenosine triphosphate
BSA - bovine serum albumin
DFO – Deferoxamine Mesylate
DNA – deoxyribonucleic acid
DTT - dithiothreitol
E1 - ubiquitin-activating enzyme
E2 - ubiquitin-conjugating enzyme
E3 - ubiquitin ligase
EDTA - ethylenediaminetetraacetic acid
FAC – Ferric Ammonium Citrate
HEK 293- human embryonic kidney cell line
HEK 293T - human embryonic kidney cell line expressing large T antigen
HeLa – human cervical carcinoma cell line
HEPES - 4-(2-hydroxyethyl)-1-piperazineethanesulfonic acid
Hr - Hemerythrin
IP - immunoprecipitation
IPTG - isopropyl β-D-thiogalactopyranoside
IRE – Iron Responsive Element
IRP – Iron Regulatory Protein
MG132 - proteasome inhibitor Z-Leu-Leu-CHO
PAGE - polyacrylamide gel electrophoresis
PBS – Phosphate Buffered Saline
PCR - polymerase chain reaction
RNA – ribonucleic acid
rNTP – ribonucleoside triphosphate
SDS - sodium dodecyl sulfate
S100 – soluble cytosolic fraction obtained after centrifugation at 100,000 x *g*
SCF - Skp1, Cul1, F-box containing ubiquitin ligase enzyme (E3)
Sf9 – Spodoptera frugiperda ovarian cell line.
siRNA - small interfering RNA
Tris - tris(hydroxymethyl)methylglycine
Ub - ubiquitin
Ubc - Ubiquitin conjugating enzyme (E2)

CHAPTER ONE

THE PHYSIOLOGY AND CELLULAR BIOLOGY OF IRON IN HUMANS

Section IA: Iron's chemical properties in biology

Among the many essential nutrients for life, iron holds high standing for its role in various and sundry cellular processes. For example, iron is required for the synthesis of DNA, sterols, and iron is employed in electron transport within the mitochondria. Therefore, iron's position in evolutionary biology supersedes genomic DNA, membrane lipid bilayers, and aerobic respiration (Crichton, 2009).

Iron is able to play these roles, in addition to others discussed below, by the ease of its transition from the 2+ to 3+ oxidation states and vice versa, or in other words, its low energy of activation. As a result, living organisms use iron as a cofactor within enzymes to catalyze the oxidation and reduction of metabolites. For instance, iron is used in the synthesis of DNA by ribonucleotide reductase, an enzyme that removes the hydroxyl group from the 2' position of ribonucleotides (rNTPs) by a radical based mechanism requiring iron to transition from the 2+ to the 3+ oxidation state (Nordlund and Eklund, 1995). This example is but one of the several dozens of iron dependent reactions that sustain our lives.

Because of these critical functions, organisms have developed processes to optimize iron utilization. While this is true, iron is also precious to living

organisms because it is only bioavailable in trace amounts. In fact, iron's concentrations in natural water reservoirs is micromolar, orders of magnitude less than that of other divalent metal cations such as magnesium and calcium (Crichton, 2009). Therefore, organisms have developed sophisticated means for iron acquisition from their environment and iron transport within their bodies.

Iron levels must also be tightly regulated in organisms due to the ease of which it can catalyze toxic radical species. This occurs through the same chemical properties that favor its use in biology – the transition between its 2+ and 3+ oxidation states (Crichton, 2009; Galaris and Pantopoulos, 2008). As shown in Figure I-1, free iron can engage in Fenton chemistry (Fenton, 1894). Here, iron can form hydroxyl radicals that react with macromolecules (e.g. nucleic acids, lipids, and proteins) and cause irreversible damage. This process is especially evident in cellular necrosis, where free iron release caused by injurious stimuli that catalyze the formation of reactive oxygen species (ROS) causing oxidative stress and ultimately, cell death (Galaris and Pantopoulos, 2008). Myocardial infarctions and neurodegenerative diseases are two examples where pathogensis of these disease states are attributable to oxidative stress and necrosis (Rogers et al., 2002). As a result of the utility, scarcity, and reactivity of iron, humans have developed a vast and rich repertoire of cellular and physiological processes to maintain iron homeostasis.

Section IB: Iron in Human Physiology

In addition to serving as cofactors in cellular enzymes necessary for life, iron is required for the synthesis of the heme prosthetic group critical for the oxygen transport via erythrocytic hemoglobin. Moreover, the majority of body iron stores reside within erythrocytes, and is estimated to be 1.8g out of 4.0g, or approximately half (Hentze et al., 2004). Other significant iron rich sites in the body are the liver (1g, ~25%) and the bone marrow (400mg, ~10%), and the remainder of the iron is evenly distributed throughout the body (Hentze et al., 2004). Erythrocytes are also turned over daily by phagocytosis in the liver by Kupffer cells and the spleen by splenic macrophages, and this recycled iron (approximately 25mg per day) must be safely and efficiently transported back to the bone marrow, the site of erythropoiesis (Hentze et al., 2004; Wrighting and Andrews, 2008). Lastly, approximately 3-4mg of iron is lost from the body through regular sloughing of cells from intestinal mucosa, and from blood loss either through menstruation or trauma (Wrighting and Andrews, 2008). This iron loss must be replenished by iron derived from our diet. To meet these demands of iron utilization and loss, and to also overcome the deleterious properties of iron solubility and reactivity, humans possess tightly regulated means of dietary uptake and transport of iron.

Iron is obtained in our diet in two forms: heme (largely from meat products) and inorganic ferric iron (found in cereals, legumes, and vegetables).

Both forms are absorbed in the proximal part of the small intestine, or the duodenum (Lynch, 2005; Muckenthaler et al., 2008). The cells responsible for iron uptake, insestinal epithelial cells (IECs), must utilize several enzymes to transport iron from their apical surface facing the intestinal lumen, to their basolateral surface facing the blood stream.

Intestinal cells take up two forms of dietary iron: heme, and inorganic iron salts. While the identity of the heme transporter remains controversial (Qiu et al., 2006), uptake mechanisms for inorganic iron are well understood and occur through the action of Divalent Metal Transporter 1 (DMT-1). DMT-1 was first described by the identification of the gene responsible for anemia in a rat strain fed a normal diet (Fleming et al., 1998). It was later found to be a member of the conserved dication proton symport membrane channels, and DMT-1 requires iron to be reduced prior to intestinal epithelial cell uptake (Fleming et al., 1997). Evidence supports the attribution of this role to the STEAP family of ferri reductases, as they may function in the apical surface of intestinal epithelial cells, since their mRNA has been shown to be expressed in the duodenum through *in situ* hybridization (Ohgami et al., 2005). Furthermore, mice lacking STEAP3 display deficiency of iron uptake in erythroid cells (Ohgami et al., 2005)

Once iron is reduced and enters the IEC, it is then exported through the basolateral membrane by transmembrane protein ferroportin (Muckenthaler et al., 2008), and iron is reoxidized to +3 by the copper feroxidase hephastin (Andrews,

2008). Upon reaching the blood stream, iron then binds a serum protein, Transferrin (Tf) and enters the physiological cycle of Tf and Transferin Receptor (TfR).

Tf, a serum protein, binds two molecules of iron to function as a serum carrier. Tf is secreted into the serum by hepatocytes (Andrews, 2008; Wrighting and Andrews, 2008). Iron laden Tf is then binds TfR receptor by all cells in the body, especially TfR1. This Tf-TfR complex, or holo TfR, is then brought into the cell through receptor mediated endocytosis (Figure I-3). The endosomal vesicle is then acidified by the V_oATPase, and the low pH promotes iron to dissociate from Tf and TfR. The liberated iron is then reduced by STEAP3 and transported along with protons into the cytosol by DMT-1 for use by the cell (Hentze et al., 2004). Tf and TfR are then recycled, where Tf is secreted into the serum and TfR relocates to the plasma membrane. The apo, or iron free Tf then begins the Tf-TfR cycle again, but can acquire iron from cells aside from the IEC, including hepatocytes and macrophages. However, instead of Hephaestin, iron is oxidized to the 3+ state by the serum protein Ceruloplasmin, a copper containing feroxidase (Hentze et al., 2004).

While IECs and Tf-TfR cycle provides a robust uptake and transport system to deal with the scarcity and solubility of iron, humans do not have a means to secrete iron when its levels are excessive (Beutler, 2006). Instead, excess iron is sequestered within cells, especially hepatocytes, in an inert oxidized

precipitate within the cavity of a large polymeric assembly of the ferritin protein (discussed in Section IC). Additionally, iron uptake through IECs is decreased and ferroportin mediated secretion of iron into the blood stream is downregulated (Ganz, 2005). The physiological signal that governs this process at the systemic level, is the peptide hormone hepcidin.

Hepcidin was first described as a serum peptide secreted by hepatocytes in response to iron overload (Pigeon et al., 2001). It is transcriptionally induced by inflammatory cytokines through the JAK/STAT signaling pathway (Ganz, 2005). It was later found that hepcidin lowers serum iron concentrations, and thus deprived a critical nutrient from pathogens such as bacteria (Ganz, 2005). Further investigation by several groups, including Nicolas et al., found that hepcidin was also upregulated by a high iron diet (Nicolas et al., 2002). Moreover, these varied stimuli resulted in the same hepcidin mediated effect – lowered serum iron concentrations.

Further investigation led to the elucidation of a mechanism responsible for lowering serum iron concentrations. Studies employing ^{57}Fe demonstrated that duodenum from mice with high serum hepcidin concentrations exhibited lower iron uptake and transport, and that hepcidin also reduced iron export from macrophages and hepatocytes (Ganz, 2005; Muckenthaler et al., 2008). Taken together, these early findings proved the liver could respond to inflammation or increased dietary iron concentrations by secreting a peptide hormone that lowered

serum iron through a reduction in dietary iron uptake and iron secretion from systemic stores.

How hepcidin mediates these phenomena, or the identity of its receptor, was not elucidated until a study by Nemeth et al. In their report, Nemeth et al. demonstrated that ferroportin, the critical iron transporter in IECs, hepatocytes, and macrophages, was a physiological receptor for hepcidin (Nemeth et al., 2004). Once ferroportin binds hepcidin, it undergoes internalization and is ultimately degraded through a lysosome mediated process (De Domenico et al., 2007). The end result of this hepcidin driven process is that iron export from the intestine, hepatocytes, and macrophages is attenuated, and serum iron levels decrease (Figure I-4).

In summary, iron uptake, distribution, and sequestration are all regulated in human physiology to achieve a fine balance between iron deficiency and iron overload. If this is not achieved, pathological manifestations arise, as seen in anemia (a state of iron deficiency) and hemochromatosis (a state of iron overload) (Figure I-5). The pathways of iron trafficking in the body are well understood, especially systemic adaptations and responses to iron deficiency and iron overload. However, a fundamental question remains, and that is how the body senses iron concentrations to maintain iron homeostasis. To begin to understand this question, we must focus our attention to iron homeostasis at the cellular level.

Section IC: Cellular Iron Homeostasis

In cells, iron must be maintained at optimum levels for biological processes. These include metabolic synthesis and catabolism, oxygen transport and storage, mitochondrial electron transport and ATP production, and catalysis of post-translational modifications important in cell signaling. As discussed in Section IA, however, excess iron is deleterious and cytotoxic.

To achieve balance between necessity and excess, cellular iron homeostasis is achieved through the coordination of iron uptake, storage, utilization, and export. These processes are controlled by the Tf-TfR cycle, ferritin and ferritin like proteins, heme and Fe-S cluster assembly machinery, and ferroportin, respectively. Ferroportin, to a large extent, falls under the control of hepcidin, a regulator of systemic iron homeostasis and does not exhibit significant iron dependent regulation in a cell autonomous fashion (Andrews, 2008; Ganz, 2005). Iron uptake, storage, and utilization, however, have been demonstrated to be controlled in a cell autonomous fashion by the Iron Regulatory Protein/ Iron Responsive Element (IRP/IRE) network.

Approximately twenty five years ago, the field of iron homeostasis was focused on an archetype system of iron uptake and iron storage – two opposing processes that acted in concert to balance cellular iron levels (Wallander et al., 2006). In this system, Transferrin Receptor 1 (TfR1) and ferritin served as the two cellular proteins whose levels varied inversely to one another as a function of iron

(Figure I-7). It was well known that isolated primary cells, especially hepatocytes, when treated with iron rich medium, would robustly express the iron storage protein ferritin and downregulate TfR-1. Ferritin, when upregulated, assembles a 24 subunit polymer core, and sequestrates high cellular iron concentrations into an inert ferric hydroxyl phosphate mineral core (Fishback, 1969; Harrison, 1974). Additionally, downregulated TfR-1 levels results in a decrease of iron uptake from the culture medium (Casey et al., 1988).

If one were to place cells in the opposite scenario, that is a culture medium with high concentrations of an iron chelator (e.g. deferoxamine), or an iron depleted medium, ferritin levels would decrease and TfR1 levels would increase. As expected, the net effect is decreased iron sequestration in ferritin and increased iron uptake. This leads to an increase in cellular iron concentrations relative to the culture medium. While these observations were reproducible and quite robust, the mechanism could not be explained by conventional models of gene regulation (i.e. transcriptional regulation). Furthermore, treatment of cells with transcriptional inhibitors could not completely block these iron dependent changes, especially with respect to ferritin (Hentze et al., 1987). It was not until Hamish Munro hypothesized that post-transcriptional regulation regulated iron homeostasis, did our understanding of iron dependent regulation of ferritin and TfR1 begin to progress.

The post-transcriptional regulation of ferritin first postulated by Munro, was later demonstrated in his laboratory in experiments showing ferritin mRNA transcripts able to bind to cytosolic proteins in gel-shift experiments in liver extracts taken from rats treated with high iron (Leibold and Munro, 1988). Hentze et al. were able to identify the mRNA element essential for this behavior, and showed that it resided on the 5' untranslated region (UTR) of both the ferritin light chain (FTL) and heavy chain (FTH) mRNA transcripts (Hentze et al., 1987). Furthermore, they showed that this Iron Responsive Element (IRE) could be transferred onto a heterologous gene, Chloramphenicol Acetyl Transferase (CAT), and confer iron dependent regulation (Hentze et al., 1987). Thermodynamic structural predicting programs found that the IRE folded into a stem loop structure, and later studies show that this stem-loop structure is highly conserved in vertebrates (Piccinelli and Samuelsson, 2007).

By using the IRE-CAT heterologous gene fusion product, it was found that the ferritin IRE actually *repressed* mRNA translation in iron deficient conditions and that in iron replete conditions this repression was relieved. These findings, in conjunction with earlier observations of a cytosolic binding protein, suggested that in iron depleted conditions, a trans-acting cytosolic protein bound to the IRE in ferritin's 5'UTR and functioned as a translational repressor. With respect to TfR1, later studies revealed that it also contains an IRE which binds to a trans-acting cytosolic protein (Casey et al., 1988). TfR1's IRE, unlike ferritin,

resides within the 3' UTR of its mRNA transcript, and when the cytosolic protein binds to the TfR1 IRE, the mRNA half life is increased in cells, and *in vitro* RNAse protection assays demonstrate this be due to a mechanism of reduced RNAse endonucleolytic cleavage (Wallander et al., 2006). In summary, Munro's post-transcriptional regulation involves IREs, which, when iron is high, do not bind a cytosolic protein resulting in derepression of ferritin translation (increased ferritin expression) and an increase in TfR1 endonucleolytic cleavage (decreased TfR1 expression). When iron is low, ferritin translation is repressed, and TfR1 mRNA is protected from degradation, and this is mediated by IREs being bound by a trans-acting cytosolic protein. IREs have later been identified in many other genes involved in iron homeostasis including the iron importer DMT-1, the rate limiting step in erythroid heme synthesis aminolevulinc acid synthase (ALAS2), and several others listed in Table I-1.

The identity of the trans-acting protein that bound to IREs was revealed by Rouault et al., who used an *in vitro* synthesized IRE to affinity purify the cytosolic binding protein from human liver extracts (Rouault et al., 1989). The protein, named Iron Regulatory Protein (IRP), was cloned, and its coding sequence was identified to be homologous to mitochondrial aconitase (Rouault, 2006). In mammals, there are two IRPs, IRP1 and IRP2 (Rouault, 2006). IRP1 functions as the source of mammalian cytosolic aconitase, whereas IRP2 lacks

this activity. As discussed below, low iron levels promote IRP/IRE binding whereas high iron levels abolish this activity.

Together, IRP1 and 2 are essential regulators of mammalian iron homeostasis. This is underscored by the observation that mice null for both IRP1 and IRP2 in the intestine (the site of iron uptake) exhibit profound misregulation of iron homeostasis and neonatal lethality (Galy et al., 2008). Global IRP1 and IRP2 deficiency results in embryonic lethality at the blastocyst stage, but it is unclear whether this is due to disrupted iron homeostasis (Smith et al., 2006). Global IRP2 deficiency in mice, however, results in microcytic anemia and iron overload in the intestine and liver (LaVaute et al., 2001; Meyron-Holtz et al., 2004a). Interestingly, mice lacking IRP2 also have a higher rate of neurodegenerative disease compared to wild type littermates. The phenotype in these mice consists of bradykinesia, tremor, and gait abnormalities. Consistent with these findings is abnormal iron accumulation in ferritin like particles within the brain and spinal cord of these mice (Zhang et al., 2005).

In cells, low iron promotes IRP binding activity in cells whereas high iron abolishes this activity. How iron levels control IRP binding activity is distinct for IRP1 and IRP2. For IRP1, it was observed that in iron replete states, the cytosolic aconitase activity was upregulated and IRE binding was downregulated. In iron deficient states, the activities are reversed (Hentze and Kuhn, 1996). These findings suggested that IRP1 contains an iron dependent switch in its aconitase

active site, where iron replete states form an Fe-S cluster and iron deficient states unmask an IRE binding pocket (Hentze and Kuhn, 1996). This model has received significant support from an X-ray crystal structure of IRP1 bound to an IRE, where it was shown that the IRE binding site resides within a pocket vacated by the Fe-S cluster (Walden et al., 2006). Therefore, with respect to IRP1, cells are able to sense iron concentrations and post-transcriptionally regulate ferritin and TfR through this iron dependent aconitase switch (Figure I-8).

IRP2, unlike IRP1, cannot form an Fe-S cluster within its active site due to mutation in one of the Fe-S cluster binding cysteines. Instead, it was found that when cells were iron replete, the half-life of IRP2 protein decreased (Guo et al., 1995; Samaniego et al., 1994). Furthermore, when cells were deprived of iron through iron chelators such as DFO, the IRP2 accumulates due to an increased half-life. This phenomenon was found to be mediated by proteasome dependent degradation (Guo et al., 1995; Samaniego et al., 1994) (Figure I-8).

The proteasome is a large multisubunit complex that functions in quality control and turnover of most proteins in the cell (Ardley and Robinson, 2005; Hershko and Ciechanover, 1998). The signal that targets proteins to the proteasome either occurs through the unfolded protein pathway, or through the conjugation of a small protein, ubiquitin, to lysine side chains by formation of an isopeptide bond between the lysine ε-amino group and the c-terminal glycine of ubiquitin (Hershko and Ciechanover, 1998). Polyubiquitin chains can then form,

by further isopeptide linkages between ε-amino group of the initial ubiquitin (usually K-48) and the c-terminal glycines of additional ubiquitins (Figure I-9). The resulting polyubiquitin chains then serve to initiate proteasome catalyzed degradation of the targeted protein.

Like most proteins that undergo proteasome dependent degradation, IRP2 is also shown to be ubiquitinated, and like its degradation, requires iron (Figure I-10) (Hanson et al., 2003; Iwai et al., 1998). Like most proteins, IRP2's ubiquitination depends on the enzyme cascade of an E1 ubiquitin activating enzyme, an E2 ubiquitin conjugase, and an E3 ubiquitin ligase (Figure I-9). In humans, there exists one E1 enzyme, dozens of E2s, and over 600 E3 ligases (Ardley and Robinson, 2005; Hershko and Ciechanover, 1998). The E3 ubiquitin ligase is often the enzyme that confers specificity and regulation in the ubiquitination and degradation of a given protein (Ardley and Robinson, 2005). E3 ligases exist in several classes, the most common being HECT (Homologous to E6 Carboxy Terminus), RING (Really Interesting New Gene), or SCF (Skp, Cullin, F-box) (Figure I-11). These E3 ligases either constitutively ubiquitinate their protein substrates, or their activity can be upregulated in response to a signal, often a post-translational modification of an amino acid side chain on the E3 ligase's substrate protein (Ardley and Robinson, 2005). For example, the Hypoxia Inducible Factor alpha (HIF-α) subunit is known to be ubiquitinated by the SCF class E3 ligase, VHL as a function of oxygen concentration (Semenza, 2007). It

was later found by several groups that hydroxylation of prolines within HIF-α's VHL binding site was the signal that upregulated HIF-α's ubiquitination (Ivan et al., 2001; Jaakkola et al., 2001). Interestingly, a family of conserved prolyl hydroxylases (HPH, ENGLN) employ iron in the enzyme active site to catalyze a reaction involving an exotic Fe IV peroxo intermediate to catalyze the reduction of molecular oxygen and hydroxylation of HIF-α prolines and a cosubstrate 2-oxoglutarate (Bruick and McKnight, 2001; Epstein et al., 2001; Ivan et al., 2002; Ozer and Bruick, 2007). As discussed in Chapter 4, these enzymes serve as a hub for the cross-talk between iron and oxygen homeostasis.

With the HIF paradigm in mind, it was believed that an iron dependent post translational modification could occur in a region specific to IRP2. Also, with the observations that IRP2, but not IRP1, is ubiquitinated and degraded in response to high iron concentrations, and given that IRP1 and IRP2 share greater than 60% amino acid identity, it was believed that an amino acid region unique to IRP2, and not IRP1, could confer this iron dependent degradation. A 73 amino acid cysteine rich region in IRP2 shows no homology with IRP1 was investigated by the Rouault laboratory (Iwai et al., 1995). This region, named the Iron Degradation Domain (IDD), was shown to undergo cysteine oxidation when incubated *in vitro* with iron and oxygen (Iwai et al., 1998). Furthermore, experiments in cell culture demonstrated that deletion of the IDD resulted in an IRP2 that was refractory to iron dependent degradation. With these data, a

candidate IRP2 E3 ligase was identified (Yamanaka et al., 2003). This E3 ligase, termed Heme Oxidized IRP2 E3 Ligase -1 (HOIL-1), was shown to bind to the IDD of IRP2, and ubiquitinate IRP2 *in vitro* in the presence of iron. Further studies by the Iwai group showed that the IDD could also bind heme through a conserved cysteine, and heme binding also facilitated HOIL-1 mediated ubiquitination of IRP2 in cultured cells (Ishikawa et al., 2005). Taken together, a model suggested that the IDD of IRP2 responds to the iron replete state through cysteine oxidation or heme binding, promoting the association of the E3 ligase HOIL-1. Through the ensuing polyubiquitination, IRP2 is then targeted for proteasomal degradation. As a result, IRP2 IRE binding activity decreases and the IRE containing mRNAs promote a decrease of iron uptake and an increase of iron utilization and sequestration.

The proposed mechanisms of IRP2's iron dependent degradation and IRP1's iron sulfur cluster switch provided biologists with an elegant paradigm. In cells, two distinct and overlapping regulatory mechanisms afford tight molecular control of iron homeostasis. However, evidence began to emerge that challenged this model's validity, particularly the iron dependent degradation of IRP2.

Section ID: Paradigm Lost – Controversy and Outstanding Questions

During the late 1990's and early 2000's, several reports involving animal models and primary cell culture questioned the veracity of the models of IRP2's regulation and IRP1's iron sulfur cluster switch. With respect to IRP2's iron dependent degradation, the first reports questioned the cysteine oxidation model and the necessity for the entire IDD's 73 amino acid region (including heme binding). Bourdon et al. first showed that systematic mutation of all of the cysteines in the IDD did not affect IRP2's iron dependent degradation (Bourdon et al., 2003). This observation was later corroborated by Hanson et al. and Wang et al. where the entire IDD was removed, and IRP2 was still found to be degraded in an iron dependent manner (Hanson et al., 2003; Wang et al., 2004). This observation was also reproduced in our laboratory (Figure I-12).

The above findings contradict Iwai et al's initial observation that deletion of the IDD serves to stabilize IRP2 regardless of iron conditions. However, one can reconcile these apparent contradictions by considering that all of these experiments rely on exogenous expression of IRP2 in cell culture. When IRP2 is expressed at high levels, its iron dependent degradation can be saturated. In this setting, wild type IRP2 and IRP2 lacking the IDD both lack any iron dependent degradation in the cell (Wang et al., 2004). Thus, the IRP2 lacking the IDD in Iwai et al's report may have been expressed at saturating levels, while reports showing that the IDD was unnecessary employed IRP2 expressed at unsaturated

levels. Thus, the IDD is not required and is "dispensable" in cell culture models, and perhaps in the natural physiological setting (Pantopoulos, 2004).

In addition to the IDD controversy, the relevance of HOIL and the heme binding properties of IRP2 became suspect. For example, *in vitro* ubiquitination reactions are used to show that HOIL is essential for robust ubiquitin conjugation to IRP2 *in vitro* (Yamanaka et al., 2003) . However these reactions contain high concentrations of E1 and E2 UbCH5, and have high background activity that HOIL addition may slightly enhance in a stochastic manner. We have found in our laboratory that IRP2 can be ubiquitinated *in vitro* in similar reaction conditions with high concentrations of E1 and E2 UbCH5 (Figure I-13). In addition to these *in vitro* findings, no data has been published showing that loss of HOIL expression, either by RNA interference or in knockout mice, results in inappropriate IRP2 accumulation. A HOIL knockout mouse has been characterized, but to date, no study has been published examining deficiencies in IRP2 regulation in this mouse (Tokunaga et al., 2009). HOIL's importance has also been challenged by Zumbrennen et al., who show that HOIL knockdown in HEK293 cells does not abolish IRP2's iron dependent degradation (Zumbrennen et al., 2008).

With respect to the heme binding properties of IRP2, a report describing purification of recombinant IRP2 found that the IDD was susceptible to proteolysis, and that heme binding to IRP2 was dependent on this *in vitro*

proteolyzed IRP2 product (Dycke et al., 2007). Because this proteolysis of IRP2 is not observed in the physiological setting, this raises the likelihood that heme binding to IRP2 is an *in vitro* artifact. Moreover, when one examines the initial report describing the heme binding properties of the IRP2, the data that shows weak Soret band absorption (Ishikawa et al., 2005) that may result from non-specific heme binding to IRP2. Regardless, the heme binding region of IRP2 lies within the IDD, which as discussed, is not essential for IRP2 regulation. The weak data of heme binding and iron dependent cysteine oxidation led investigators to believe that iron must regulate IRP2 in some other manner. As a result, the field of cellular iron homeostasis returned to its original questions of iron sensing and IRP2 ubiquitination.

As regulation of IRP2 became again, an open question, IRP1's simple and elegant regulatory paradigm began to have more complex mechanisms ascribed to it. In physiological studies involving mice, it was found that IRP1 binding activity did not change as a function of dietary iron, unlike IRP2 which does response to dietary iron (Meyron-Holtz et al., 2004b). These data suggested that the iron sulfur cluster switch might be diminished in the physiological setting versus cell culture. Further investigations found that IRP1's iron sulfur cluster switch was sensitive to oxygen concentrations. That is, in previous studies in cell culture, the iron sulfur switch occurred in ambient oxygen tensions (~20%) (Hentze and Kuhn, 1996). However, in tissues, particularly the liver, a major site of

physiological iron homeostasis, oxygen tensions are much less (~2-3%). When primary cells were grown from mouse liver and bone marrow, it was found that IRP1's iron sulfur cluster switch functioned in 20% oxygen, but not at physiological oxygen concentrations (Meyron-Holtz et al., 2004b). With the possibility that the iron sulfur cluster switch may not completely explain IRP1's iron dependent regulation *in vivo*, additional studies on other mechanisms of its regulation were carried out in cell culture.

These additional studies found an intriguing, albeit modest mode of IRP1 regulation. It was found that IRP1 lacking an iron sulfur cluster – its IRE binding form – was degraded in an iron dependent manner like IRP2. This only became evident when a variant IRP1 was exogenously expressed containing point mutations in conserved cysteine residues critical for iron sulfur cluster assembly (Clarke et al., 2006; Wang et al., 2007).

In cells, the vast majority of IRP1 (~90%) resides in the aconitase state (Rouault, 2006), and therefore immunoblots of IRP1 from cell extracts could not discern a change in the 10% of IRP1 through iron dependent degradation. However, despite this 9:1 ratio of aconitase to IRE binding states, it can be argued that regulation of the 10% in the IRE binding form is consequential to gene expression. Therefore, iron dependent degradation of IRP1 could be an important mechanism for its regulation *in vivo*. Furthermore, the E3 ligase that controls

IRP1's degradation could be the same as the one that regulates IRP2 in an iron dependent manner.

With these revelations, outstanding questions have resurfaced regarding cellular iron homeostasis. It is important to answer these questions not just to understand a fundamental process in human physiology, but also to understand iron homeostasis in human disease. Understanding cellular iron homeostasis is especially important with respect to iron absorption by the intestine, iron trafficking within the body, and also the pathophysiology of iron misregulation in cellular necrosis, iron overload, anemia, and neurodegeneration (See Chapter IV for a further discussion of iron and disease).

In the context of understanding an important cellular process that could impact human health, we asked the following questions at the start of this dissertation research project:

1. **What is identity of the E3 ligase responsible for IRP2's, and perhaps IRP1's, iron dependent ubiquitination?**

2. **What is the cellular iron sensor?**

3. **How does the cellular iron sensor translate iron concentrations into a signal that modulates E3 ubiquitin ligase activity?**

TABLE I-1. Genes containing Iron Response Elements.

Gene Symbol	UTR	Protein Name	Proposed Function
ALAS2[a]	5’	5’ Aminolevulinic Acid Synthase	Heme synthesis
APP[b]	5’	Amyloid Precursor Protein	Alzheimer’s Disease pathogenesis
CDC14A[c]	3’	Cell Division Cycle Homolog A	Phosphatase; Cell Cycle
DMT1[a]	3’	Divalent Metal Transporter 1	Intestinal iron import
EPAS1[d]	5’	HIF-2α	Hypoxia induced transcription
FTH[a]	5’	Ferritin Heavy Chain	Iron storage
FTL[a]	5’	Ferritin Light Chain	Iron storage
mACO[c]	5’	Mitochondrial Aconitase	Citrate-isocitrate conversion
SLC40A1[a]	5’	Ferroportin	Iron export
SNCA[d]	5’	alpha-synuclein	Synucleinopathy pathogenesis
TFRC[a]	3’	Transferrin Receptor 1	Cellular iron uptake

a. Hentze et al., 2004.
b. Lee and Anderson, 2006.
c. Piccinelli and Samuelsson, 2007.
d. Sanchez et al., 2007.
e. Olivares et al., 2009

(1) $Fe^{2+} + H_2O_2 \rightarrow Fe^{3+} + HO\cdot + HO^-$

(2) $Fe^{3+} + O_2\cdot^- \rightarrow Fe^{2+} + O_2$

Figure I-1.

Fenton Reaction. Free iron can catalyze formation of toxic hydroxyl radicals from hydrogen peroxide as shown in (1). The resulting Fe^{3+} is regenerated back to the Fe^{2+} Fenton catalyst by oxidizing superoxide to oxygen as shown in (2). (Prousek, 2007)

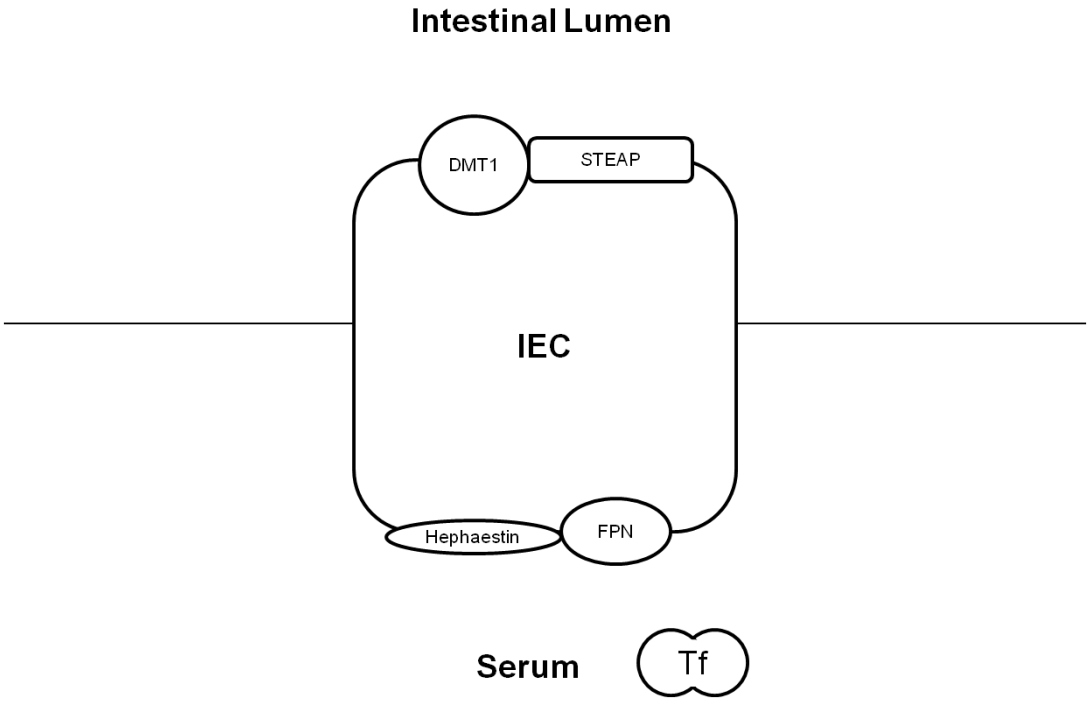

Figure I-2.

Iron uptake by Intestinal Epithelial Cells. Iron from the intestinal lumen is reduced by the STEAP ferrireductases and imported by DMT1. Iron is then exported into the bloodstream through ferroportin (FPN) and reoxidized by Hephaestin to bind to serum transferrin.

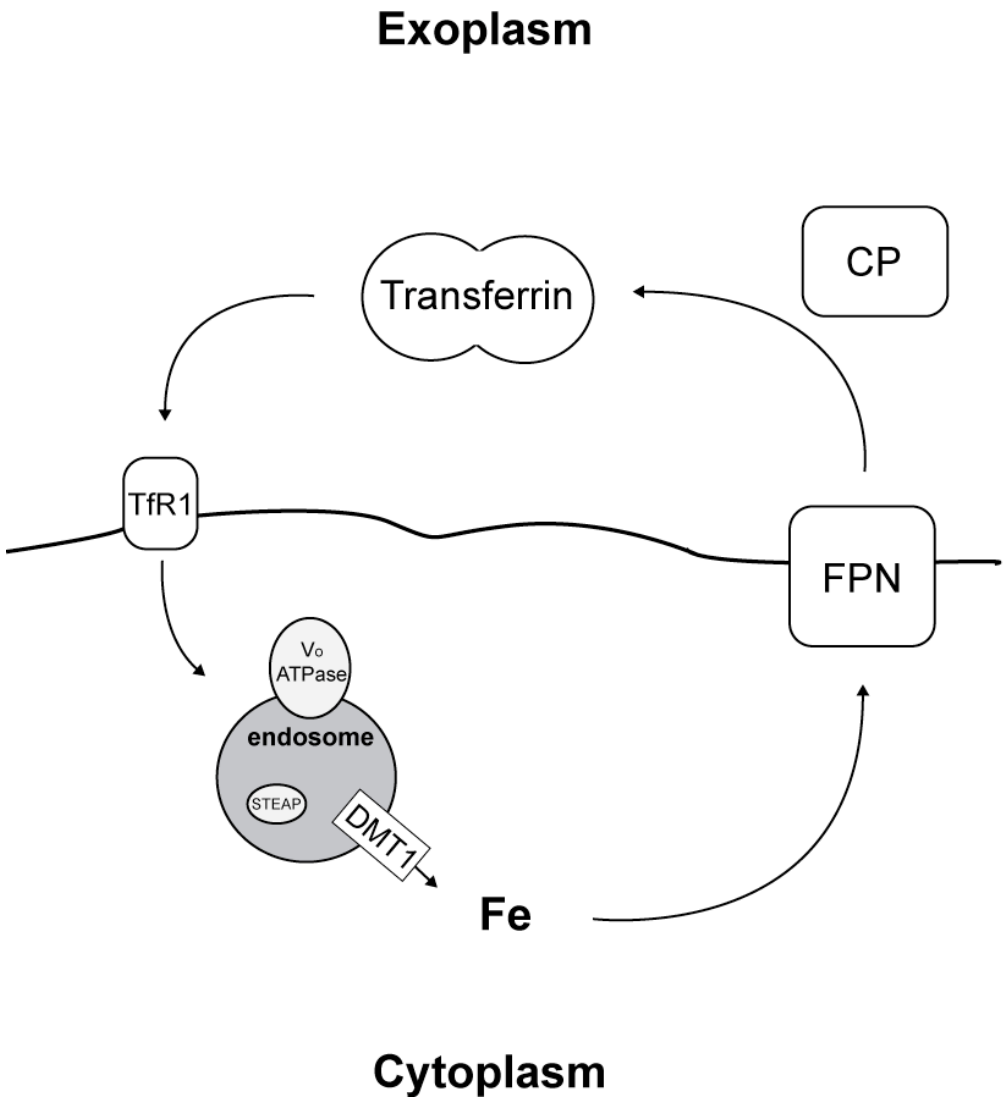

Figure I-3.

Transferrin and Transferrin Receptor Cycle. Transferrin bound iron undergoes receptor mediated endocytosis upon interaction with TfR. The endosome is then acidified by the vacuolar ATPase (V_0) and liberated ferric iron is reduced to ferrous (2+) iron by STEAP ferrireductases. DMT-1 then exports ferrous iron into the cytosol. In certain cells (intestinal epithelial cells (IECs), hepatocytes, and macrophages), iron is exported by ferroportin, and is reoxidized back to the 3+ state (hephaestin on IECs, ceruloplasmin for all others) where it binds to Tf and the Tf-TfR cycle is repeated in other parts of the body.

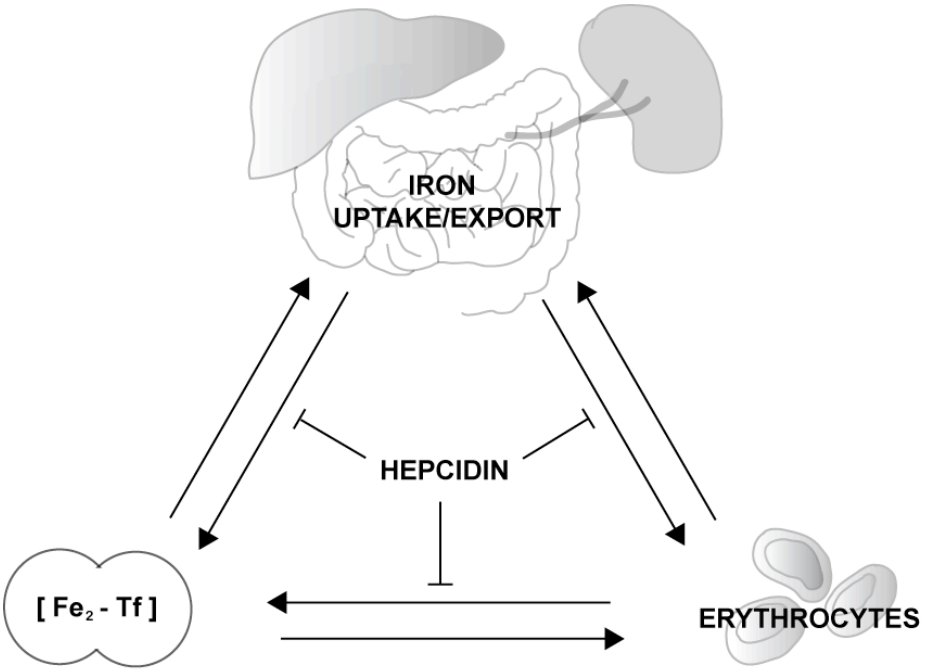

Figure I-4.

Hepcidin regulation of systemic iron homeostasis. Systemic iron homeostasis is mediated largely by iron uptake through the intestine, and release of iron stores from hepatocytes or splenic and hepatic macrophages that derive iron from phagocytosed senescent erythrocytes. In response to elevated iron concentrations or inflammatory stimuli, hepcidin is secreted by the liver and downregulates ferroportin export of iron into the blood stream from either intestinal epithelial cells, or from macrophages. The end result is a decrease in systemic iron availability until the hepcidin stimulus diminishes (either cessation of inflammation, or a return to normal levels of systemic iron availability).

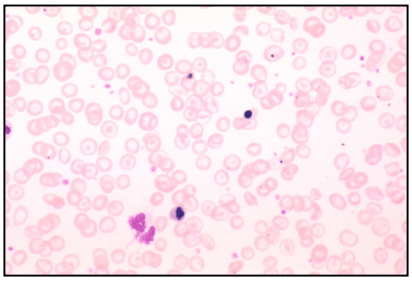

Figure I-5.

Iron Deficiency Anemia. Peripheral blood smears from a patient with iron deficiency anemia (left) or iron overload (right). In addition to constitutional symptoms (pallor, lethargy, dizziness), erythrocytes are hypochromic and microcytic due to insufficient iron for heme synthesis and red blood cell maturation. Image provided by the PEIR digital library.

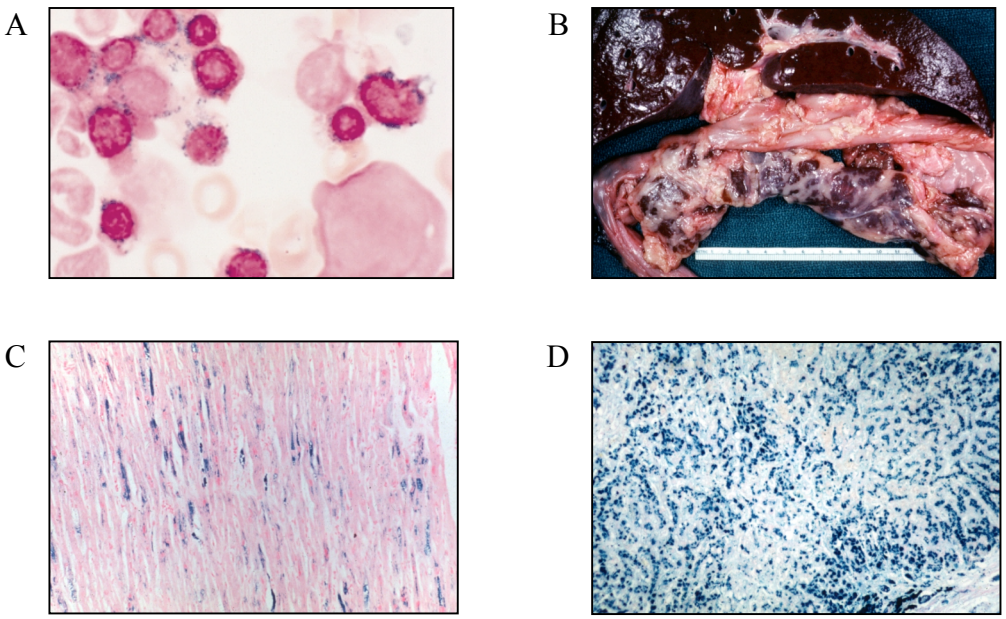

Figure I-6

Iron overload. Erythrocytes contain sideroblast bodies composed of inorganic iron hydroxyphosphate deposits (A). (B) Classic rust brown color of liver and pancreas from a patient with hemochromatosis. (C) Ferric iron staining (Prussian Blue staining) in cardiac muscle section (D) Prussian blue staining of liver section. Iron overload can result in heart failure, liver cirrhosis and pancreatic insufficiency due to cytotoxic accumulation of iron. Images are provided by the PEIR digital library.

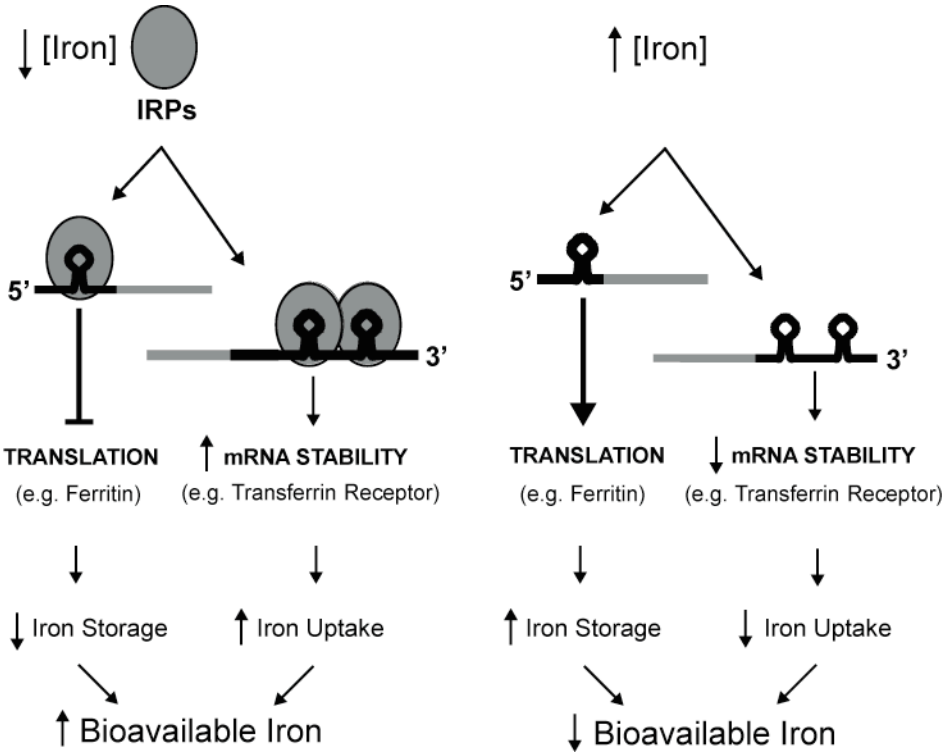

Figure I-7.

A prototypical system of iron homeostasis in mammalian cells. In response to low iron concentrations (left), cells downregulate ferritin synthesis and upregulate transferrin receptor expression. This is mediated by Iron Regulatory Proteins (IRPs) which bind Iron Responsive Elements (IREs, stem loop structures) in mRNA 5' or 3' untranslated regions. IRP binding to 5' IREs result in translational repression (e.g. ferritin), while IRP binding to 3' IREs result in increased halflife of the mRNA transcript (e.g. transferrin receptor). In the state of high cellular iron (right) IRPs do not bind to IREs, and mRNAs with 5' IREs are no longer translationally repressed (i.e. genes such as ferritin are then upregulated) and mRNAs with 3' IREs are more susceptible to endonucleolytic degradation by RNAses.

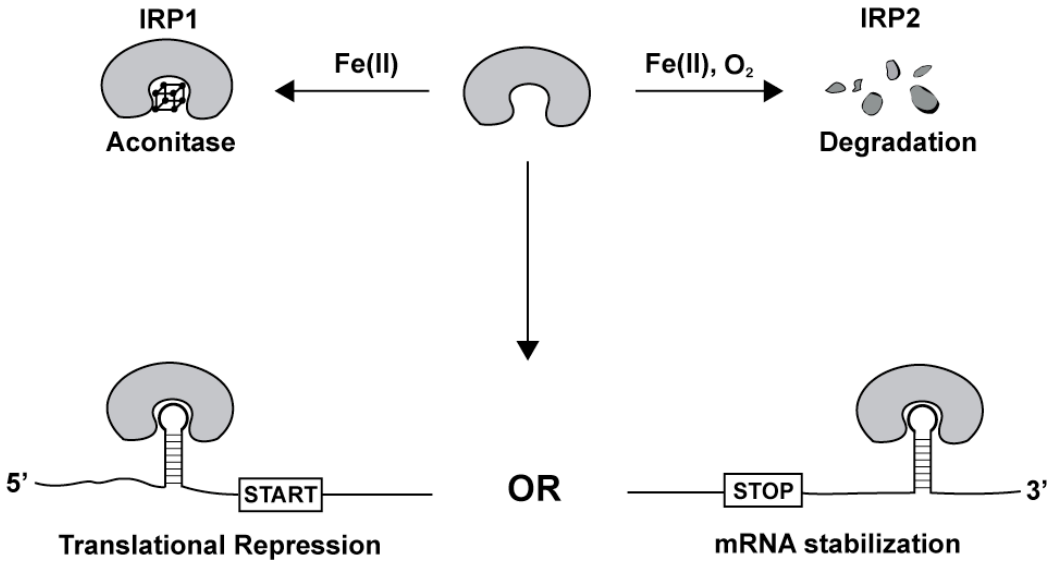

Figure I-8.

Iron dependent regulation of IRP1 and IRP2. In low iron states, IRPs bind to IREs within mRNAs to post-transcriptionally regulate genes involved in iron homeostasis. In high iron, IRP1 assembles an iron sulfur cluster within its IRE binding site, and is thus unable to bind IREs. IRP2, unable to assemble an iron sulfur cluster, is instead ubiquitinated and degraded by the proteasome. In addition to iron, oxygen appears to be required for IRP2 degradation since iron treated cells incubated in ambient 20% oxygen degrade IRP2 more rapidly than iron treated cells grown in 1% oxygen, or hypoxia (Pantopoulos, 2004).

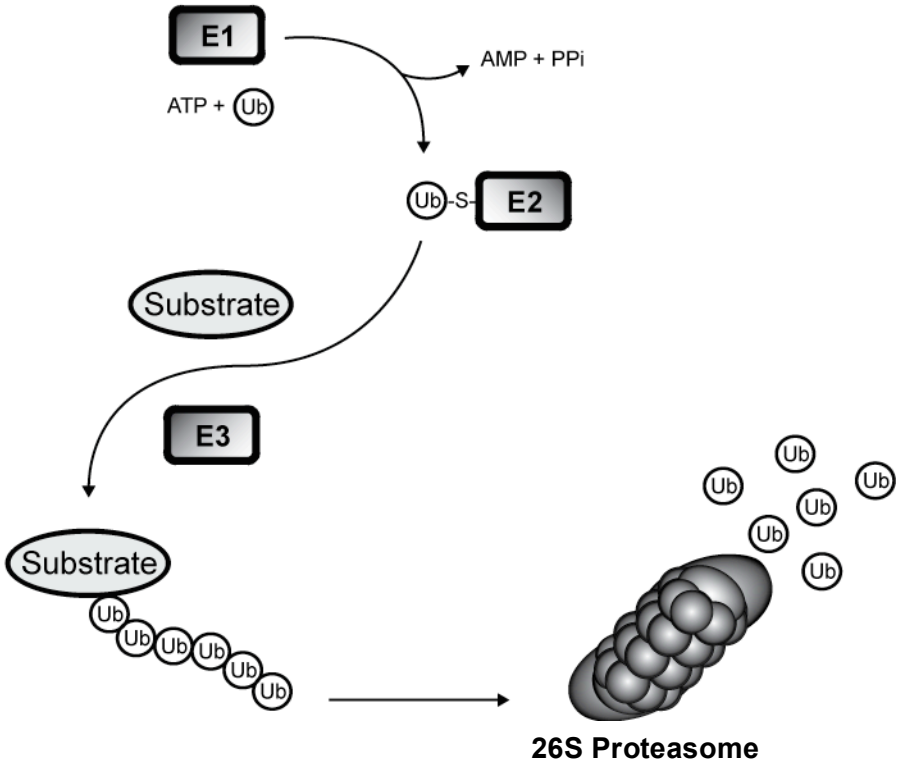

Figure I-9.

Ubiquitination of proteins depends on a cascade of E1, E2, and E3 activities. The C-terminal glycine of ubiquitin is first activated by AMP ribosylation catalyzed by E1. The high energy phospho-ester bond allows for ubiquitin to be conjugated to E2 ubiquitin conjugase through a thioester bond on a conserved cysteine residue. The E2-conjugated ubiquitin is then placed onto lysine residues of protein substrates to be targeted for proteasome degradation by an E3 ubiquitin ligase. The E3 ubiquitin ligase can also catalyze polyubiquitination on protein substrates. These polyubiquitin chains facilitate proteasome degradation through the 26S proteasome.

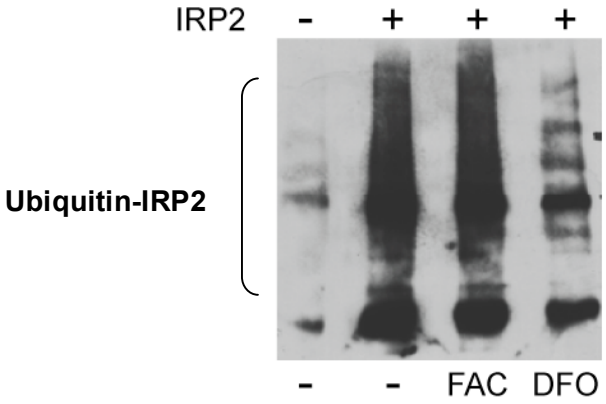

Figure I-10.

Iron-dependent IRP2 ubiquitination. HeLa cells were transfected with a FLAG-tagged IRP2 expression construct followed by treatment for 1 hr with the proteasome inhibitor. The cells were incubated for 5 hr with vehicle (-), 50 μM Ferric Ammonium Citrate (Iron), or 100 μM DFO. Flag-tagged IRP2 was immunoprecipitated and subjected to SDS PAGE and Western blot analysis using a monoclonal mouse anti-ubiquitin antibody (Santa Cruz P4D1). These data are consistent with other published findings (Hason et al., 2003) that IRP2 ubiquitination is iron dependent.

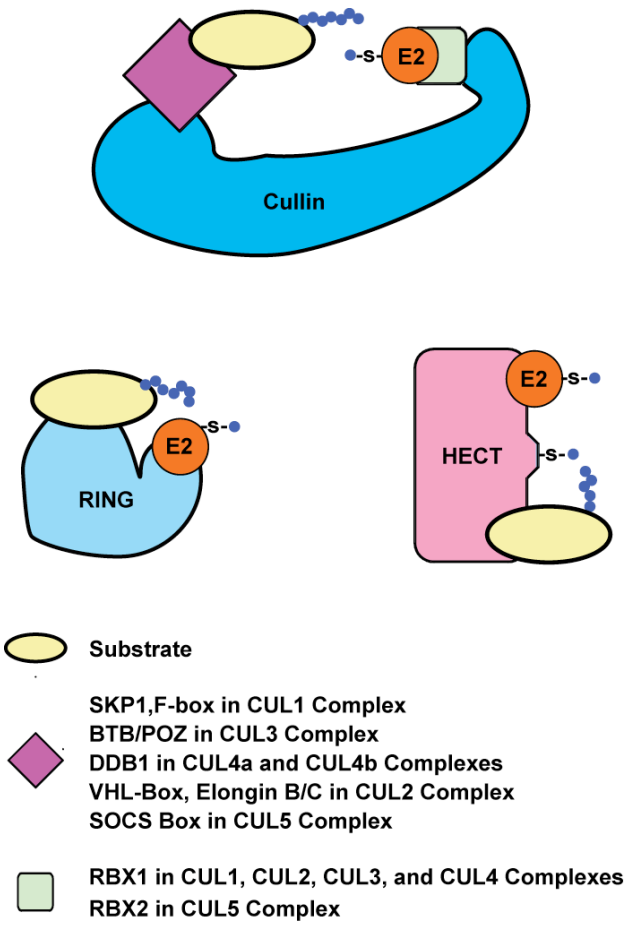

Figure I-11.

Classes of E3 ubiquitin ligases in the human genome. In general, E3 ligases promote the transfer of ubiquitin from E2s to substrate proteins targeted for proteasomal degradation. Cullin class E3 ligases are a family of E3 ligase complexes that employ a Cullin protein as a scaffold for adaptor proteins involved in substrate recruitment, and Ring Box (RBX 1 and 2) proteins responsible for E2 recruitment. RING finger E3 ligases bind E2 through its RING domain, and directly bind substrates to bring them in proximity to the E2, facilitating direct ubiquitin transfer from the E2 to the substrate. HECT domain E3 ligases utilize a similar mechanism, but directly transfer ubiquitins from E2s to substrates through a ubiquitin thioester intermediate which takes place on a conserved cysteine residue within the HECT domain. (Ardley and Robinson, 2005)

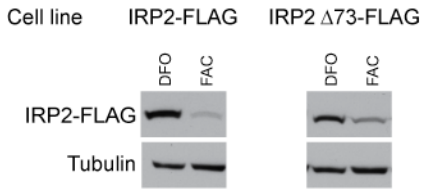

Figure I-12

(Courtesy of Joel Thompson). Deletion of the cysteine rich 73 amino acid region in IRP2 does not preclude iron dependent degradation. Stable HEK293 cells constitutively expressing FLAG tagged wild type or Δ73 IRP2 were treated with either 100μM deferoxamine (DFO) or ferric ammonium citrate (FAC) overnight. IRP2 levels were then visualized by immunoblotting against the FLAG-epitope.

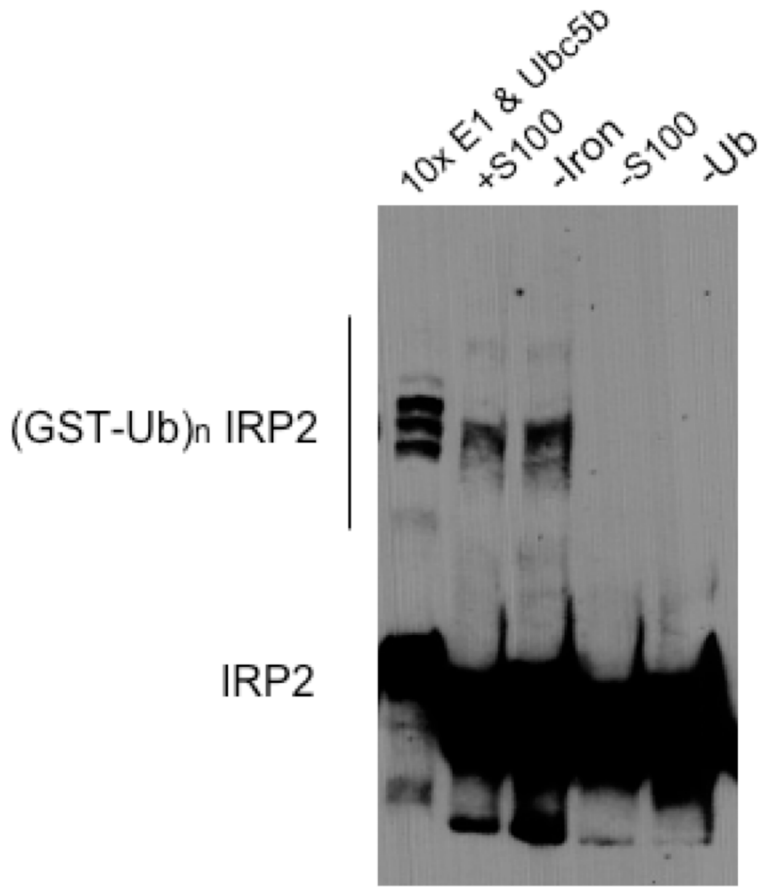

Figure I-13.

in vitro ubiquitination assays reveal that excess many fold excess of E1 and E2 can reconstitute IRP2 ubiquitination seen with ten fold less E1, E2, and HeLa S100 as a source of E3 activity. Reactions were carried out as described in methods (Chapter III), except that a mouse monoclonal IRP2 antibody was employed instead of FLAG to detect IRP2 ubiquitination (here shown as discrete bands due to the use of GST-Ubiquitin). These conditions are similar to that of Yamanaka et al. and suggest that HOIL *in vitro* ubiquitination of IRP2 may be due to high background E1 and E2 activity.

CHAPTER TWO

APPROACHES TO UNDERSTANDING CELLULAR IRON SENSING AND IRP2 REGULATION

Section IIA - Overview of Approaches

How cells sense iron and in turn modulate IRP2's iron dependent ubiquitination have remained open questions since the turn of this century. While many groups have attempted to approach this problem through systematic analysis of regions in the IRP2 protein, these approaches have produced controversial findings (Pantopoulos, 2004). To address the questions of iron sensing, the identity of the IRP2 E3 ligase, and how iron sensing is translated to IRP2 ubiquitination and degradation, three unbiased approaches were initiated: Biochemical purification of IRP2 ubiquitination activity from cell free extracts; affinity purification of IRP2 from extracts of cells treated with iron and proteasome inhibitor; and a high throughput cell based screen to identify genes that whose expression is suppressed by RNA interference, result in IRP2 accumulation.

Section IIB - Biochemical purification of *in vitro* IRP2 ubiquitination

A classical biochemical approach was first undertaken to identify regulators of IRP2, including the relevant iron sensor(s) and responsible

ubiquitin-ligase complex. This strategy was chosen because it offered several advantages, chief among them is that it made few assumptions as to the identity/nature of the relevant factors, providing an unbiased opportunity to identify components of the IRP2 regulatory pathway.

To identify factors responsible for iron stimulated ubiquitination of IRP2, the biochemical approach required both an *in vitro* assay that faithfully recapitulated iron-dependent ubiquitination of IRP2 and a source of lysate containing the responsible regulatory machinery. As IRP2 is expressed in many cell lines, we initially chose HeLa cells as a potential source of lysate as they are available on large scale (~100 L cultures) from Biovest International Inc./National Cell Culture Center. To verify that HeLa cells express the appropriate regulatory machinery, we transfected these cells with a Flag-tagged IRP2 expression construct. Following transfection, the cells were incubated in the presence of a proteasome inhibitor to block IRP2 degradation prior to addition of either iron or the iron chelator desferrioxamine (DFO) to promote or block IRP2 ubiquitination, respectively. As shown in lanes 3 and 4 of Figure II-1, immunoprecipitated IRP2 from the iron-treated cells displays a broad ladder of higher molecular weight species indicative of polyubiquitination that is absent in the sample from cells incubated with DFO. These data demonstrate that HeLa cells express the machinery to recognize elevated iron levels and selectively ubiquitinate IRP2.

Using the soluble fraction of HeLa cell lysates following a 100,000 x *g* centrifugation step (HeLa S100) we were able to establish an *in vitro* assay that appeared to recapitulate IRP2 ubiquitination in an iron-dependent manner (Figure II-2). Having validated our assay and identified a source of material containing the active components necessary for iron sensing and IRP2 ubiquitination, we began to biochemically purify the activity to identify these responsible factors.

The assay (and subsequent modified versions) described in Figure II-2 was used to begin to purify the regulatory components of iron-dependent IRP2 ubiquitination. HeLa S100 fraction was subjected to standard biochemical purification steps including ammonium sulfate precipitation, and liquid chromatography using columns that resolve proteins on the basis of a variety of properties including size, charge, and hydrophobicity (*e.g.* Source Q, Mono Q, Mono S, Phenyl Sepharose, Butyl Sepharose, DEAE Sepharose, CM sepharose, and heparin. Eluted fractions were incubated with the purified Flag-IRP2 substrate in buffer supplemented with ubiquitin, ubiquitin aldehyde, an ATP regeneration system, and iron. An example of a purification step is provided in Figure II-3.

Fractionation removed key factors required for general ubiquitination (*e.g.* an ATP-dependent ubiquitin activating enzyme (E1) and ubiquitin transferase (E2)) early in the process, so fractions were supplemented with recombinant preparations of these proteins. E1 was purchased from a commercial source and

bacterial expression constructs for E2 proteins were kindly provided by the laboratory of Dr. Zhijian Chen (UT Southwestern).

Conventionally, one characterizes the activity over multiple procedures to devise a large scale protocol from the most effective purification steps. After sequential purification of the activity across several columns, the most purified fractions of the activity would be subjected to polyacrylamide gel electrophoresis and proteins would be visualized by silver staining. Individual band(s) co-eluting with the enzymatic activity would then be identified by mass spectrometry. As there are likely to be several relevant activities required for iron-dependent ubiquitination, including an "iron sensor" and a substrate specific ubiquitin ligase (E3) that need not reside within the same protein, we anticipated carrying out several sequential purifications in which fractions containing one activity are added back to the assay mixture in the course of further purifying a second activity. Once the responsible protein for one activity had been identified, we planned to supplement our reactions with that factor before embarking on subsequent fractionation/purification of the first activity.

However, after a year of effort, our progress was hindered by several *in vitro* artifacts including purification of an E3 ligase activity for a protein that cross-reacted with the FLAG antibody, purification of a high molecular weight product that cross-linked with IRP2 in an iron dependent manner, and high background from recombinantly expressed IRP2. These artifacts continued to

surface despite reoptimization of assay conditions and changing the source of E3 activity and type of IRP2 substrate. Ultimately, we concluded that biochemical purification of IRP2 ubiquitination activity was not the most optimal approach because our *in vitro* assay was not sufficiently sensitive or specific. Furthermore, we refocused our efforts more promising approaches, discussed in Sections IIC and IID.

Section IIC – Identification of IRP2 interacting proteins through affinity purification.

The E3 ligase, or other proteins involved in IRP2's iron regulation, could potentially be identified through affinity purification of IRP2 since these proteins often have a semi-stable interaction (Chen et al., 2005; Song et al., 2005). To identify IRP2 interacting proteins, a HEK293 stable cell line expressing an N-terminal HA tag and a C-terminal 3XFLAG tag was employed. Importantly, the tandem tagged IRP2 faithfully recapitulated endogenous IRP2's iron dependent degradation (i.e. accumulates upon DFO treatment, and diminishes upon treatment with Ferric Ammonium Citrate (FAC)) (Figure II-4).

In work carried out by a rotation student, Julio Ruiz, cells were grown in the presence of iron to induce IRP2's E3 ligase activity. Cells were also treated with a proteasome inhibitor, MG132, to prevent degradation of the HA-IRP2-3XFLAG protein. As a negative control, the stable cell line was similarly treated

with DFO and MG132. In addition, a parental HEK293 cell line lacking the HA-IRP2-3XFLAG transgene was treated in an identical manner. Lysates from these four conditions were then immunoprecipitated with anti-FLAG antibodies, washed, and IRP2 and interacting proteins were eluted with a 3X-FLAG peptide. The eluates were then subjected to SDS-PAGE followed by silver staining to identify bands specific to the FAC treated HA-IRP2-3XFLAG stable cell line (Figure II-5). For protein identification, FLAG eluted proteins from the FAC treated stable cells were subjected to in solution trypsin digestion, followed by reverse phase liquid chromatography and tandem Mass Spectrometry analysis. As expected, the greatest amount of tryptic peptides identified corresponded to IRP2. In addition to several identified IRP2 interacting proteins, three candidate E3 ligases were found. These E3 ligases were Ring Finger 111 (RNF111), NS1-Binding Protein (NS1-BP), and Cullin 1 (CUL1). A complete list of all peptide identifications can be found in the Appendix.

Of the three candidate E3 ligases, CUL1 was found to be required in IRP2's iron dependent regulation. CUL1, as discussed in Chapter I, functions as a scaffold protein in a four protein SCF complex class of E3 ligases (Willems et al., 2004). CUL1's requirement in IRP2 degradation was demonstrated by siRNA knockdown of the CUL1 in HA-IRP2-3XFLAG cells treated with iron (Figure II-6). Here, CUL1 knockdown results in inappropriate IRP2 accumulation in iron replete cells.

The SCF class of E3 ligases are protein complexes composed of a static core of SKP1, which binds to the N-terminus of the CUL1 scaffold protein, and RBX1 which binds to CUL1's C-terminus (Willems et al., 2004) (Figure I-11). A variable F-box protein, which dictates substrate specificity, then interacts with this three protein complex by interacting with SKP1 through its eponymous F-box domain. Because the subunits of the SCF complex are at equal molar stochiometries, it is unusual that CUL1, and not SKP1, RBX-1 and a specific F-box protein, was identified by mass spectrometry. However, it should be noted that the confidence score for the CUL1 identification was low, and only a single peptide was identified. In this situation, it is possible that low abundance for SKP1, RBX1, and the F-box were below the threshold for detection that was sufficient for CUL1 identification. Regardless, this affinity purification approach provided the first clue to identify the E3 ligase responsible for IRP2's iron dependent regulation.

Because CUL1 was identified in an early affinity purification attempt, further optimization of the procedure may have identified all components of the putative SCF complex. However, we instead chose to undertake a complementary approach, and undertook an unbiased siRNA screen of 800 candidate E3 ligases. If this independent and unbiased approach also identified an SCF complex as a candidate IRP2 E3 ligase, it would have provided support for our initial CUL1 finding.

Section IID – A High throughput siRNA screen to identify an IRP2 E3 ligase.

Because our *in vitro* biochemical purification was artifact prone, and also because there was a possibility that affinity purification of IRP2 may not copurify all components of an E3 ligase complex, we developed an alternative cell based approach. This approach utilized siRNA suppression to serve as a loss of function screen for genes important in IRP2's iron dependent degradation. We hypothesized that suppressing protein levels of the IRP2 E3 ligase under high iron conditions would result in increased IRP2 protein levels.

While we could measure IRP2 protein levels by immunoblotting, we opted instead for a more high throughput and quantitative method to measure levels for IRP2. The method we chose for this purpose was a proprietary technology from Perkin Elmer, AlphaScreen (Figure II-7). Amplified Light Proximity Homogenous Assay (ALPHA) involves generation of light only when beads conjugated with donor and acceptor fluorophores are brought within close proximity (~200nm). Here, excitation of the Donor beads with long wavelength light (680 nm) results in the generation of singlet oxygen molecules with a limited lifetimes, restricting their radius of diffusion in solution. If the Acceptor bead is within ~200 nm of the Donor bead, a thioxene derivative embedded within the Acceptor bead will react with singlet oxygen. The ensuing chemiluminescent

reaction transfers energy to a fluorophore within the Acceptor bead that emits light at a shorter (520-620 nm) wavelength (Ullman et al., 1994).

To employ this technology for our siRNA screen, HEK 293 cells were stably transfected with a plasmid expressing human IRP2 fused to an N-terminal HA epitope tag and a C-terminal FLAG epitope tag under the control of a constitutive CMV promoter. A clonal cell line was selected that accumulated high levels of HA-IRP2-FLAG in cells depleted of iron upon treatment with the iron chelator deferoxamine mesylate (DFO), and low levels of HA-IRP2-FLAG in cells incubated in the presence of excess iron (Ferric Ammonium Citrate; FAC) in a manner comparable to endogenous IRP2 (Figure II-8). As an alternative to Western blot analysis, HA-IRP2-FLAG protein accumulation levels could also be assessed in whole cell lysates using a high throughput luminescent proximity assay (AlphaScreen; Figure II-8). Relative HA-IRP2-FLAG levels as measured by AlphaScreen strongly correlate with IRP2 levels detected by Western blot analysis (Figure II-8). Furthermore, siRNA knockdown of CUL1 results in an increase in ALPHA screen signal, as does knockdown of SKP1 and RBX1 (Figures II-9, II-10, and II-11). These data show that AlphaScreen is a high fidelity reporter of IRP2 stabilization, and that a CUL1 containing SCF class E3 ligase may be involved in IRP2 regulation.

To identify candidate E3 ubiquitin ligase components responsible for iron-dependent IRP2 ubiquitination, a library of 800 siRNA pools (Qiagen), each

designed to suppress expression of an individual human gene, was assembled. Included in the library were siRNAs for genes encoding proteins known to play a role in ubiquitination as well as proteins containing domains found within previously identified E3 ligase complexes (Ardley and Robinson, 2005; Hershko and Ciechanover, 1998; Li et al., 2008; Willems et al., 2004). To serve as a positive control for siRNA transfection in this screen, siRNAs targeting the D1 subunit of the vacuolar ATPase were employed. When the D1 subunit is suppressed in cells, acidification of the endosome is attenuated, and receptor mediated endocytosis is compromised (personal communication, Michael G. Roth, UT Southwestern). In this setting, transferrin-TfR mediated iron uptake is blocked at the stage of endosomal acidification. As a result, cells incubated with moderate iron concentrations mimic iron chelator (DFO) treatment. IRP2 then accumulates at low iron concentrations, but is degraded at higher iron concentrations as measured by AlphaScreen (Figure II-10). At higher iron concentrations, iron is believed to be take up by cells through non specific means, such as calcium and other divalent cation channels (Hentze et al., 2004). This behavior allowed us to interrogate positive hits in the siRNA screen to see whether their function was at the level of receptor mediated endocytosis or at intracellular levels.

With these findings providing sufficient validation, the screen was then performed by Joel Thompson in conjuction with the UT Southwestern

High-Throughput Screening Facility. The results of the screen provided a major breakthrough in our understanding cellular iron sensing and IRP2 ubiquitination. Our detailed findings are presented in the next chapter.

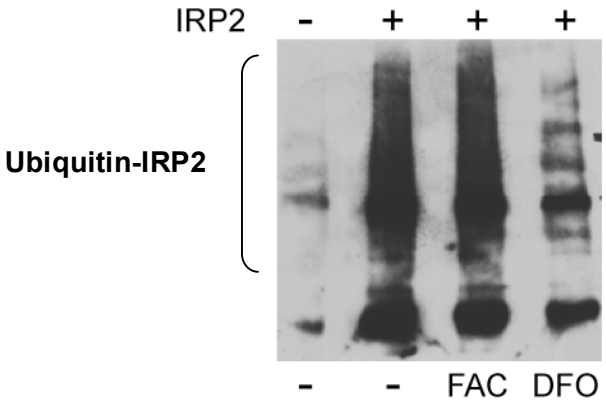

Figure II-1.

HeLa cells contain iron-dependent IRP2 ubiquitination activity. HeLa cells were transfected with a FLAG-tagged IRP2 expression construct followed by treatment for 1 hr with the proteasome inhibitor. The cells were incubated for 5 hr with vehicle (-), 50 μM Ferric Ammonium Citrate (Iron), or 100 μM DFO. Flag-tagged IRP2 was immunoprecipitated and subjected to SDS PAGE and Western blot analysis using an anti-ubiquitin antibody.

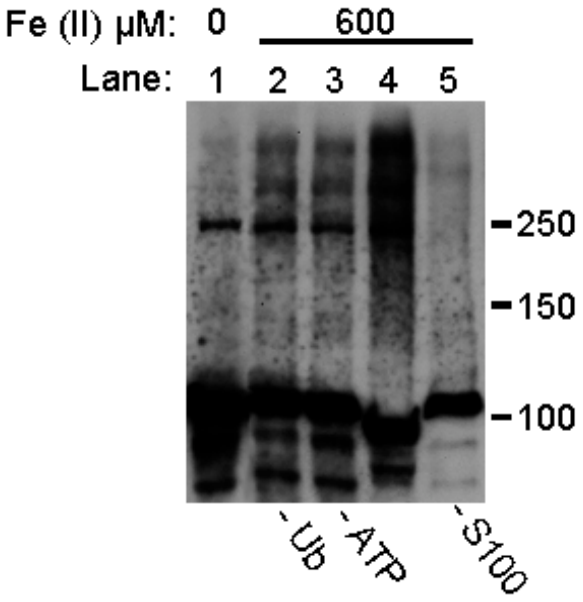

Figure II-2.

Iron stimulated ubiquitination of IRP2 *in vitro*. To prepare the IRP2 substrate, HEK-293 cells stably-transfected with a Flag-tagged IRP2 expression constructed were grown the presence of DFO for 10 hours to block IRP2 ubiquitination. IRP2 was subsequently purified by immunopreciptation from the resulting cell lysates using an anti-Flag antibody. Immunopreciptated IRP2 was then incubated in the presence of HeLa S100 lysate, ubiquitin, ubiquitin aldehyde (an inhibitor of deubiquitinating enzymes), and an ATP regeneration system in the absence (Fig. 3 lane 1) or presence (Fig. 3 lane 4) of ferrous sulfate for 1hr at 37°C. Samples were resolved by SDS PAGE and analyzed by Western blotting using an anti-FLAG antibody. A broad laddering pattern of higher molecular weight species is indicative of efficient polyubiquitination as demonstrated in lane 4. Removal of iron, ubiquitin, the ATP regeneration mixture, or HeLa S100 lysate (lanes 1, 2, 3, and 5 respectively) results in the loss of apparent ubiquitination activity.

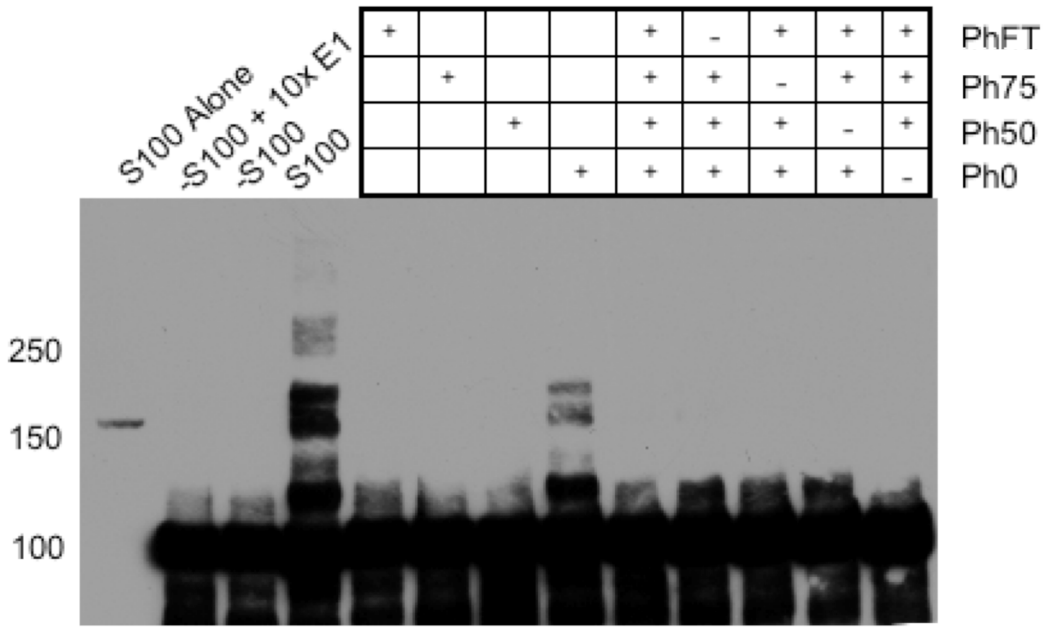

Figure II-3.

Fractionation of *in vitro* ubiquitination of IRP2. 10mg of HeLa S100 was incubated with 20% ammonium sulfate in Hepes buffer pH 7.4. The supernatant after a 20,000 x g spin (input, or S100) was then equilibriated on a 1mL HiTrap Phenyl HP column, and equilibriated in a 20% ammonium sulfate Hepes buffer. Fractions were then collected by step wise gradient elution of starting buffer and elution buffer (Hepes pH 7.5 20mM KCl). Fractions were then dialyzed in Buffer A and fractions were normalized by volume to the input. Reactions were then carried out as described in the methods, with the exception that a GST-tagged ubiquitin was employed which gives a discrete banding pattern (Chapter III). Reactions were then stopped with sample buffer, resolved by SDS-PAGE, and activity was visualized by immunoblotting for FLAG-IRP2. Activity appears to fractionate in the Ph0 fraction (0% starting buffer, 100% elution buffer), but activity is not fully recoverable, and combining all fractions show that Ph0 is essential. While this activity appears to be amenable to purification, the activity was ultimately found to be an artifact (the activity shown is not IRP2 ubiquitination, but an unidentified protein that cross-reacts with the FLAG antibody).

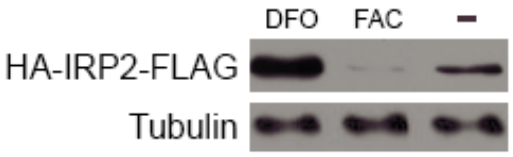

Figure II-4.

FLAG immunoblots from HA-IRP2-3XFLAG HEK293 stable cells lysates demonstrate that the affinity tagged IRP2 is regulated in a physiological manner. Cells were either treated with iron chelator (DFO), iron (FAC), or vehicle (-) and incubated for twenty hours prior to immunoblotting.

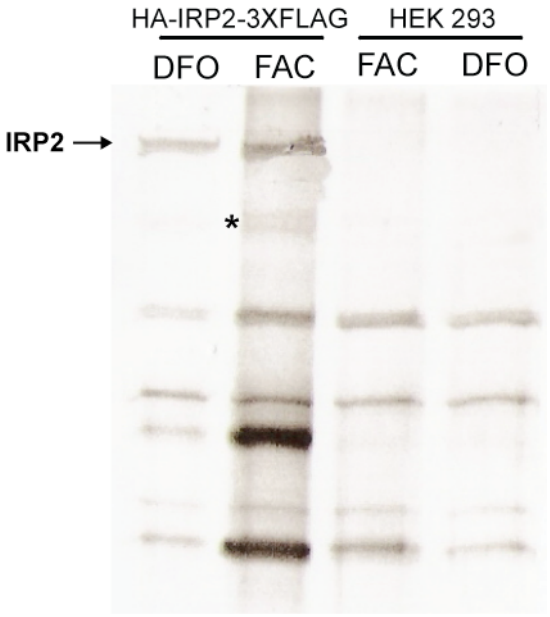

Figure II-5.

Courtesy of Julio Ruiz. Silver stained SDS PAGE from FLAG affinity purification of HEK 293 parental cells (Untransfected) or cells expressing FLAG-tagged IRP2 (HA-IRP2-3XFLAG). Lysates were generated from iron depleted (DFO), or iron replete (FAC) cells that were preincubated with the proteasome inhibitor MG132. A specific band purified from the HA-IRP2-3XFLAG is indicative of IRP2, and a specific co-purifying band is indicated by an asterisk. Proteins that copurified with FLAG affinity purified IRP2 were subjected to in solution trypsin digestion and peptides were identified by LC-MS.

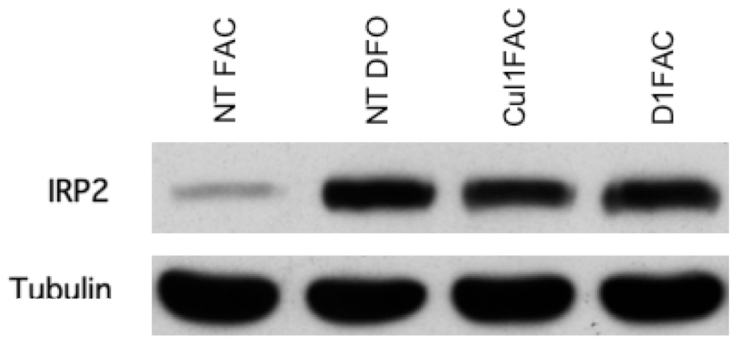

Figure II-6.

Courtesy of Julio Ruiz. IRP2 immunoblots demonstrate that siRNA suppression of CUL1 or the D1 subunit of the vacuolar ATPase results in inappropriate IRP2 accumulation in high iron conditions. Cells were transfected with Non-targeting (NT), CUL1 siRNA oligo number 1 (Table III-1) or D1 siRNA (Table III-1) for 48 hours. The media was then changed and cells were then incubated with either 100 micromolar DFO or FAC overnight.

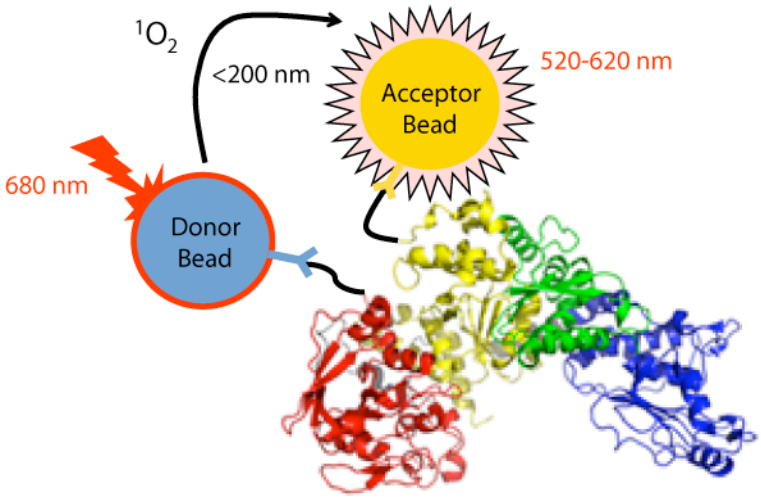

Figure II-7.

A high throughput assay to identify the IRP2 E3 ligase(s). Cells are reverse transfected with siRNA in opaque plates and treated with excess iron. Cells are then lysed, and lysates are incubated in the presence of Donor beads coated with α-HA antibodies and Acceptor beads coated with α-FLAG antibodies. Excitation of the Donor beads with long wavelength light (680 nm) results in the generation of singlet oxygen molecules with a limited lifetimes, restricting their radius of diffusion in solution. If the Acceptor bead is within ~200 nm of the Donor bead, a thioxene derivative embedded within the Acceptor bead will react with singlet oxygen. The ensuing chemiluminescent reaction transfers energy to a fluorophore within the Acceptor bead that emits light at a shorter (520-620 nm) wavelength (Ullman et al., 1994). When HA-IRP2-FLAG is present in whole cell lysates, the α-HA Donor beads and α-FLAG Acceptor beads are brought into close proximity as reflected by an amplified luminescent signal. Conversely, incubation of cells in the presence of excess iron (FAC) prior to lysis results in low accumulation of HA-IRP2-FLAG and a corresponding decrease in signal. siRNAs targeting a putative IRP2 E3 ligase would result in an abnormal high signal in cells treated with FAC. The IRP structure was obtained from the Protein Data Bank (2IPY).

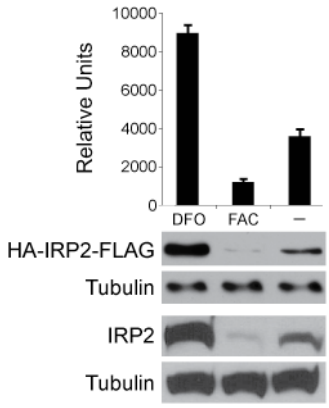

Figure II-8.

Assessment of IRP2 protein accumulation under iron deplete (DFO) or iron replete (FAC) conditions using the AlphaScreen assay (top), by Western blot analysis of the HA-IRP2-FLAG reporter protein (α-FLAG antibody; middle) or endogenous IRP2 in the parental HEK 293 cell line (bottom). Tubulin immunoblots served as loading controls. Data are presented as the mean of three samples, with error bars indicating the standard error of the mean.

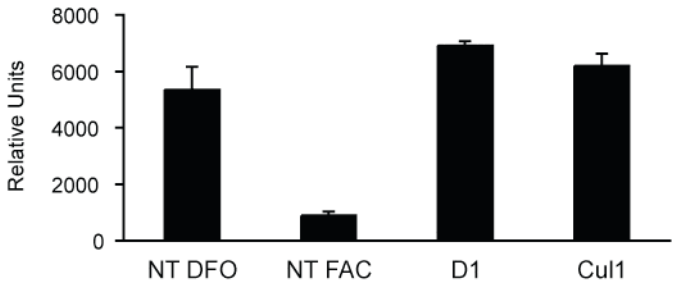

Figure II-9.

AlphaScreen readout of HA-IRP2-3XFLAG cells transfected with either Non-targeting (NT), D1, or CUL1 siRNA either with DFO or FAC. Data are presented as the mean of three samples plus or minus the standard error of the mean (error bars).

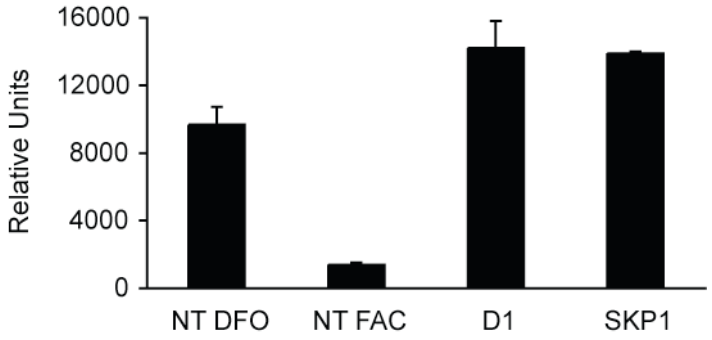

Figure II-10.

AlphaScreen readout of HA-IRP2-3XFLAG cells transfected with either Non-targeting (NT), D1, or SKP1 siRNA either with DFO or FAC. Data are presented as the mean of three samples plus or minus the standard error of the mean (error bars).

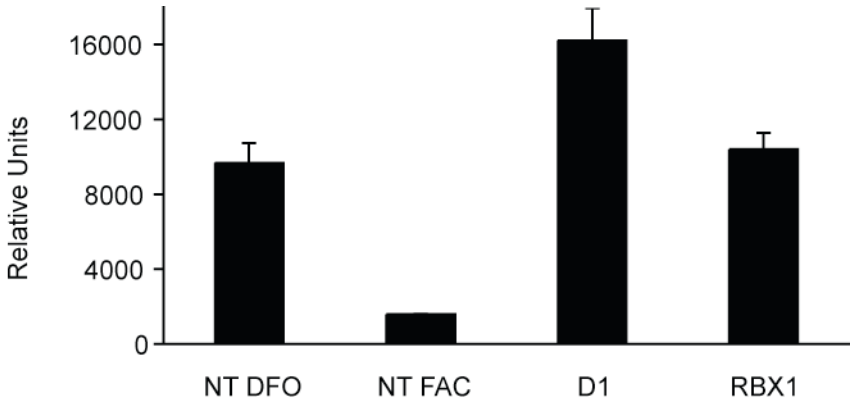

Figure II-11.

AlphaScreen readout of HA-IRP2-3XFLAG cells transfected with either Non-targeting (NT), D1, or RBX1 siRNA either with DFO or FAC. Data are presented as the mean of three samples plus or minus the standard error of the mean (error bars).

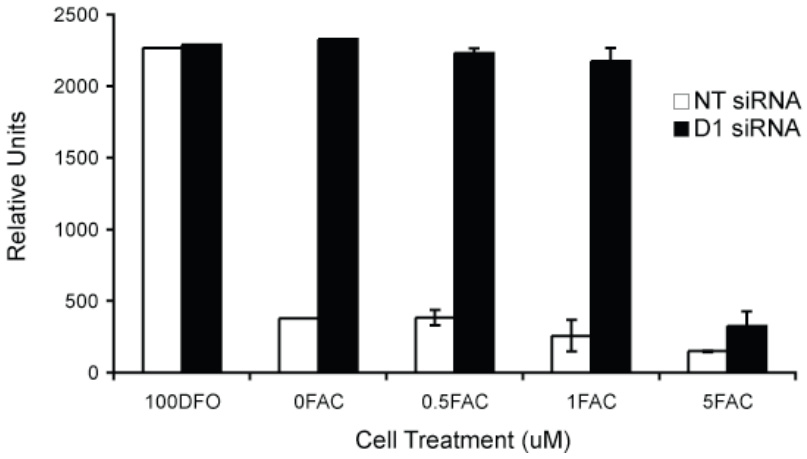

Figure II-12.

AlphaScreen readout of HA-IRP2-3XFLAG cells transfected with either Non-targeting (NT) or D1 siRNA either with DFO or increasing amounts of FAC. Data are presented as the mean of three samples plus or minus the standard error of the mean (error bars).

CHAPTER THREE

CRUCIAL STEP IN IRON HOMEOSTASIS: FBXL5 BINDS CELLULAR IRON TO PROMOTE THE UBIQUITINATION OF IRON REGULATORY PROTEINS

Introduction

How iron regulates IRP2 degradation was an outstanding question in the field of iron homeostasis. To elucidate how IRP2 is regulated, we sought to identify E3 ligase components required for its iron dependent regulation in cells. To this end, we carried out an siRNA screen described in Section IID, that employed a cell based assay for measuring IRP2 stability. After we carried out the screen, we were able to identify a candidate SCF E3 ligase. Further experiments not only validated our initial finding, but were also able to elucidate a mechanism uniting iron sensing, IRP2 regulation, and the regulation of genes responsible for cellular iron homeostasis. The results supporting these findings are presented in this chapter.

Section IIIA - Identification of a SKP-CUL-F-box E3 Ubiquitin Ligase Complex Required for Iron-Dependent IRP2 Degradation

HEK 293 cells were stably transfected with a plasmid expressing human IRP2 fused to an N-terminal HA epitope tag and a C-terminal FLAG epitope tag under the control of a constitutive CMV promoter. A clonal cell line was selected

that accumulated high levels of HA-IRP2-FLAG in cells depleted of iron upon treatment with the iron chelator deferoxamine mesylate (DFO), and low levels of HA-IRP2-FLAG in cells incubated in the presence of excess iron (Ferric Ammonium Citrate; FAC) in a manner comparable to endogenous IRP2 (Figure II-4). As an alternative to Western blot analysis, HA-IRP2-FLAG protein accumulation levels could also be assessed in whole cell lysates using a high throughput luminescent proximity assay (AlphaScreen; Figure II-7). Relative HA-IRP2-FLAG levels as measured by AlphaScreen strongly correlate with IRP2 levels detected by Western blot analysis (Figure II-8).

To identify candidate E3 ubiquitin ligase(s) responsible for iron-dependent IRP2 ubiquitination, a library of 800 siRNA pools (Qiagen), each designed to suppress expression of an individual human gene, was assembled. Included in the library were siRNAs for genes encoding proteins known to play a role in ubiquitination as well as proteins containing domains found within previously identified E3 ligase complexes (Ardley and Robinson, 2005; Hershko and Ciechanover, 1998; Li et al., 2008; Willems et al., 2004). The reporter cells were transfected with the siRNAs in 96-well plates and incubated in the presence of excess iron prior to determination of relative HA-IRP2-FLAG accumulation by AlphaScreen. In most cases, transfection of cells with individual siRNA pools had little effect on iron-dependent degradation of the HA-IRP2-FLAG reporter. However, siRNA-mediated repression of a small subset of targeted genes resulted

in inappropriate accumulation of HA-IRP2-FLAG under iron replete conditions (data not shown).

The greatest increase in HA-IRP2-FLAG accumulation under iron replete conditions was observed upon transfection with siRNAs targeting expression of the F-box-containing FBXL5 protein (Figure III-1). F-box containing proteins typically assemble within SCF E3 ubiquitin ligase complexes composed of common core components SKP1, Cullin 1 (CUL1), RBX1, and a variable F-box-containing protein (Willems et al., 2004). CUL1 functions as a scaffolding protein, interacting with RBX1 at its C-terminus and indirectly interacting with the F-box protein through the SKP1 adaptor protein at its N-terminus. RBX1 is a ring-finger protein that recruits an ubiquitin-conjugated E2 enzyme to the complex. In addition to the common F-box motif, F-box proteins feature domains responsible for recruiting particular substrates to individual SCF complexes to facilitate ubiquitin conjugation. The resulting transfer of ubiquitin from E2 to substrates promote their recognition by the proteasome (Hershko and Ciechanover, 1998). In addition to FBXL5, CUL1, SKP1, and RBX1 were also identified in the unbiased siRNA screen. Compared with a non-targeting (NT) control siRNA, knockdown of *FBXL5* expression by either of two independent siRNAs (FBXL5 #1 or #2) leads to complete stabilization of HAIRP2-FLAG under iron replete conditions (Figure III-1). Analogous results were observed by Western blot analysis of endogenous IRP2 levels in HEK 293 (Figures III-1) and

HeLa (Figure III-2) cells. Suppression of the core SCF subunits SKP1, CUL1, and RBX1 also resulted in partial stabilization of IRP2 under iron replete conditions (Figure III-1). Similar results were observed for two independently selected clonal cell lines containing a tetracycline (Tet)-inducible FBXL5 shRNA (Figure III-3). Unlike the parental HEK 293 TRex cell line that properly degrades endogenous IRP2 upon FAC-treatment, IRP2 is stabilized in FAC-treated FBXL5 shRNA clonal cell lines in the presence, but not absence, of Tet.

Given the apparent differences in IRP1 and IRP2 regulation, despite a greater than 60% amino acid identity between the two proteins, early studies focused on the role of a cysteine-rich 73 amino acid insertion unique to IRP2 (Iwai et al., 1995). Oxidation of multiple cysteine residues in this region following an increase in cytosolic iron concentration was proposed to recruit a candidate E3 ligase, heme-oxidized IRP2 ubiquitin ligase-1 (HOIL-1) (Iwai et al., 1998; Yamanaka et al., 2003). However, deletion of these 73 amino acids does not preclude iron dependent IRP2 degradation and RNAi-mediated knockdown of HOIL-1 expression in HEK 293 cells does not result in inappropriate IRP2 accumulation in the presence of excess iron (Bourdon et al., 2003; Hanson et al., 2003; Wang et al., 2004; Zumbrennen et al., 2008). Consistent with this finding, HEK 293 cell lines stably transfected with either a FLAG-tagged wildtype or IRP2-Δ73 expression construct featured reduced IRP2 accumulation under iron replete conditions when transfected with a nontargeting (NT) control siRNA.

However, knockdown of FBXL5 expression led to accumulation of both proteins (Figure III-4). Furthermore, it has recently been reported that the apo form of IRP1, like IRP2, can be targeted for proteasomal degradation under iron replete conditions (Fillebeen et al., 2003) though the physiological relevance of these observations remains under investigation. Such regulation is most easily observed for IRP1 variants containing mutations to Cys ligands (3C>3S) used to bind Fe-S clusters (Clarke et al., 2006). Little change in IRP1 levels was observed in FAC-treated HEK 293 cell lines stably expressing myc-tagged wildtype (WT) IRP1 following transfection with three independent FBXL5 siRNAs. Conversely, a myc-tagged 3C>3S IRP1 variant responded in an analogous manner to endogenous IRP2 (Figure III-5). Together, these data suggest that FBXL5 can recognize both IRP1 and IRP2, likely through a shared element.

IRP2's reduced half-life under iron replete conditions is accompanied by decreased RNA binding activity and changes in expression of IRE-containing mRNAs (Guo et al., 1995). To demonstrate that the IRP2 inappropriately accumulating in iron replete cells upon FBXL5 knockdown is functional, an electrophoretic mobility shift assay (EMSA) was performed. The HA-IRP2-FLAG HEK 293 cell line was treated with control NT or FBXL5 siRNAs and incubated in the presence of FAC or DFO. Lysates from these cells were incubated with a ^{32}Pradiolabeled IRE, and IRP/IRE complexes were resolved in a nondenaturing gel. In NT control samples, less IRE/IRP complex was observed in

FAC-treated cells as both IRP1 (increased Fe-S cluster assembly) and IRP2 (proteasomal degradation) RNA-binding activities were low. Knockdown of FBXL5 expression under iron replete conditions increased total IRE binding activity (IRP1/2) to levels similar to those observed under iron deficient conditions (Figure III-6). Because human IRP1/IRE and IRP2/IRE complexes migrate similarly, antibodies were added to supershift individual complexes. Supershifting with an α-IRP1 antibody revealed that while IRP1's RNA binding activity is sensitive to cellular iron availability (compare lanes 6 and 7), FBXL5 knockdown had little effect on IRP1's IRE binding activity. This result suggests that FBXL5 knockdown does not simply reduce cellular iron uptake or availability. In contrast, supershifting with an α-FLAG antibody demonstrated that the increased IRP2 levels in FAC treated cells results in a corresponding increase in total IRP2 RNA-binding activity (Figure III-6).

To determine whether increased IRP2 IRE binding activity following FBXL5 suppression results in misregulation of IRE containing genes, the expression of an IRP target was measured. Normally, when bioavailable iron levels are high and IRP1/2 have minimal IRE binding activity, TfR1 mRNA levels are low due to increased endonucleolytic cleavage (Koeller et al., 1989) though TfR1 expression is also regulated by iron at the level of transcription (Rao et al., 1986). However, in the Tet-inducible FBXL5 shRNA cells, loss of FBXL5 expression resulted in a ~2.5 fold increase in TfR1 mRNA accumulation under

iron replete conditions as measured by qRTPCR (Figure III-7). Together these results demonstrate that siRNA-mediated FBXL5 suppression results in inappropriate accumulation of IRP2 under iron replete conditions and increased IRP2 IRE binding activity with concomitant misregulation of IRP target genes.

Section IIIB - FBXL5 Interacts with IRP2

While the results in Figures III-1 to III-7 indicate that FBXL5 contributes to iron-dependent IRP regulation, these data do not address whether these effects are direct or indirect. To investigate whether FBXL5 interacts with IRP2, a plasmid encoding V5-tagged FBXL5 was transfected into IRP2-FLAG HEK 293 cells. Anti-FLAG immunoprecipitates were resolved by SDS-PAGE and immunoblotted with antibodies against the FLAG or V5 epitope tags. Interaction between FBXL5-V5 and IRP2-FLAG was observed as α-FLAG antibodies co-immunoprecipitate FBXL5-V5 (Figure III-8 left panel). As a negative control, V5-tagged FBXL5 was transfected into the parental (HEK) cell line. Immunoprecipitation with anti-FLAG M2 resin and subsequent immunoblotting revealed that FBXL5-V5 does not interact with the FLAG antibody or resin alone (Figure III-8 left panel). Next, to assess FBXL5 interaction with endogenous IRP2, extracts from HEK 293T cells stably expressing FLAG-tagged FBXL5 were immunoprecipitated with anti-FLAG M2 resin. The anti-FLAG resin precipitated IRP2 from HEK FBXL5-FLAG cells but not from the control

parental cell line (Figure III-8 right panel). These results indicate that FBXL5 associates with IRP2.

Section IIIC - SCF ^{FBXL5} Polyubiquitinates IRP2 *in vitro*

To investigate whether the interaction between FBXL5 and IRP2 in co-immunoprecipitation assays reflects an E3 ligase:substrate relationship, recombinant SCF ^{FBXL5} was prepared. Coexpression of FLAG-tagged FBXL5 with untagged SKP1, CUL1, and RBX1 in insect cells followed by FLAG affinity purification results in co-purification of SCF^{FBXL5} complex components as assessed by Western blot analysis (Figure III-9, left). An FBXL5 variant lacking the F-box domain does not assemble a SCF complex (Figure III-9, right). Interestingly, the CUL1 protein that copurifies with FBXL5 has a larger apparent molecular weight than the majority of overexpressed CUL1 in the input lysate, possibly due to preferential association of neddylated CUL1 in SCF complexes (Bornstein et al., 2006; Wu et al., 2000). Immunoblotting these fractions with a monoclonal anti-human Nedd-8 antibody supports this hypothesis, as a cross reacting band at the approximate size is only present in the wild type FBXL5 FLAG immunoprecipitates (data not shown). However, the specificity of this antibody to Nedd8 in these samples is questionable.

FLAG-affinity purified fractions were then tested for E3 ligase activity. FLAG-affinity purified SCF^{FBXL5}, but not ΔF-box variant has ubiquitination

activity (Figure III-10). This activity is dependent on E1, E2, ATP, and ubiquitin. Parallel reactions were carried out with K_0-GST-Ub (discussed below) to show a laddering pattern distinct from that of unmodified ubiquitin (Figure III-11). Interestingly, when these reactions were incubated with cytosolic extract, activity was increased suggesting the presence of an enhancing factor.

To further purify the SCF complex, FLAG-purified SCF^{FBXL5} was subjected to an additional gel filtration chromatography step (Figure III-12). The peak fraction (SCF) contained roughly stoichiometric amounts of each SCF^{FBXL5} component as observed in a silver-stained SDS-polyacrylamide gel (Figure III-13). Purified SCF^{FBXL5} is able to ubiquitinate recombinant IRP2 *in vitro* only when supplemented with purified E1 and E2 (UbcH5a) enzymes, ATP as an energy source, and ubiquitin (Ub) (Figure III-14). Addition of excess iron (50 μM ferrous sulfate) had no effect on the observed activity (Figure III-14). As further evidence of *in vitro* ubiquitination, a laddering pattern observed for IRP2 in the presence of wildtype ubiquitin, indicative of polyubiquitination (Figure III-14), differed in reactions performed with GST-tagged ubiquitin lacking lysines, and thus unable to form polyubiquitin chains (K_0-GST-Ub). Here, a smaller number of discrete product bands were observed, consistent with mono-GST-ubiquitination of several IRP2 lysines (Figure III-15). Furthermore, with tubulin as a substrate in parallel reactions, no ubiquitination activity was observed, suggesting that SCF^{FBXL5} is not simply promiscuous *in vitro* (Figures

III-16 and 17).

Section IIID - FBXL5 Protein Accumulation is Regulated by Iron and Oxygen Availability

The lack of an effect of iron on SCF^{FBXL5} *in vitro* ubiquitination activity suggests that iron dependent activity occurs at a step prior to substrate binding and ubiquitination by an assembled SCF^{FBXL5} complex. One such step is the level of FBXL5 protein present in cells *i.e.* in a steady state, SCF^{FBXL5} activity in cells is proportional to the amount of FBXL5 protein. To determine if FBXL5 levels are regulated by iron, we treated HEK FBXL5-FLAG cell lines with either DFO or FAC and examined the lysates by Western blot analysis. These data revealed that FBXL5-FLAG protein levels are low when iron is limiting but increase dramatically under iron replete conditions (Figure III-18). To determine whether endogenous FBXL5 protein accumulation levels are likewise regulated as a function of iron availability, IRP2 and FBXL5 levels were examined in the parental and Tet-inducible FBXL5 shRNA cell lines. Endogenous FBXL5 could only be detected from HEK 293 cells by immunoprecipitating with rabbit polyclonal antibodies raised against bacterially expressed full length FBXL5 followed by Western blot analysis using a goat polyclonal α-FBXL5 antibody. As was observed for the stably transfected FBXL5-FLAG protein, endogenous FBXL5 accumulates under iron replete conditions but is substantially lower when iron is limiting (Figure III-19). RNAi-mediated knockdown of FBXL5 expression

using the Tet-inducible shRNA cells confirmed that the product detected by immunoblotting was FBXL5 (Figure III-19). These data suggest that iron-dependent regulation of IRP2 may be conferred through changes in FBXL5 accumulation.

To determine whether iron-dependent FBXL5 protein regulation occurred on a time scale relevant to IRP2 responses, HEK FBXL5-FLAG cells were incubated overnight with either DFO or FAC then switched to high or low iron conditions, respectively, and harvested 1, 2, 4, or 6 hours later. Consistent with IRP2's reported half-life (Guo et al., 1995), endogenous IRP2 protein levels fully accumulate within six hours following iron deprivation and conversely drop within six hours after addition of excess iron. FBXL5-FLAG protein levels are inversely regulated over the same period (Figure III-20).

Many F-box proteins are themselves regulated at the level of protein stability via ubiquitin mediated proteasomal degradation (Jin et al., 2004; Yen and Elledge, 2008). To test whether FBXL5 is regulated by proteasomal degradation, HEK FBXL5-FLAG cells were incubated with the proteasome inhibitor MG132 or vehicle alone (DMSO) prior to addition of either DFO or FAC for an additional six hours. MG132 treatment resulted in increased accumulation of FBXL5-FLAG under both conditions (Figure III-18). Because endogenous FBXL5 mRNA levels do not change significantly as a function of iron (Figure III-7) and iron-dependent regulation of exogenous FBXL5-FLAG does not require elements from the

FBXL5 promoter or UTRs, these data indicate that FBXL5 is post-translationally regulated in an iron-dependent manner.

IRP2 is regulated not only in response to iron but also O_2 availability as IRP2 accumulates under hypoxic conditions even when iron levels are high (Hanson et al., 2003). To test whether FBXL5 protein accumulation is affected by O_2 availability, HEK FBXL5-FLAG cells were grown in iron replete conditions under normoxia or hypoxia (1% O_2). FBXL5-FLAG levels from iron replete cells were substantially lower when grown under hypoxia (Figure III-21). These data suggest that both iron- and O_2-dependent regulation of IRP2 are mediated by reciprocal effects on the stability of the IRP2 E3 ligase component, FBXL5.

Section IIIE - The N-Terminal Domain of FBXL5 Confers Iron- and O_2-Dependent Regulation

Human FBXL5 is 691 amino acids in length and contains multiple protein domains in addition to the defining F-box, including two series of leucine rich repeat (LRR) regions, comprised of at least three putative LRRs elements each (Appendix). LRRs frequently promote protein-protein interactions and may act to bind substrates (Jin et al., 2004). Between the two series of LRRs is a region we termed the Cys-rich region due to the high number of conserved cysteine residues found among the vertebrate homologs. FBXL5 also contains a highly conserved

N-terminus. To identify the region of FBXL5 that confers iron-dependent regulation, a series of V5 epitope tagged FBXL5 deletion mutants (Figure III-22) were transfected into HEK 293T cells followed by incubation with DFO or FAC. As observed for the full length (FL) protein, all but one deletion construct showed preferential accumulation under conditions of excess iron. In contrast, the FBXL5 ΔNterm protein accumulated at constitutively high levels under both conditions (Figure III-23). Additional deletion analysis demonstrated that residues 162-197 of FBXL5 were not required for normal iron regulation (data not shown). Moreover, expression of residues 1-161 of FBXL5 demonstrated that this region was sufficient for iron-dependent regulation (Figure III-24).

To determine whether the hemerythrin (Hr) domain of FBXL5 could target a heterologous protein for iron- and O_2-dependent regulation, HEK 293T cells were transfected with FLAG tagged constructs consisting of the domain fused to either the N-terminus (Hr-Luc) or C-terminus (Luc-Hr) of firefly luciferase. While luciferase (Luc) activity measured from cellular lysates was unaffected by iron availability, both Hr-Luc (~2.5x) and Luc-Hr (~2.0x) luciferase activities were higher in lysates from FAC treated cells (Figure III-25). Relative luciferase activity correlated with changes in fusion protein accumulation. Incubation under hypoxic conditions also blocks fusion protein accumulation and luciferase activity under iron-replete conditions while having no effect on the Luc

control (Figure III-25). These results suggest that the FBXL5 hemerythrin domain is sufficient to confer iron- and O_2-dependent regulation.

Section IIIF - The FBXL5 N-Terminus Encodes an Iron-Binding Hemerythrin Domain

PSI-BLAST searches (Altschul et al., 1997) with FBXL5 residues 1 to 200 identified the sequences of two protein structures that form a hemerythrin-like four helix up and down bundle with an additional C-terminal helix that packs against the core. A multiple sequence alignment between the FBXL5 sequences, the PSI-BLAST identified structures (2p0n and 3cax), and the next closest hemerythrin-like structures (2avk and 1hmo) was generated with PROMALS-3D (Pei et al., 2008) and manually adjusted based on alignments generated with two sensitive sequence-based structure recognition methods, COMPASS (Sadreyev and Grishin, 2003) and HHPRED (Soding et al., 2005). As shown in Figure III-26, the FBXL5 N-terminus is predicted to contain five conserved alpha-helices with several key conserved residues (see Appendix for alignment).

Proteins containing hemerythrin domains were first identified in marine invertebrates and more recently found in bacteria (French et al., 2008). Structural studies of several hemerythrins demonstrate that these alpha-helical bundles bind metals, frequently iron, through the imidazole and carboxylate groups of amino acid side chains (Stenkamp, 1994) (Figure III-27). The diiron centers of

hemerythrins can in turn reversibly bind oxygen and can function as O_2-transport proteins, oxygen sensors, and metal storage depots (French et al., 2008). As compared to known hemerythrins (Holmes et al., 1991; Isaza et al., 2006), the FBXL5 family retains six out of seven invariant Fe-binding ligands. Typically, five histidine residues from hemerythrin form a diiron site buried within the helix bundle, with three coordinating one Fe (two of which correspond to FBXL5 H80 and H126) and two coordinating a second Fe (corresponding FBXL5 H15 and H57). Two hemerythrin carboxylates (corresponding to FBXL5 E61 and E130) bridge the irons. Structural modeling suggests that an invariant FBXL5 carboxylate residue (likely either E58 or E131) acts as the third ligand coordinating one Fe (data not shown).

To investigate the prediction that the N-terminus of FBXL5 encodes a functional hemerythrin domain, residues 1-161 were recombinantly expressed and purified from *E. coli* (Figure III-28). The wildtype (WT) FBXL5 hemerythrin domain copurified with iron as assessed using the iron detecting reagent ferene (Figure III-29). The molar ratio of iron to FBXL5 in these preparations was calculated to be 1.1:1.0, suggesting approximately half of the protein contained a diiron center. Mutation of one of the conserved bridging carboxylates (E61A) was sufficient to abolish iron binding (Figure III-29). UV-VIS absorption spectra for ferene bound to iron liberated from the hemerythrin domain showed a uniform peak with a maximum at 593 nm that was insensitive to the addition of the

copper-specific chelator thiourea (data not shown), characteristic of iron bound to ferene (Hennessy et al., 1984).

The iron atoms present in diiron μ-oxo centers have d-orbital electrons with small energy gaps between their Highest Occupied Molecular Orbital (HOMO) and Lowest Unoccupied Molecular Orbital (LUMO). As a result, diiron centers are able to absorb light in the UV-Visible spectrum (Kurtz, 1990). Moreover, the UV-visible spectrum of hemerythins have characteristic absorbances that change as a function of the oxidation state of the diiron center (Zhang and Kurtz, 1992; Zhang et al., 1991). Therefore, to verify that FBXL5's hemerythrin domain forms a diiron μ-oxo center, we measured the UV-Visible absorbance spectra of FBXL5's hemerythrin domain. Spectra of the WT Hr domain in the absence of reducing agent show a broad absorbance peak around 330nm (Figure III-30), characteristic of oxidized diiron μ-oxo centers within hemerythrins (Zhang et al., 1991). Notably, this absorption decreases upon reduction with dithionite to remove oxygen (Figure III-30). The effect of oxygen concentrations were also investigated on the UV-VIS absorbance of FBXL5's diiron center (Figure III-31). Here, the absorbance of the diiron center decreased after the Hr domain was reduced and equilibriated in an anaerobic chamber. The absorbance increased upon equilibriation with ambient oxygen, which corresponds with previous reports that the diiron absorbance increases upon oxygen binding. Taken together, these data suggest that the iron bound to

FBXL5's Hr domain has features consistent a diiron μ-oxo center that can bind oxygen.

Circular dichroism (CD) spectrometry shows that the WT domain has significant alpha helical content with minima at 207 and 222nm (Greenfield, 2006). In contrast, the spectrum of the E61A mutant that is unable to bind iron is indicative of an unstructured protein (Figure III-32). Treatment of the WT domain with dithionite ($Na_2S_2O_4$) to remove O_2 had little effect on the helical content, though subsequent addition of an iron chelator (*o*-phenanthroline) induced a partial loss of helical structure as indicated by a decrease in molar ellipticity (Figure III-33) (Zhang and Kurtz, 1992). Structural changes were less severe when chelator was added without prior addition of dithionite (Figure III-34) suggesting that in the oxidized state, iron is less susceptible to removal perhaps consistent with observations of shorter bond distances between Fe(III) and protein in oxyhemerythrin as compared with Fe(II)-protein bond lengths in the deoxy-state (Stenkamp, 1994). Thermal denaturation experiments (Figure III-35) revealed that treatment of the hemerythrin domain with dithionite and *o*-phenanthroline lowers both the T_m and cooperativity of unfolding, indicating these reagents destabilize the tertiary fold of the domain (Greenfield, 2006). Together, these results confirm that the FBXL5 N-terminus can fold into an alpha helical-rich structure capable of binding both iron and oxygen, consistent with predictions that this region encodes a hemerythrin domain.

Section IIIG – A Preliminary X-Ray Crystal Structure of FBXL5's Hr Domain at 1.8 Angstroms

To complement spectroscopic studies of the isolated recombinant FBXL5-Hr domain, an X-Ray crystal structure of FBXL5's Hr domain was obtained. For this finding, the Hr domain of FBXL5 was purified in a strategy outlined in the Appendix, and individual plate crystals were grown and isolated as described in the methods. Diffraction data were collected by Chad Brautigam and the structure was solved by Diana Tomchick (Structural Biology Laboratory core facility, UT Southwestern) statistics for the initial model are described in the Appendix.

The structure of FBXL5's Hr domain correlates well with its predicted structure (Figure III-26). As shown in Figure III-36, the Hr domain is composed of four alpha helices forming a hydrophobic core, with a fifth helix packing against the bundle. Interestingly the third helix is disrupted in sequences flanking a residue that coordinates the hexacoordinate iron (Figure III-36).

Electron density within the hydrophobic core corresponds to a diiron μ-oxo center, with one iron atom being hexacoordinate and the other iron atom being pentacoordinate (Figure III-37). This density was also recorded using anomalous scattering by data collection at the Fe inflection point (Appendix). The pentacoordinate iron in this structure would canonically serve as the oxygen binding site within a hemerythrin. However, no ordered electron density

corresponding to oxygen was observed in this model. This is somewhat surprising, since crystals were grown in ambient oxygen concentrations, which is sufficient to obtain crystals of oxy-hemerythrin in previous reports (Holmes et al., 1991) and were also sufficient to cause a change in the UV-Visible spectrum of FBXL5's Hr domain. One explanation, though, is that reducing agent was included as an additive in crystallization conditions (4mM 2-ME, 0.5mM TCEP) and could have kept the diiron center in the 2+ state, greatly reducing oxygen affinity.

Examination of the amino acid side chains responsible for coordinating iron shows that FBXL5's Hr domain largely follows the scheme previously observed in hemerythrins (Figure III-37). The X-ray crystal structure, however, does not provide the identity of the final iron binding residue of the hexacoordinate iron, since the electron density proximal to this ligand's position is poorly defined. Furthermore, the third helix where this amino acid resides (residues 67-84) is unstructured, preventing deduction of the identity of the sixth binding residue. One way to overcome these limitations would be to obtain the structure of FBXL5's Hr domain when it is bound to oxygen (discussed in Chapter IV). Additionally, data in cell culture show that in low oxygen concentrations, FBXL5's Hr domain is destabilized (Figure III-21). How oxygen binding mediates increased stability of FBXL5's Hr domain is further discussed in chapter IV.

Section IIIH - Summary

A unifying hypothesis to combine the data presented in Sections IIIA-IIIH, is that in the folded iron-bound state, a degron is sequestered within the hemerythrin fold, inaccessible to an E3 ubiquitin ligase that targets FBXL5 for degradation (Figure III-38). Under these iron replete conditions, FBXL5 accumulates and assembles into a SCF^{FBXL5} E3 ligase complex. If the hemerythrin domain is unable to assemble a diiron center (*e.g.* iron deficient conditions), the domain unfolds to reveal a degron for an as-yet unidentified ubiquitin ligase. Degradation of FBXL5 precludes the assembly of a SCF complex allowing IRP2 to accumulate and bind IREs. Similarly, O_2 binding is predicted to further stabilize the hemerythrin helical bundle, while hypoxic conditions that favor the less stable deoxyhemerythrin state render the hemerythrin switch more susceptible to proteasomal degradation. Consistent with this model, small N-terminal deletions compromise the ability of the hemerythrin domain to fold in the presence of iron. Thus, unregulated exposure of the degron disrupts iron dependent regulation and leads to constitutively low levels of protein accumulation (Figure III-39). Likewise, point mutations to the iron-binding ligands observed in our crystal structure cause FBXL5 to accumulate at low levels, consistent with an iron-insensitive unfolded hemerythrin domain (Figure III-40). However, larger deletions of the FBXL5 N-terminus eventually remove

the putative degron resulting in constitutively high levels of FBXL5 accumulation in an iron-independent manner (Figure III-39).

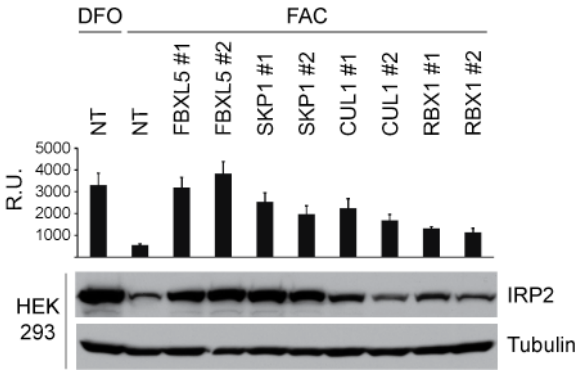

Figure III-1.

Courtesy of Joel Thompson. Stabilization of IRPs under iron-replete conditions following RNAi-mediated suppression of SCF^{FBXL5} using the AlphaScreen assay (top), and by Western blot analysis of endogenous IRP2 in HEK 293 cells (bottom).

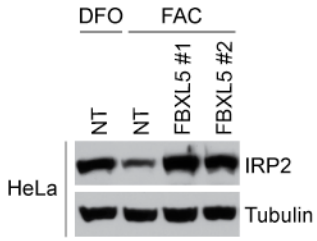

Figure III-2.

Courtesy of Joel Thompson. Stabilization of IRP2 under iron-replete conditions following RNAi-mediated suppression of SCF^{FBXL5} by Western blot analysis of endogenous IRP2 in HeLa cells.

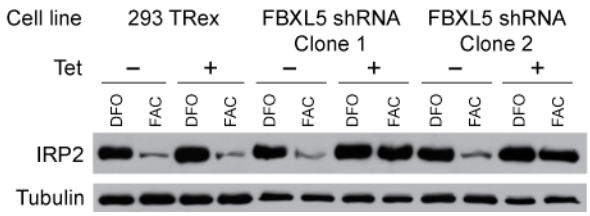

Figure III-3.

Stabilization of endogenous IRP2 under iron-replete conditions following RNAi-mediated suppression of SCF^{FBXL5} using shRNA inducible HEK293 TRex cells.

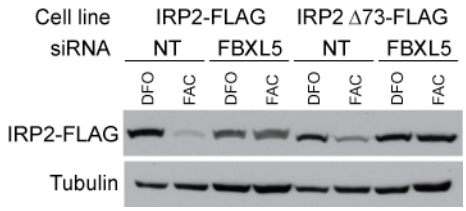

Figure III-4.

Courtesy of Joel Thompson. Stabilization of IRP2 under iron-replete conditions following RNAi-mediated suppression of SCF^{FBXL5} using western blot analysis of stably-transfected tagged IRP2 constructs.

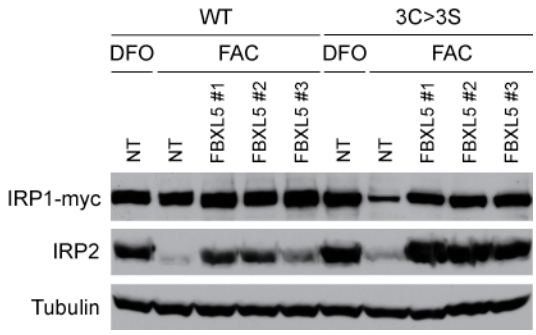

Figure III-5.

Courtesy of Joel Thompson. Stabilization of IRP2 under iron-replete conditions following RNAi-mediated suppression of SCF^{FBXL5} using western blot analysis of stably-transfected tagged IRP2 constructs.

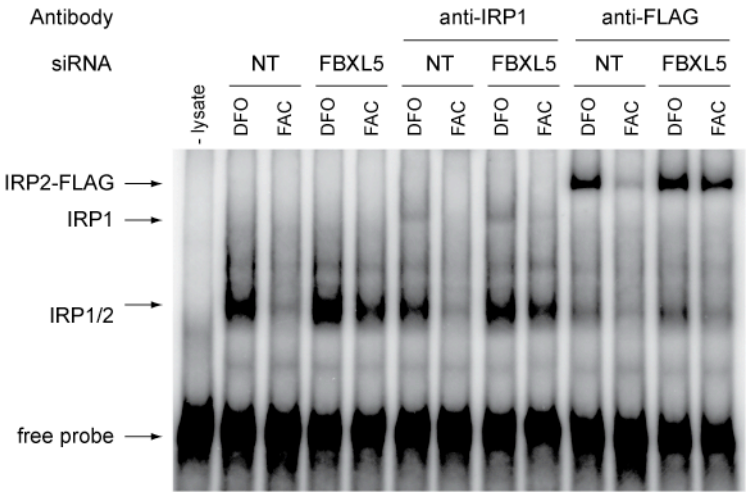

Figure III-6.

Courtesy of Joel Thompson. RNA-binding activity of IRP1 and IRP2 from cell lysates following siRNA-mediated suppression of *FBXL5* expression in HEK293 cells.

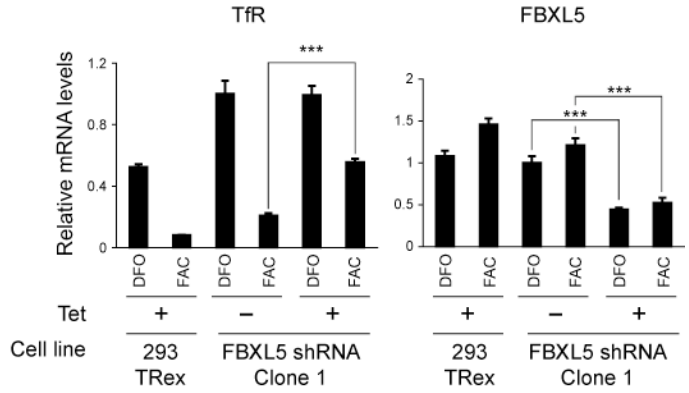

Figure III-7.

Relative TfR1 and FBXL5 mRNA accumulation levels. Values are expressed as the mean plus or minus the standard error. *** = p<.001 by Student's T-test.

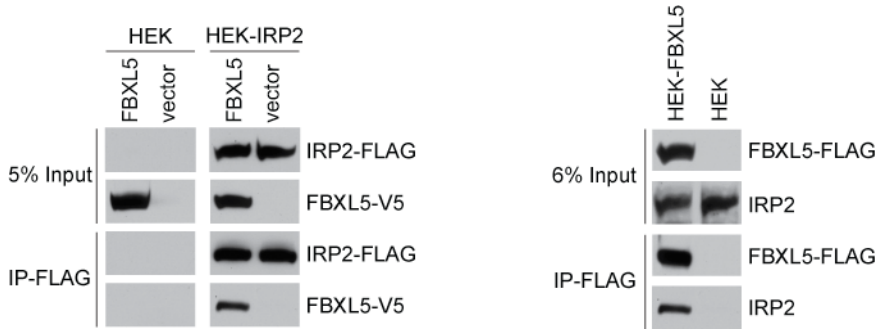

Figure III-8.

Courtesy of Joel Thompson. Co-immunoprecipitation of FBXL5-V5 and FLAG-IRP2-FLAG (left) or endogenous IRP2 and FBXL5-FLAG following FLAG immunoprecipitation of lysates from transfected HEK 293 cells (right).

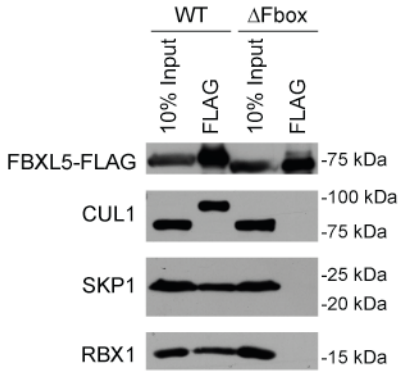

Figure III-9.

Western blot analysis of FLAG immunoprecipitates from insect cells co-expressing SKP1, CUL1, and RBX1 with either full length FLAG-FBXL5, or FLAG-FBXL5 lacking the F-box domain.

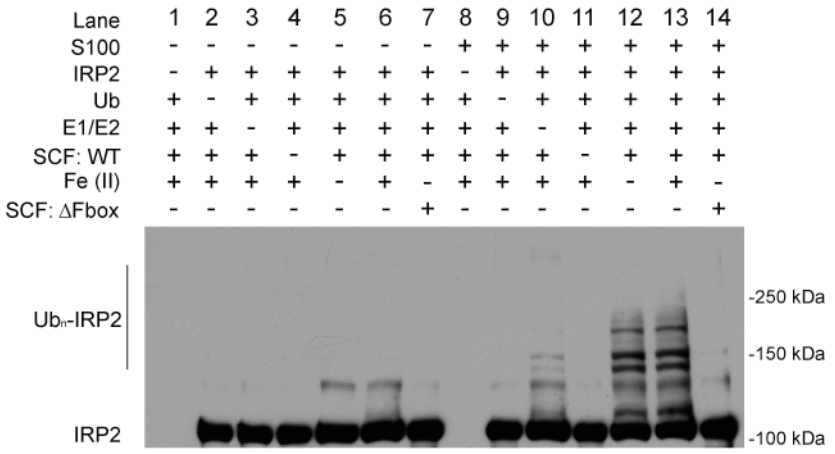

Figure III-10.

Recombinant SCF^{FBXL5} ubiquitinates IRP2 in *in vitro* assays containing wildtype ubiquitin.

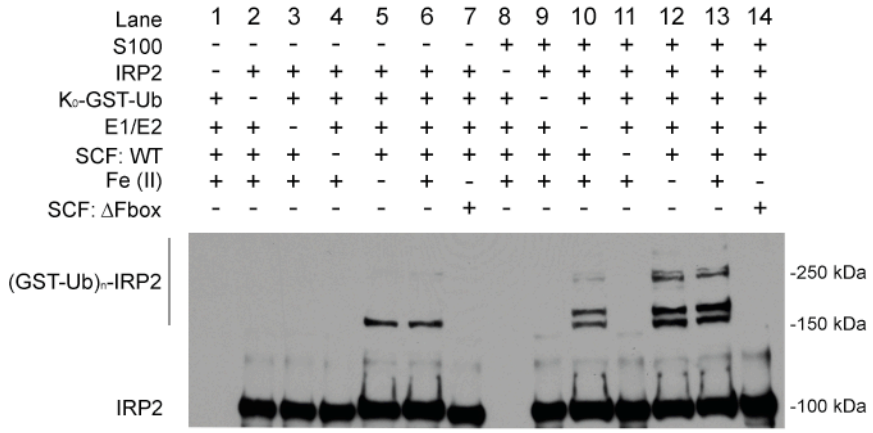

Figure III-11.

Recombinant SCF^{FBXL5} ubiquitinates IRP2 in *in vitro* assays containing GST-tagged ubiquitin lacking lysines (K_0).

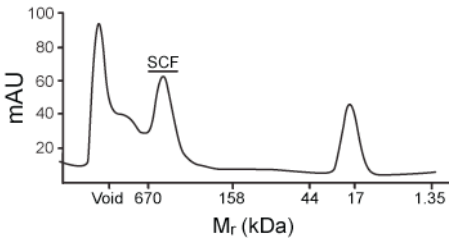

Figure III-12.

UV-chromatogram of the peak fraction (SCF) from a Superdex-200 gel-filtration column loaded with FLAG-purified SCF^{FBXL5}

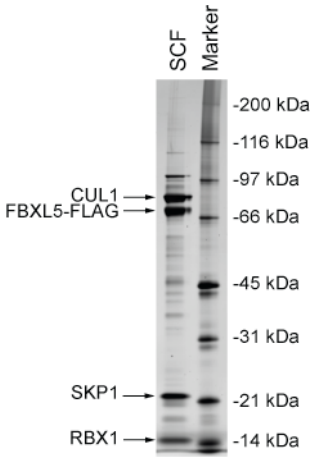

Figure III-13.

Silver stain of the peak fraction (SCF) from a Superdex-200 gel-filtration column loaded with FLAG-purified SCF^{FBXL5}

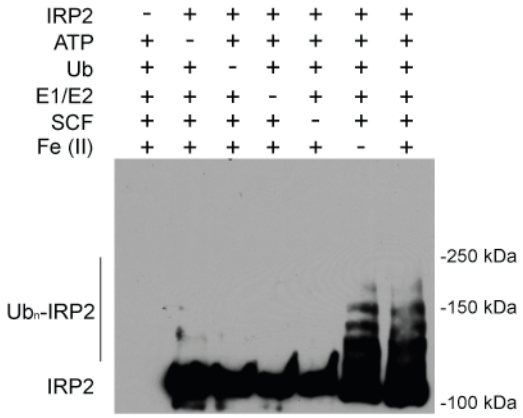

Figure III-14.

Recombinant and size exclusion purified SCF^{FBXL5} ubiquitinates IRP2 in *in vitro* assays containing wildtype ubiquitin.

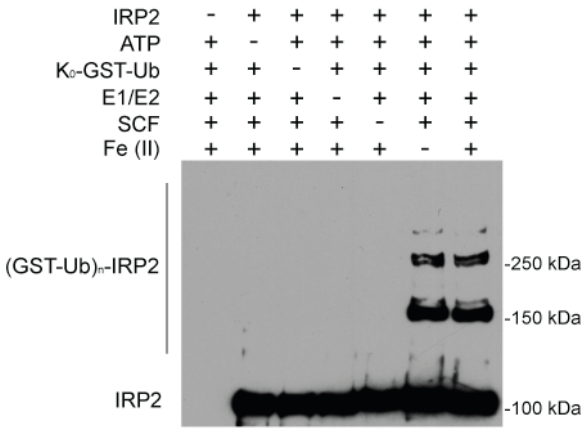

Figure III-15.

Recombinant and size exclusion purified SCF^{FBXL5} ubiquitinates IRP2 in *in vitro* assays containing GST-tagged ubiquitin lacking lysines (K_0).

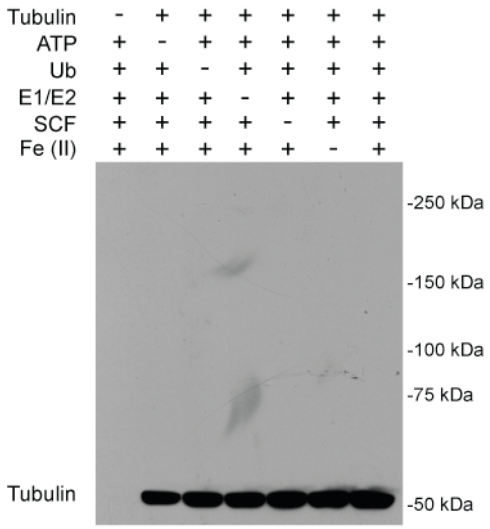

Figure III-16.

Recombinant SCF^{FBXL5} does not ubiquitinate tubulin *in vitro*. Reactions were carried out in an identical manner to those in Figure III-14, except tubulin was used as a substrate instead of IRP2.

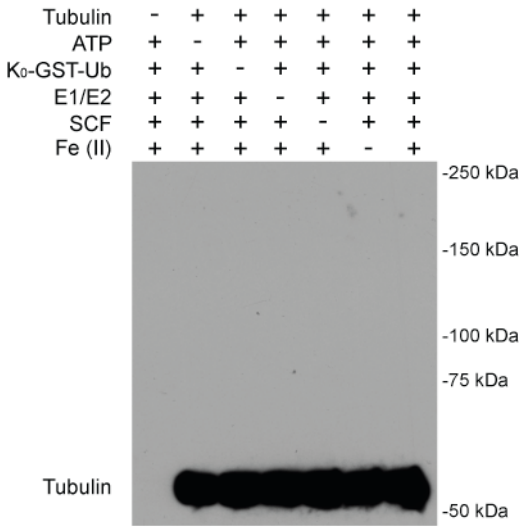

Figure III-17.

Recombinant SCF^{FBXL5} does not ubiquitinate tubulin *in vitro*. Reactions were carried out in an identical manner to those in Figure III-15, except tubulin was used as a substrate instead of IRP2.

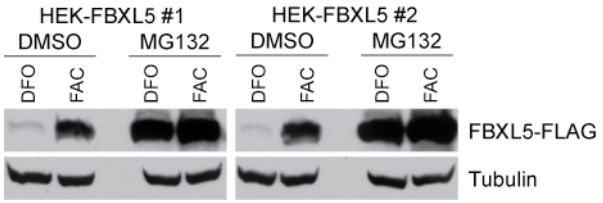

Figure III-18.

Courtesy of Joel Thompson. Assessment of FBXL5 protein accumulation under iron-deplete (DFO) or iron-replete (FAC) conditions by Western blot analysis of stably-transfected FBXL5-FLAG.

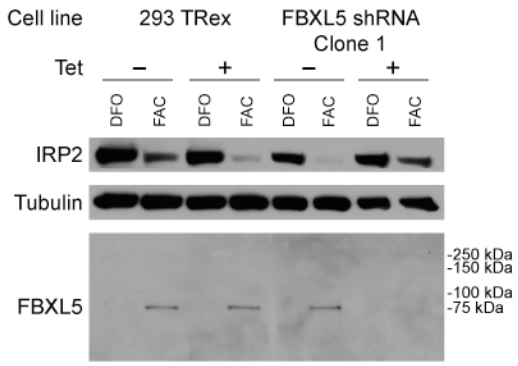

Figure III-19.

Assessment of FBXL5 protein accumulation under iron-deplete (DFO) or iron-replete (FAC) conditions by Western blot analysis of endogenous FBXL5.

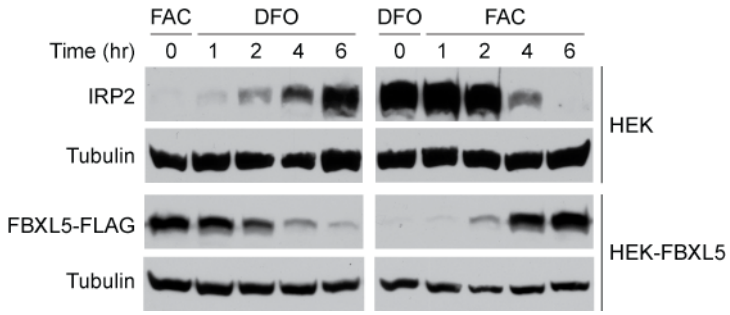

Figure III-20.

Courtesy of Joel Thompson. Assessment of FBXL5 protein accumulation under iron-deplete (DFO) or iron-replete (FAC) conditions by Western blot analysis of stably-transfected FBXL5-FLAG.

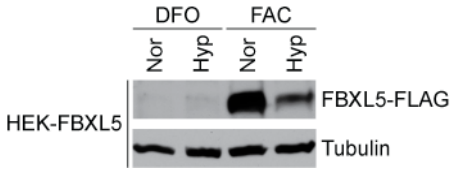

Figure III-21.

Courtesy of Joel Thompson. Assessment of FBXL5 protein accumulation under iron-deplete (DFO) or iron-replete (FAC) conditions by Western blot analysis of stably-transfected FBXL5-FLAG. Nor = normoxia = 20% Oxygen. Hyp = hypoxia = 1% Oxygen.

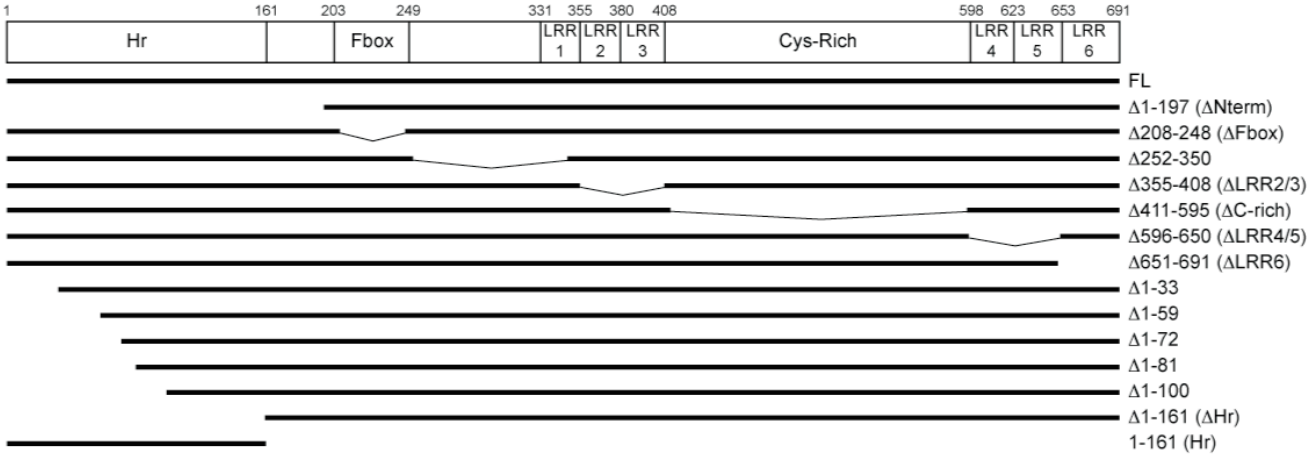

Figure III-22. Schematic of FBXL5 deletion constructs. Human FBXL5 is 691 amino acids in length and contains multiple protein domains in addition to the defining F-box, including two series of leucine rich repeat (LRR) regions, comprised of at least three putative LRRs elements each. Between the two series of LRRs is a region we termed the Cys-rich region due to the high number of conserved cysteine residues found among the vertebrate homologs. FBXL5 also contains a highly conserved N-terminus (Hr).

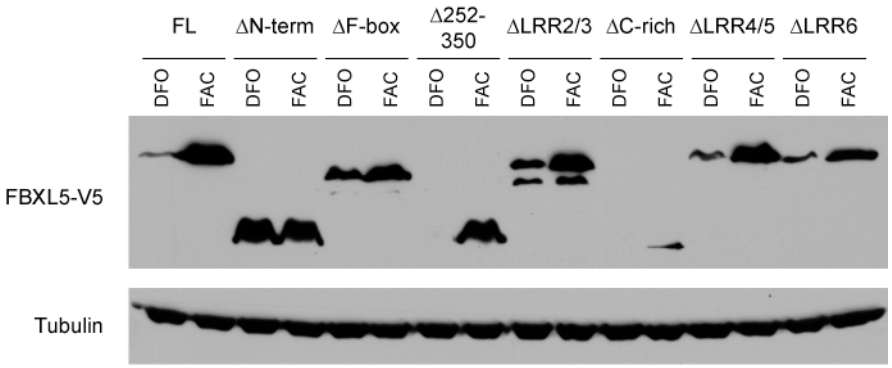

Figure III-23.

Courtesy of Joel Thompson. Assessment of FBXL5 protein accumulation under iron-deplete (DFO) or iron-replete (FAC) conditions by Western blot analysis of transiently-transfected FBXL5 deletion constructs. Tubulin, loading control.

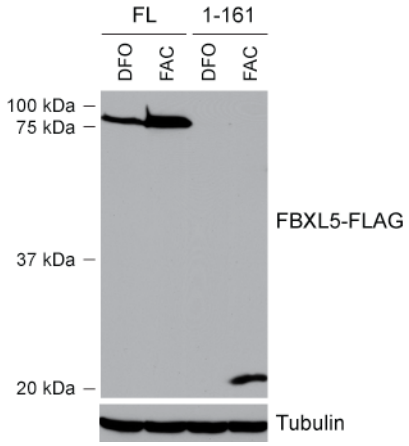

Figure III-24.

Courtesy of Joel Thompson. Assessment of FBXL5 protein accumulation under iron-deplete (DFO) or iron-replete (FAC) conditions by Western blot analysis of transiently-transfected FBXL5 deletion constructs. Tubulin, loading control.

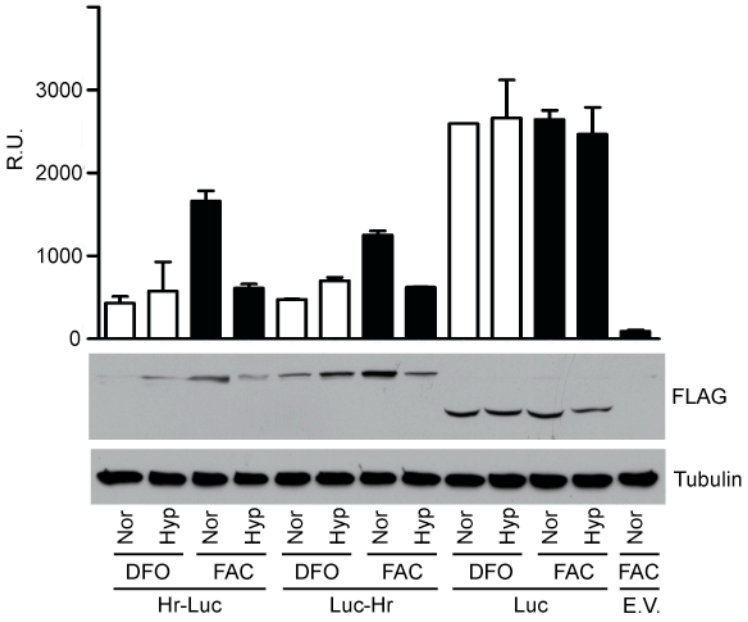

Figure III-25.

Courtesy of Julio Ruiz. Luciferase activity (upper panels) and protein accumulation levels (lower panels) in HEK 293 cells transiently transfected with FBXL5 Hemerythrin (Hr)-luciferase (Luc) fusion constructs. Tubulin, loading control.

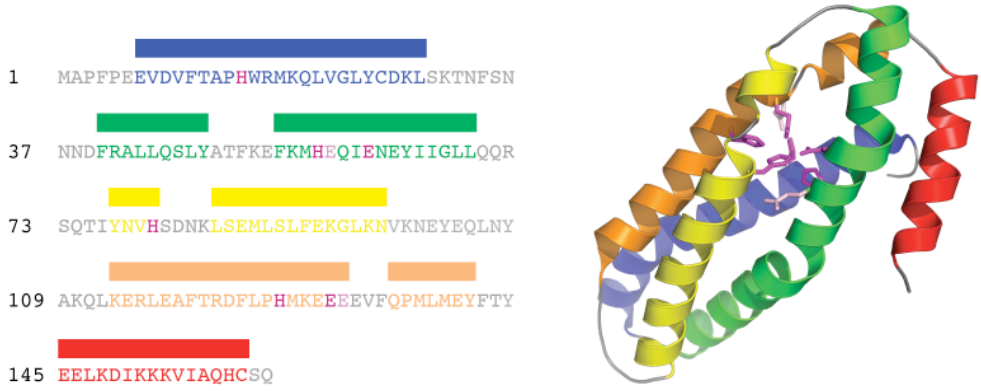

Figure III-26.

Courtesy of Lisa Kinch. Schematic of the predicted alpha helices (bars) and iron binding ligands (magenta) in the FBXL5 Hr domain. Helical bounds for FBXL5 were determined by combining information from helices observed in Hr structures and FBXL5 helices predicted from sequence alignments (left). (right) Model of the FBXL5 hemerythrin domain mapped upon a solved hemerythrin structure (2p0n).

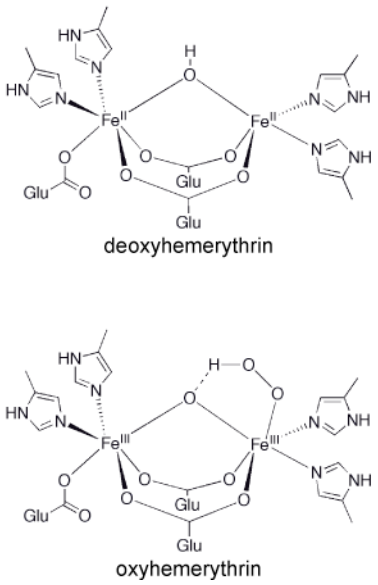

Figure III-27.

Model of FBXL5's predicted oxy- and deoxyhemerythrin diiron center.

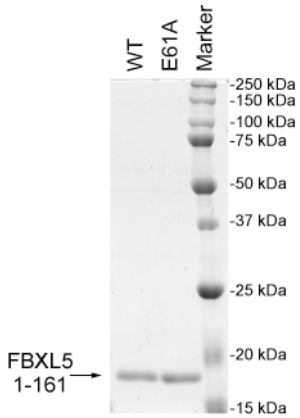

Figure III-28.

Coomassie blue staining of recombinantly expressed and purified wildtype (WT) and variant (E61A) FBXL5 hemerythrin domain.

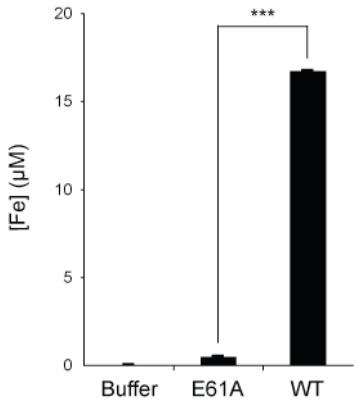

Figure III-29.

Iron content of recombinantly expressed and purified wildtype (WT) and variant (E61A) FBXL5 hemerythrin domain.

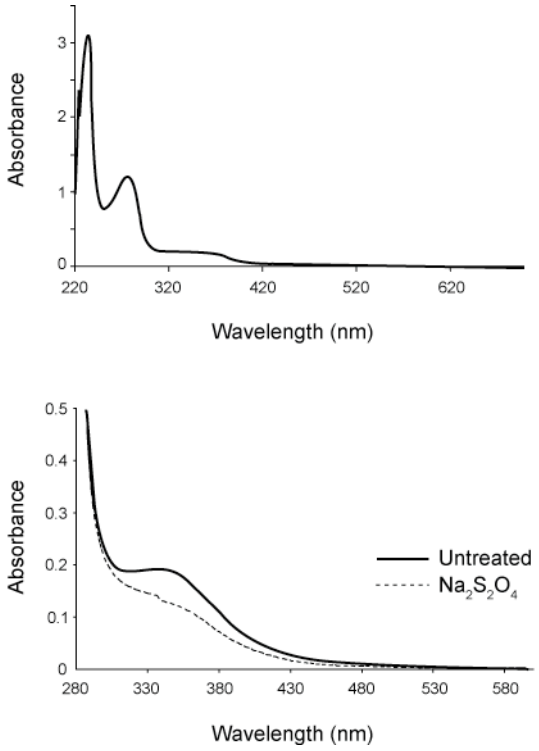

Figure III-30.
UV chromatogram of the WT FBXL5 Hr domain protein before and after dithionite addition

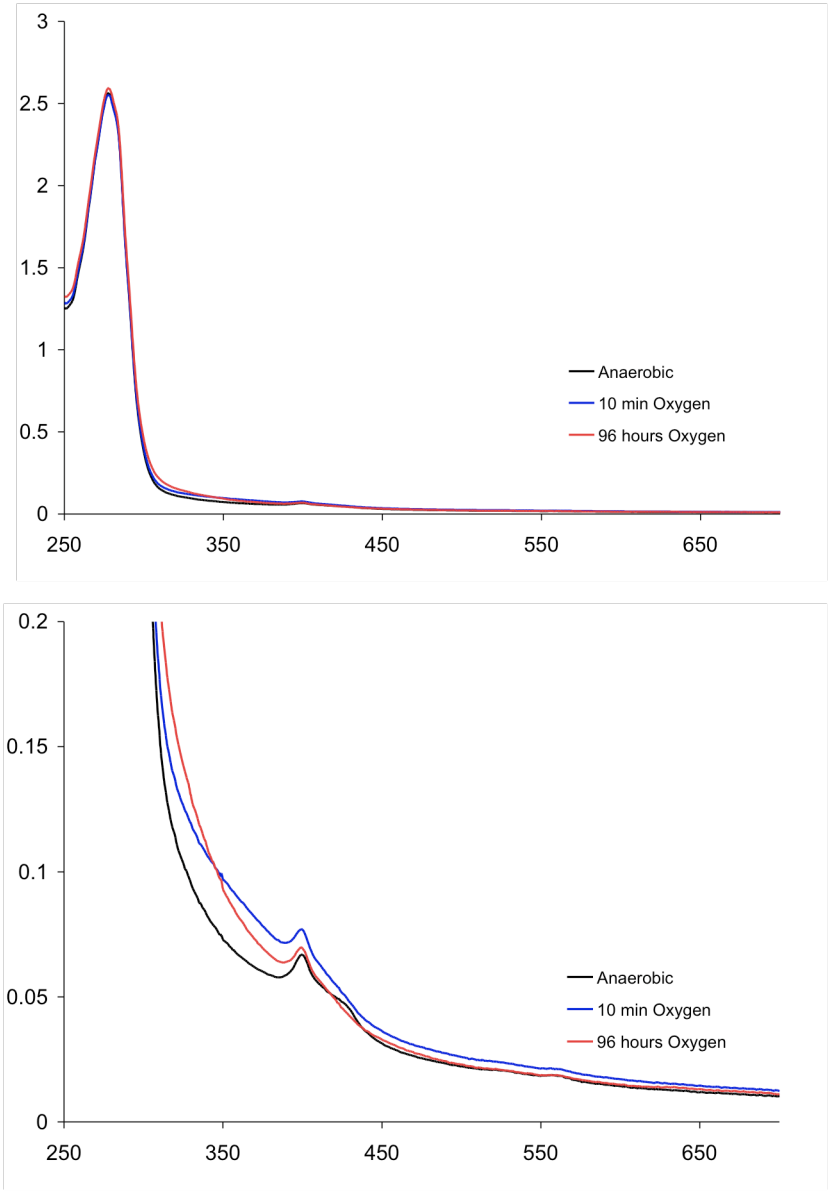

Figure III-31.

UV chromatogram of the WT FBXL5 Hr domain protein before and after exposure to oxygen subsequent to dithionite reduction and anaerobic incubation.

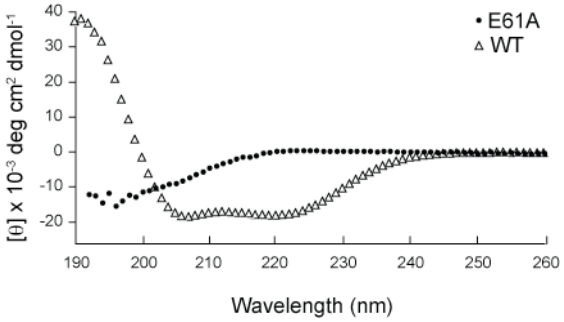

Figure III-32.

Circular Dichroism spectra of recombinantly expressed and purified wildtype (WT) and variant (E61A) FBXL5 hemerythrin domain.

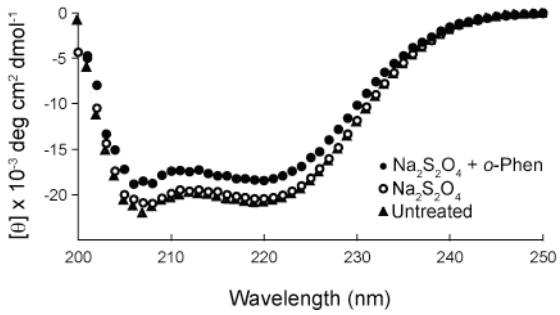

Figure III-33.

Circular Dichroism measurement of the WT Hr domain treated with dithionite, with and without iron chelator (*o*-Phen).

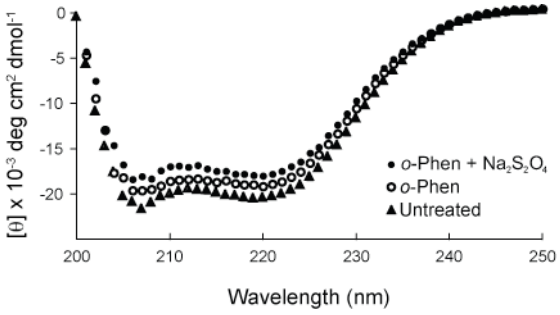

Figure III-34.

Circular Dichroism measurement of the WT Hr domain treated with iron chelator (*o*-Phen), with and without dithionite.

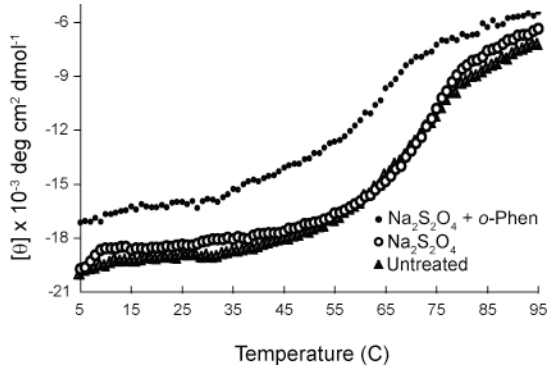

Figure III-35.

Circular Dichroism measurement of ellipticity at 222nm as a function of thermal denaturation of the WT Hr domain treated with dithionite with and without iron chelator (*o*-Phen).

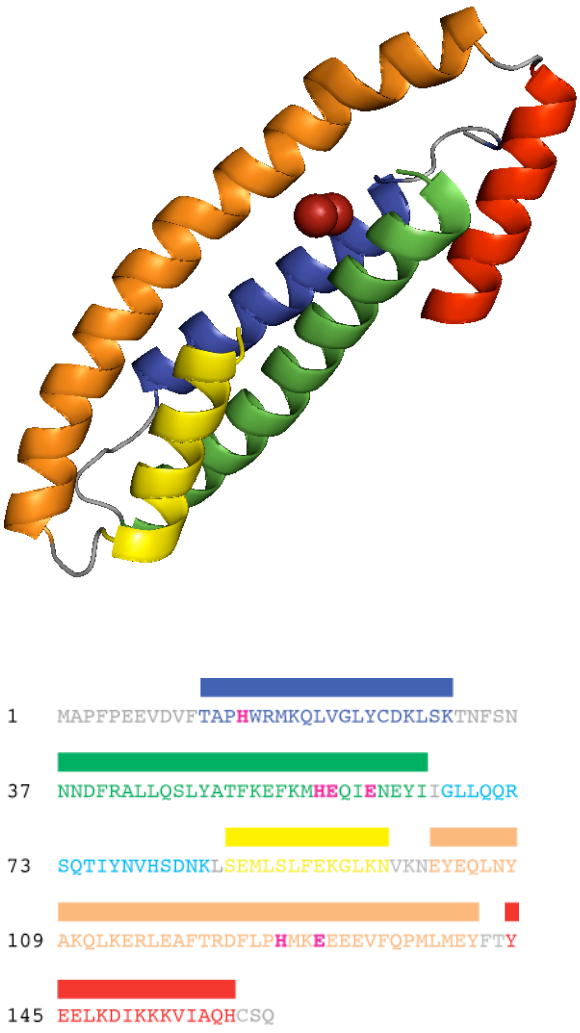

Figure III-36.

Initial model of the FBXL5 hemerythrin domain in the deoxy state. Boundaries of alpha helices are indicated by bars. Iron coordinating residues are (bridging, E61, E130; hexacoordinate iron, E58, H126; pentacoordinate iron, H15, H57) indicated in magenta. Unassigned amino acid residues are highlighted in cyan. The sixth coordinating ligand of the hexacoordinate iron lies within unassigned residues (cyan) and is potentially either N78 or H80.

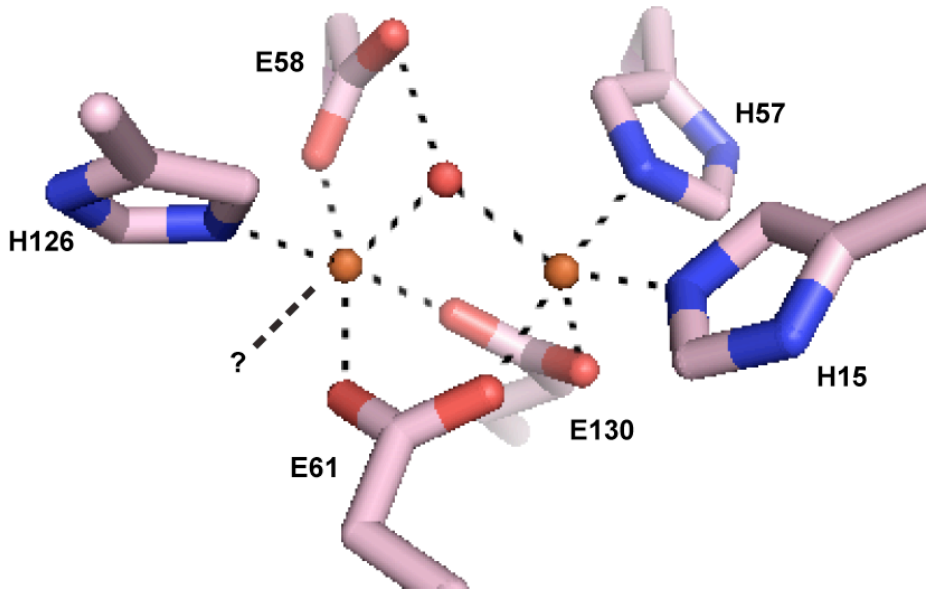

Figure III-37.

Initial model of the diiron site of FBXL5's hemerythrin domain. The missing sixth ligand for the hexacoordinate iron is marked as ?.

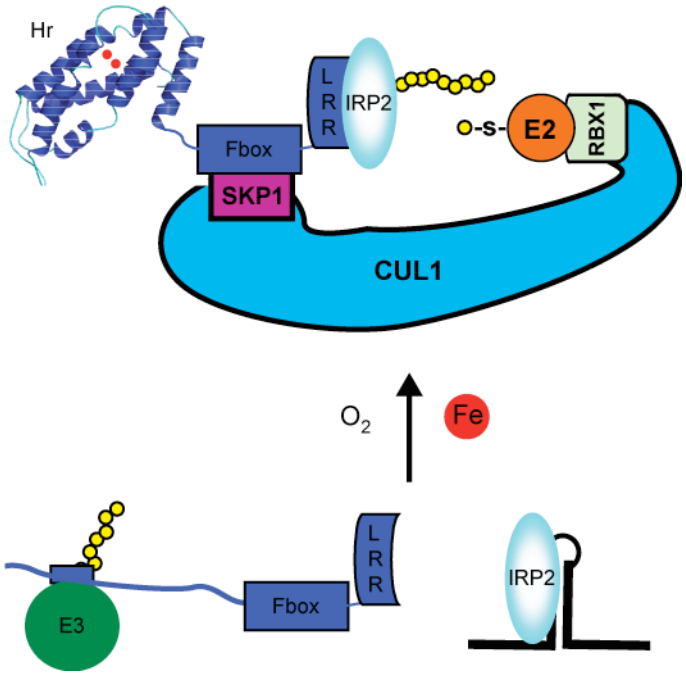

Figure III-38.

Model of FBXL5's role in mammalian iron homeostasis. In iron and oxygen deficient states, the hemerythrin domain of FBXL5 is unstructured, allowing for the exposure of an amino acid recognition element for an as yet unidentified E3 ligase. This putative E3 ligase mediates the ubiquitination (yellow circles) and degradation of FBXL5, resulting in increased IRP2 levels and regulation of IRE containing mRNAs. In iron and oxygen replete states, FBXL5 accumulates since the hemerythrin domain is able to fold and sequester the recognition element that targets it for degradation. FBXL5 then assembles into an SCF complex that targets IRP2 for ubiquitination and degradation.

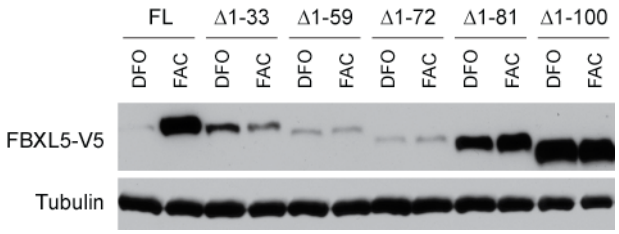

Figure III-39.

Courtesy of Joel Thompson. Immunoblots for V5 tagged FBXL5 N-terminal deletion constructs.

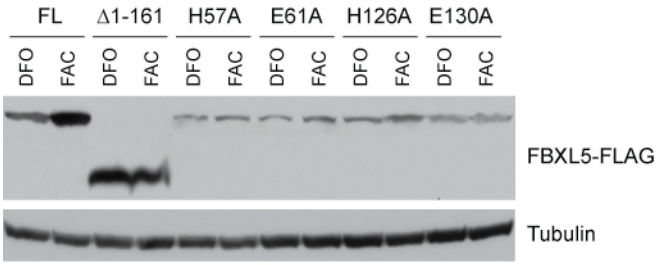

Figure III-40.

Courtesy of Joel Thompson. Assessment of FBXL5 protein accumulation under iron-deplete (DFO) or iron-replete (FAC) conditions by Western blot analysis of transiently-transfected FBXL5 mutation constructs. Tubulin, loading control.

Section III I- MATERIALS AND METHODS

Cell Culture and Reagents

Cell lines were grown in Dulbecco's Modified High Glucose Eagle Medium (HyClone). Tetracycline inducible cells were supplemented with 10% tetracycline-free fetal bovine serum (Clontech) while all other cells were supplemented with 10% fetal bovine serum (Atlanta Biologicals). Low (1%) O_2 incubations were carried out in a hypoxic chamber (Coy Laboratory Products). Transient transfections of plasmid DNA were carried out using Lipofectamine 2000 (Invitrogen) according to the manufacturer's instructions. Typically, $5x10^4$ cells were plated per well of a 24-well plate and incubated for 16 hr followed by transfection with 500 ng of DNA. Neomycin-resistant cells stably expressing epitope-tagged IRP2 or FBXL5 proteins were isolated over two rounds of clonal selection in the presence of 400 μg/mL G418 (Research Products Inc). IRP1 and $IRP1^{3C>3S}$ Flp-In T-Rex HEK 293 cells were kindly provided by R. Eisenstein.

FBXL5 shRNA knockdown cells were generated by stable transfection of HEK 293 TRex cells (Invitrogen) with pSuperior vector (Oligoengine) encoding the FBXL5 shRNA:

5′gaucccGCACAACACUGCUCUCAGAuucaagagaUCUGAGAGCAGUGUUG UGCuuuuua-3′. Individual cell lines were isolated over two rounds of clonal selection in the presence of 1 μg/mL puromycin (Sigma). FBXL5 shRNA

expression was induced upon addition of 1 μg/mL tetracycline hydrochloride (Sigma) to the culture medium for 72 hr.

RNAi

Transient transfections of siRNAs (Table III-1; Dharmacon) were carried out using Lipofectamine 2000 (Invitrogen) according to the manufacturer's instructions. Typically, $2x10^4$ cells were reverse transfected in 24-well plates with 20 pmoles siRNA duplex/well. Following 48 hr incubation, cells were treated with either 100 μM ferric ammonium citrate or 100 μM deferoxamine and incubated an additional 16 hr.

Plasmids

Human FBXL5 cDNA (NM_012161) was amplified from a human placenta cDNA library (kindly provided by C. Mendelson) using the oligonucleotides 5′-GGAGTCTAGAACCTTCGCCAGAGCGGCAGCAGG and 5′-GGAGGGATCCACCATGGCGCCCTTTCCTGAAGAAGTGGAC and cloned into the pcDNA3.1-V5 vector (Invitrogen). FBXL5 cDNA was subcloned into the pCI-FLAG vector (kindly provided by X. Wang) using the 5′GGAGGTCGACTCATTCGCCAGAGCGGCAGC and 5′-GGAGGGATCCACCATGGCGCCCTTTCCTGAAGAAGTGGAC

oligonucleotides. Human IRP2 was amplified from a human cDNA library using the oligonucleotides

5′-AATTGGATCCACCATGGACGCCCCAAAAGCAGGATAC and

5′-CCTCCTCTAGATGAGAATTTTCGTGCCACAAAG and cloned in frame with a C-terminal 3xFLAG epitope tag into the pcDNA3.1 vector. The oligonucleotide

5′TCGGATCCATGGCCGCCTACCCCTACGACGTGCCCGACTACGCCGGT

GACGCCCCAAAAGCAGG was used to incorporate an N-terminal HA tag. Where appropriate, the overlap extension PCR method was utilized to construct deletion and point mutants using oligonucleotides listed in Table III-2. Full length human IRP2 was cloned into the pPICZb vector (Invitrogen) in frame with C-terminal 1xMyc and 6xHIS epitope tags, and then cloned into the yeast centromeric shuttle vector pRS316 (kindly provided by B. Tu) downstream of the S. Cerevisiae GAL1 promoter. The vector was transformed into a protease deficient *S. cerevisiae* W303 strain using a standard Lithium Acetate protocol (Gietz and Woods, 2002). Transformants were isolated and maintained on SD-URA medium. All constructs were confirmed by sequencing.

Immunoblot Analysis

Samples were resuspended in SDS sample buffer and proteins were resolved by SDS-PAGE prior to immunoblot analysis. Rabbit anti-IRP1 antibody

was kindly provided by R. Eisenstein. The Myc 9E10 antibody was purified (Harlow and Lane, 1988) on protein G agarose (Roche) from 9E10 hybridoma (ATCC) grown in Hybridoma SFM media (Gibco Cat# 12045). α-FBXL5 antibody was generated from rabbits immunized with 6xHis-tagged FBXL5 (1-691) expressed in *E. coli* and further affinity-purified from serum. Additional antibodies are listed in Table III-3. Immune complexes were detected by enhanced chemiluminescence using peroxidase-conjugated secondary antibodies. Immunoblots using antibodies specific for tubulin were used as loading controls. Quantitation of immunoblots was performed using a Canon Model 30 LED Indirect Exposure Scanner and analyzed using Scion Image software (version 4.0.3.2).

AlphaScreen Assay

To identify candidate E3 ubiquitin ligase(s) responsible for iron-dependent IRP2 ubiquitination, a library of 800 siRNA pools (Qiagen), each designed to suppress expression of an individual human gene, was assembled. Included in the library were siRNAs targeting genes encoding proteins known to play a role in ubiquitination as well as proteins containing domains found within previously identified E3 ligase complexes (Ardley and Robinson, 2005; Hershko and Ciechanover, 1998; Li et al., 2008; Willems et al., 2004). HEK 293 cells stably transfected with the HA-IRP2-FLAG expression construct were reverse-

transfected with siRNA using Lipofectamine 2000 (Invitrogen) in 96-well plates. Following 48 hr incubation, cells were treated with either 25 μM ferric ammonium citrate or 100 μM deferoxamine and incubated for 16 hr. Media was removed and 50 μL assay mixture/well (1X PBS, 0.5% TritonX-100, 5 ng/μL streptavidin donor beads (PerkinElmer), 5 ng/μL M2 FLAG acceptor beads (PerkinElmer), 2 pg/μL biotinylated α-HA antibody (Genscript), 250 μM PMSF (Sigma), and 1X protease inhibitor cocktail (Sigma)) was added. Plates were incubated in the dark with gentle rocking for 4 hr and data collected with an EnVision microplate reader (PerkinElmer). Assays were performed in triplicate with bars indicating standard error.

Electrophoretic Mobility Shift Assay (EMSA)

HA-IRP2-FLAG HEK 293 cells were transfected with siRNAs and treated with either 100 μM ferric ammonium citrate or 100 μM deferoxamine for 16 hr. Cells were washed with 1X PBS, incubated in lysis buffer (20 mM HEPES (pH 7.4), 3 mM $MgCl_2$, 40 mM KCl, 5% glycerol, 0.2% Nonidet P-40, 1 mM DTT, 250 μM PMSF, 1X protease inhibitor cocktail (Sigma)), and centrifuged at 17,000g for 15 min. Lysate containing 10 μg total protein was incubated in the presence of 100 kcpm ^{32}P-labeled in vitro transcribed RNA encompassing the rat L-ferritin IRE in a reaction mixture containing 1 mM DTT, 0.06 U/μL RNase inhibitor (New England Biolabs), 5% glycerol, 20 mM HEPES (pH 7.4), 40 mM

KCl, and 3 mM $MgCl_2$ for 1.5 hr at 4°C. For supershift reactions, 1 μL of α-IRP1 antibody or α-FLAG antibody was added to the mixture. Heparin was added to 2 mg/mL and the samples incubated another 10 min at 4°C. Protein-bound DNA complexes were resolved by electrophoresis in a 5% nondenaturing polyacrylamide gel at 4° C and visualized by phosphorimager analysis.

Quantitative Real-time Reverse Transcript (qRT)-PCR

Total RNAs were prepared using the Rneasy Mini Kit (Qiagen), treated with DNAse I (Roche) and converted to cDNA using Superscript II Reverse Transcriptase (Invitrogen) and random primers $p(dN)_6$ (Roche). qRT-PCR was performed using the Power SYBR Green PCR Master Mix (ABI) on the 7900HT Fast Real-Time PCR System (ABI) using primer sets for human TfR1 (5′-GGTGACCCTTACACACCTGGATT and 5′-TGATGACCGAGATGGTGGAA), FBXL5 (5′-CTTACCCAGACTGACATTTCAGATTC and 5′-GAAGACTCTGGCAGCAACCAA), and the 18S rRNA (5′-GATATGCTCATGTGGTGTTG and 5′-AATCTTCTTCAGTCGCTCCA) control. The thermal cycle conditions were as follows: 2 min at 50°C and 10 min at 95°C followed by 40 cycles of 95°C for 15 sec and 60°C for 1 min. Melting curves were performed at 95°C for 15 sec, 60°C for 15 sec and 95°C for 15 sec. All tests were performed in triplicate and all experiments were repeated three

times. The mathematical transformations for primary data analysis were done by SDS2.0 (ABI). The amplification data were analyzed based on the equation: R (ratio) = $2^{-(\Delta Ct\ sample-\ \Delta Ct\ control)}$. The results were expressed as fold changes of the treatment groups compared to the controls. p-values were determined by using Student's unpaired t-test.

Co-Immunoprecipitations

HA-IRP2-FLAG HEK 293 cells were transiently transfected using Lipofectamine 2000 (Invitrogen). Twenty-four hours after transfection, cells were treated with 10 μM MG132 (Boston Biochem) to block IRP2 or FBXL5 degradation for 1 hr followed by incubation with 100 μM ferric ammonium citrate for an additional 6 hr. Cells were then washed with PBS, and incubated in lysis buffer containing 50 mM Tris/Cl (pH 8.0), 150 mM NaCl, 1.0% NP40, 250 μM phenylmethylsulfonyl fluoride, and 1X protease inhibitor cocktail (Sigma), and centrifuged at 17,000g for 15 min. Lysate (~500 μg) was incubated with 5 μL α-FLAG M2 affinity resin (Sigma) overnight, washed three times with lysis buffer, and the precipitates were subjected to immunoblot analysis. For co-immunoprecipitation of endogenous IRP2, reactions were carried out as described with two exceptions. Following incubation with MG132, FBXL5-FLAG expressing HEK 293T cells were treated with either 100 μM ferric ammonium citrate or 100 μM deferoxamine mesylate for 6 hrs and immunoprecipitates were

eluted from the α-FLAG M2 affinity resin using a competitor FLAG-peptide prior to immunoblotting.

Recombinant Protein Expression and Purification

Bacteria, yeast, and insect cells were cultured under standard conditions unless otherwise specified. Recombinant E1 enzyme and ubiquitin were purchased from Boston Biochem. K_0-GST-Ubiquitin was expressed in *E. coli* and purified by glutathione agarose (GE Healthcare). UbcH5a E2 was expressed and purified under similar conditions, except the GST tag was released by Thrombin protease (GE Healthcare) and removed using glutathione agarose. For recombinant IRP2 expression, yeast were grown to mid-log phase in YPGL medium and induced with galactose (2% w/v) for 16 hours (Caron et al., 1994). IRP2 was purified in anaerobic conditions (<1ppm O_2) in a Coy glovebox by Ni-NTA chromatography and gel filtration on a Superdex 200 column equilibriated in deoxygenated buffer.

SCF^{FBXL5} was expressed in Sf9 cells grown in Sf900IIM media using the Bac to Bac system (Invitrogen). Briefly, SKP1, CUL1, and RBX1 were cloned into pFastBac HT vectors and full length FBXL5, or ΔF-box FBXL5 were fused to a C-terminal 3xFLAG epitope tag in the pFastBac 1 vector. Recombinant baculovirus was generated according to the manufacturer's protocol, and SCF^{FBXL5} was expressed by infecting Sf9 cells in log phase growth. Optimal

expression was observed at 55-60 hr with a ratio of 4:1:6:6 of FBXL5:SKP1:CUL1:RBX1 viruses. Soluble SCF^{FBXL5} was purified by binding to FLAG M2 Resin and eluted with FLAG peptide. Eluted fractions were dialyzed in a Slide-A-Lyzer (MWCO 10kDa; Pierce) or subjected to size exclusion chromatography in a Superdex 200 column in buffer containing 10 mM HEPES (pH 7.5), 1.5 mM $MgCl_2$, 10 mM KCl, and 100 mM NaCl. The subset of CUL1 protein that copurifies with FBXL5 migrates slower than the majority of overexpressed CUL1 in the input lysate, though the difference between these populations has not been determined.

Wildtype and E61A FBXL5 Hr domains were amplified by PCR using the oligonucleotides 5′-GGAGGGATCCGATGGCGCCCTTTCCTGAAGAAGTG and 5′-GGATCTAGATCACTGAGAGCAGTGTTGTGCAATCAC and cloned into the pGST-parallel vector (Sheffield et al., 1999). Soluble GST-fusion proteins were expressed in *E. coli* grown in media supplemented with 100 μM ferric ammonium citrate and purified using glutathione agarose. The GST fusion tag was cleaved upon incubation with TEV protease for 6 hr at 24°C and the liberated Hr domains were purified by anion exchange chromatography (HiTrap Q, GE Healthcare).

Ubiquitination Assay

Typical reactions are composed of 10 μg ubiquitin, 1 μg IRP2, 40 ng E1, 200 ng UbCH5a, and 1-3 μg of SCF^{FBXL5} in 50 μL reaction buffer containing 10 mM HEPES (pH 7.5), 10 mM KCl, 100 mM NaCl, 1.5 mM $MgCl_2$, 1 mM DTT, 2 mM ATP, and 50 μM ferrous sulfate. Reactions were incubated at room temperature for 2 hr and resolved by electrophoresis in a 6% SDS-polyacrylamide gel. Reactions involving HeLa S100 for the purpose of biochemical purification were carried out in similar conditions, with the following exceptions: 25-30uL reaction volume; NaCl was omitted from the reaction buffer; 20ng of E1 and 300-500 ng of UbCH5b was employed as the source of E1 and E2 where appropriate; 25-30ug of HeLa or normalized fractions were used as the source of E3 activity; and the reactions were incubated for one hour at 37C prior to SDS-PAGE and immunoblotting for either the FLAG epitope or with endogenous IRP2 antibody.

Iron Content Measurement

UV-Visible spectra were measured with a Shimadzu UV-Visible Spectrophotometer (Model UV-1601). Iron content of the recombinant FBXL5 Hr domain was determined by the method of Beinert (Beinert, 1978) with the following modifications: 15.7 μM of protein in 50 mM Tris/Cl (pH 8.0) was denatured with 1.5% SDS, and 600 μM Ferene (3-(2-Pyridyl)-5,6-di(2-furyl)-1,2,3-triazine-5',5''-disulfonic acid disodium salt; Sigma) was employed as the

iron detecting reagent. Absorbance was measured at 593nm and iron content was quantified against a standard curve generated from Claritas PPT Iron Solution Standard (CLFE2-2Y). The molar ratio of iron to FBXL5 in these preparations was calculated to be 1.1:1.0, suggesting approximately half of the protein contained a diiron center. In addition, UV-VIS absorption spectra for ferene bound to iron liberated from the hemerythrin domain showed a uniform peak with a maximum at 593 nm that was insensitive to the addition of the copper-specific chelator thiourea (data not shown), diagnostic of iron bound to ferene (Hennessy et al., 1984).

Circular Dichroism

Circular dichroism (CD) measurements were performed in an AVIV 62 DS instrument with a 1 mm pathlength quartz cuvette. Protein concentrations were kept at 0.11 mg/mL (6.2 μM) to prevent protein precipitation in buffer containing 10 mM Tris/Cl (pH 7.5) and 100 mM NaCl. Measurements were taken with an averaging time of 10 sec with 5 repeats. Thermal denaturation experiments were performed in a 20 mM HEPES buffer (pH 7.5) with 100mM NaCl, and data were recorded by measuring ellipticity at 222nm from 5-95°C in 1°C increments over equilibration times of 90 sec. Sodium dithionite (Fluka) and *o*-phenanthroline (Sigma) were added at 10x molar excess under N_2 atmosphere. Melting curves measured in reverse from 95-5°C did not overlap demonstrating

that denaturation is not reversible (data not shown). Data are reported in terms of mean molar residual ellipticity.

Luciferase Gene Reporter Assay

Following 24 hr of transfection, HEK 293T cells were treated with either 100 μM ferric ammonium citrate or 100 μM deferoxamine mesylate and incubated an additional 24 hr under atmospheric (~20% O_2) or low (1%) O_2 conditions. Cells were lysed in buffer (30 mM Tricine (pH 7.8), 8 mM MgAc, 0.2 mM EDTA, 1% Triton) on ice, transferred to a 96-well plate, and ATP, CoA, β-mercaptoethanol, and D-luciferin (Molecular Probes) added to final concentrations of 375 μM, 375 μM, 50 mM, and 125 μM respectively. Luminescence was measured in a plate reader (Bio-Tek, Synergy HT). Assays were performed in triplicate with bars indicating standard error.

FBXL5 Crystallization and X-ray diffraction data collection

Crystals of FBXL5-Hr were grown using the hanging-drop vapor diffusion method from drops containing 1 μL protein (5 mg/ml) and 1 μL of reservoir solution (10% PEG 6000, 0.1M HEPES pH 6.5) and equilibrated over 50 μL of reservoir solution. Plate-like crystals appeared after 1 day at 20°C and grew to their maximal extent by 2-3 days. Crystals were large in two dimensions (0.2 x 0.5 mm) and relatively thin (0.1 mm thickness). Cryoprotection was performed by

transferring the crystals to a final solution of 25% ethylene glycol, 10% PEG 6000, 0.1M HEPES pH 6.5, increasing in 5% steps of ethylene glycol over the course of 10 minutes at 20°C. Crystals were flash frozen using liquid nitrogen. Crystals exhibited the symmetry of space group C2 with unit cell parameters of a=60.1 Å, b=75.7 Å, c=78.7 Å and β=111.8° and contained two molecules of FBXL5-Hr per asymmetric unit. Crystals diffracted isotropically to a d_{min} of 1.84 Å when exposed to synchrotron radiation. Data were indexed, integrated and scaled using the HKL-3000 program package (Minor et al., 2006). Data collection statistics are provided in the Appendix.

Phase determination and structure refinement

Phases were obtained from a two-wavelength anomalous dispersion experiment using the native iron atoms with data to a resolution of 2.5 Å. Four iron and two sulfur sites were located using the program SHELXD (Schneider and Sheldrick, 2002); this represented two single-occupancy iron sites and one methionine sulfur site per FBXL5-Hr monomer. Phases were refined with the program MLPHARE (Otwinowski, Z. 1991), resulting in an overall figure-of-merit of 0.59 for data between 44.7 and 2.5 Å. Phases were further improved by density modification and two-fold non-crystallographic averaging with the program DM (Cowtan and Main, 1998) resulting in a figure-of-merit of 0.85. An

initial model containing about 86% of all residues was automatically generated by alternating cycles of the programs ARP/wARP (Morris et al., 2004).

Additional residues were manually modeled in the programs O (Jones et al., 1991). Refinement was performed with native data to a resolution of 1.84 Å using the program PHENIX (Adams et al., 2002) with a random 5.1% of all data set aside for an R_{free} calculation. The current model contains two FBXL5-Hr monomers; included are residues 6-71,85-158 in molecule A and residues 6-66, 85-159 in molecule B and 81 waters. The R_{work} is 0.232, and the R_{free} is 0.268. A Ramachandran plot generated with Molprobity (Davis et al., 2007) indicated that 99.3% of all protein residues are in the most favored regions with the remaining 0.7% in additionally allowed regions. Phasing and model refinement statistics are provided in the previous table .

The structure shown in this report is derived from work performed on beamlines 19-BM and 19-ID at Argonne National Laboratory, Structural Biology Center at the Advanced Photon Source. Argonne is operated by University of Chicago Argonne, LLC, for the U.S. Department of Energy, Office of Biological and Environmental Research under contract DE-AC02-06CH11357.

Table III-1. siRNA Sequences

siRNA	Catalog #	Targeting Sequence
FBXL5 #1	D-012424-04	CCUUAGAGGUCUUAGCCUA
FBXL5 #2	D-012424-17	CCUCAAGAGUUAUGUCGAU
FBXL5 #3	D-012424-01	GCACAACACUGCUCUCAGA
SKP1 #1	D-003323-09	CGCAAGACCUUCAAUAUCA
SKP1 #2	D-003323-10	CCAAUAUGAUCAAGGGGAA
CUL1 #1	D-004086-03	GGUUAUAUCAGUUGUCUAA
CUL1 #2	D-004086-05	CAACGAAGAGUUCAGGUUU
RBX1 #1	D-004087-01	GAAGCGCUUUGAAGUGAAA
RBX1 #2	D-004087-03	GCAUAGAAUGUCAAGCUAA
NT	D-001210-01	

Table III-2. PCR Primers

Construct	FBXL5 Primers
Δ1-197	5'-GGAGGATCCACCATGGTGTCAGAACACTCCACAGG
Δ208-248	5'-GGTATAACCCATTACCCTGTTCATTGGGCCAGAG 5'-ATGAACAGGGTAATGGGTTATACCTGTGGAGTGTTCTGA
Δ252-350	5'-CTTTACCCTGTTATTTTAGAGCTTTGTCCTAACC 5'-GCTCTAAAATAACAGGGTAAAGATGTTTCC
Δ355-408	5'-ATTTTAGAGCTTGGAATTCTGACATCTCATC 5'-GTCAGAATTCCAAGCTCTAAAATCTGCCTAAC
Δ411-595	5'-GCTCTTGGAATTACTGGACGTGTACTTCTGTTTC 5'-CACGTCCAGTAATTCCAAGAGCTCTGGAAATC
Δ596-650	5'-CTGATCAAGAGTGTCCTTCTCTGAATGATG 5'-CAGAGAAGGACACTCTTGATCAGATTTTTCAC
Δ651-691	5'-GGTGTCTAGAACCTGCTGAAACCAAATCCTGCAGGCCTG
Δ1-161	5'-GGAGGATCCACCATGAAGGATACTGCAGAACTCCTTAGAGG
1-161	5'-GGATCTAGATCACTGAGAGCAGTGTTGTGCAATCAC
H57A	5'-GTTCAAAATGGCTGAGCAGATTGAAAATGAATAC 5'-CAATCTGCTCAGCCATTTTGAACTCCTTGAAAG
E61A	5'-GAGCAGATTGCAAATGAATACATTATTGGTTTG 5'-GTATTCATTTGCAATCTGCTCATGCATTTTG
Construct	**IRP2 Primers**
Δ73	5'- CTTCAGTAAAGAACCTGAAACAGTGTTAAA 5'-TTTCAGGTTCTTTACTGAAGTCAATTTGTA

Table III-3. Antibodies

Antibody	Vendor	Catalog #
Rabbit anti-CUL1	Santa Cruz	sc-11384
Goat anti-FBXL5	Santa Cruz	sc-54364
Mouse anti-FLAGM2	Sigma	F3165
Donkey anti-Goat HRP	Santa Cruz	sc-2056
Mouse anti-IRP2	Santa Cruz	sc-33682
Goat anti-Mouse HRP	Santa Cruz	sc-2055
Goat anti-Rabbit HRP	Santa Cruz	sc-2054
Rabbit anti-RBX1	AbCam	ab2977
Rabbit anti-SKP1	AbCam	ab10946
Mouse anti-Tubulin	Sigma	T6199
Mouse anti-V5	Invitrogen	R960-25

CHAPTER FOUR

CONCLUSIONS AND FUTURE DIRECTIONS

CONCLUSIONS

Section IVA – FBXL5's Potential Role in Mammalian Iron Homeostasis

To maintain cellular iron homeostasis, the RNA-binding activity of IRPs is responsive to changes in iron bioavailability, allowing cells to alter expression of genes controlling iron uptake, storage, utilization, and export (Rouault, 2006). Recent identification of additional IRE containing mRNAs indicates that the IRP-mediated regulation may be more extensive than originally thought (Rogers et al., 2002; Sanchez et al., 2006; Sanchez et al., 2007). Complementing decades of studies using cell culture systems, physiological roles for the IRPs have been informed by recent knockout mouse studies confirming IRP1 and 2 as key regulators of cellular, as well as systemic, iron homeostasis (Muckenthaler et al., 2008). Though data suggest that the two IRPs are partially redundant (Meyron-Holtz et al., 2004), *IRP1* ablation results in mild iron dysregulation in the kidney and brown fat (Meyron-Holtz et al., 2004), while deletion of *IRP2* results in microcytic anemia, iron overload in the liver and intestine (Galy et al., 2005), and in one setting, neurodegeneration (LaVaute et al., 2001). Global knockout of both IRP genes results in embryonic lethality (Smith et al., 2006). In contrast,

mutations that interfere with normal iron sulfur cluster biogenesis appear to lead to significant increases in apo IRP1 levels, even under iron replete conditions (Wingert et al., 2005). The resulting increase in IRE binding activity can also lead to iron overload, while simultaneously compromising heme biosynthesis in erythroid cells to cause microcytic anemia (Pondarre et al., 2006).

How changes in cellular iron availability are directly sensed, and how that information is translated to changes in IRP activity, is poorly understood particularly with respect to iron- and O_2-dependent degradation of IRP2 (Pantopoulos, 2004). The results presented here indicate that FBXL5 can assemble into a SCF E3 ubiquitin ligase complex capable of binding and polyubiquitinating IRP2. Loss of SCF^{FBXL5} expression leads to high accumulation levels of functional IRP2, even under iron replete conditions. FBXL5 is itself post-translationally regulated as a function of both iron and O_2 availability. Regulation is conferred by a hemerythrin domain that, when bound to iron, sequesters a recognition motif for an as-yet unidentified ubiquitin ligase. Oxygen binding to the diiron center may serve to further promote this process. In contrast, iron deficiency promotes the unfolding of the hemerythrin domain, resulting in FBXL5 degradation and subsequent stabilization of SCF^{FBXL5} substrates such as IRP2.

This model of iron and oxygen mediated degron sequestration is supported by both cell culture, biochemical, and x-ray crystal structure studies (Chapter III).

Interestingly, the diiron center within the crystal structure of FBXL5 lacks oxygen, suggesting that the diiron center within FBXL5 is particularly susceptible to mild reduction potentials (4mM 2-ME and 0.5mM TCEP versus ten to one hundred millimolar dithionite (Zhang et al., 1992). In this deoxy state, the third helix of FBXL5's hemerythrin is unstructured. The unstructured region also encompasses amino acids 67-84 of FBXL5, and deletion of these amino acids as shown in Figure III-39, leads to constitutive stabilization of FBXL5.

A subunit of the microtubule motor activator dynactin that plays a role in vesicular trafficking, $p150^{Glued}$, has been reported to be a SCF^{FBXL5} substrate as well (Zhang et al., 2007), however the regulation and physiological consequences of this interaction requires further investigation. Of great interest will be loss-of-function studies to examine to contribution(s) of FBXL5 to cellular and systemic iron homeostasis *in vivo*. Predicted iron-insensitive accumulation of IRP2 in the absence of FBXL5 could also result in microcytic anemia and/or iron overload, though the possible existence of additional SCF^{FBXL5} substrates could result in additional phenotypes. In light of the relationship between oxygen availability and both cellular and systemic iron homeostasis, it will also be of interest to investigate potential roles for FBXL5 as a potential cellular oxygen sensor in these, as well as other, pathways. The finding that FBXL5 contains a hemerythrin domain was particularly significant as it is the first member of the family to be described in vertebrates. The iron and O_2-binding properties of the hemerythrin

domain make it a strong candidate for the cellular sensor governing IRP2-regulated iron homeostasis. Though several F-box-containing proteins in plants have been reported to act as ligand-regulated effector proteins (Somers and Fujiwara, 2009), none have been described in metazoans. Here, FBXL5 is the first example of a metazoan F-box protein capable of binding a ligand to promote a change in activity.

FUTURE DIRECTIONS

Section IV B – The Biochemical and Cellular Regulation of FBXL5

Much work remains to characterize the biophysical and ligand-binding properties of FBXL5's Hr domain and to correlate these properties with physiological responses. Of immediate interest is characterization of FBXL5's oxygen affinity, and structural changes upon oxygen binding to the diiron center. As discussed in Chapter III, low oxygen levels result in decreased accumulation of FBXL5 protein, and these effects are mediated in part through its iron and oxygen binding hemerythrin domain. This phenomenon may be explained by our current model (Figure IV-1), that suggests that the third helix in FBXL5's hemerythrin domain is disordered when the diiron center lacks oxygen. Interestingly, glutamate residue 58 (E58) forms a hydrogen bond with the μ-hydroxyl group in this state (Figure III-37). When oxygen is bound to the diiron

center, the third helix becomes more structured, and we hypothesize that this is due to oxygen mediated displacement E58 from the μ-hydroxyl group (Figure IV-1). The physiological consequence of oxygen binding, is that a degron within this third helix is concealed. As a result, the E3 ligase responsible for the ubiquitination of FBXL5's hemerythrin domain cannot bind the degron, and FBXL5 levels accumulate under high oxygen conditions.

To test the validity of this hypothesis, we will attempt to solve the crystal structure of the diiron site bound to oxygen. To this end, crystals have been isolated for the FBXL5's Hr domain in the absence of reducing agent. In this state, the UV-VIS absorbance spectrum of the diiron center differs from protein treated with reducing agent (Figure III-30). Therefore, if oxygen truly binds to FBXL5's Hr domain, it is likely that the oxy or met state of the diiron center will be present in the X-ray crystal structure. It is also important to note that, unlike crystals grown in the presence of reducing agent, these Hr domain crystals require a higher concentration of precipitating agent (*e.g.* 10% PEG 6,000 versus 25% PEG 3,350). Preliminary diffraction data collected from these crystals suggest that the third helix is indeed more ordered. Whether these observations hold true in the final solution is yet to be seen.

While our data suggest that IRP2 and IRP1 are substrates for SCF^{FBXL5}, they need not be exclusive ubiquitination substrates, especially if one considers $p150^{Glued}$ (Zhang et al., 2007). Identification of other SCF^{FBXL5} substrates may be

achieved through affinity purifications and Mass Spectrometry to identify interacting proteins. In addition to the identity of other target proteins, it is not completely understood how FBXL5 binds its substrates. Are all Leucine Rich Regions (LRRs) required for FBXL5-substrate interaction? If not, are there distinct LRRs for IRP2, IRP1, and other substrates?

Most importantly, is the factor(s) responsible for promoting FBXL5 degradation under iron-deplete conditions. While F-box proteins have been proposed to be ubiquitinated in an autocatalytic fashion, cell culture studies show that exogenously expressed FBXL5 Hr domain maintains its iron regulation despite eliminating its E3 ligase activity by deletion of the F-box domain required for its assembly into an E3 ligase complex (Figure IV-2). Furthermore, knockdown of endogenous FBXL5 expression does not affect iron mediated stability of transiently transfected FBXL5, arguing against the possibility that FBXL5 ubiquitinates itself in *trans* (Figure IV-2). Therefore, the identity of the E3 ubiquitin ligase responsible for FBXL5's Hr domain mediated degradation remains an open question. With the approaches discussed in Section IIB-IID, one could identify the E3 ligase responsible for this process.

To identify genes outside of E3 ligases responsible for FBXL5's degradation in iron deficient conditions, one can simply expand the 800 gene library to include all coding genes in the human genome. This "genome wide" siRNA screen could identify genes that either directly affect FBXL5 stability, or

are more generally involved in maintenance of cytosolic iron concentrations.

As discussed in Section IIIH, the degradation of FBXL5 through its Hr domain is mediated by a degron. Work to delineate the exact boundaries and mechanism of degron recognition is being undertaken by our laboratory. Of particular interest would be amino acid residues that may serve as a site for post translational modifications (*e.g.* hydroxylation of proline residues within HIF-α's degron) required for E3 ligase recognition.

Section IVC – The Role of FBXL5 in Physiology and Disease

In work currently being undertaken in our laboratory, mice null for *FBXL5* expression will be generated to characterize its role in physiological iron homeostasis. Our data suggest that eliminating *FBXL5* expression *in vivo* will result in inappropriate IRP2 and apoIRP1 levels despite high iron levels. In this state, cells that are iron replete would continue to take up iron through increased TfR1 expression, and downregulate iron sequestration by translational suppression of ferritin. If this were to occur globally in an organism, the end result would be iron overload throughout all tissues with a concomitant microcytic anemia, since IRPs repress ALAS2 expression in erythroid cells.

A scenario similar to this description has been observed in zebrafish, where IRP1 is iron insensitive and inappropriately upregulated in the *Shiraz*

mutant, due to a defect in iron sulfur cluster machinery responsible for converting IRP1 to its aconitase form in iron replete states (Wingert et al., 2005). Since zebra fish are an excellent disease model for the hematological disorders (Amatruda and Zon, 1999), studies in this system are being undertaken to understand FBXL5 in vertebrate physiology.

With regards to hepcidin regulation (introduced in Chapter I), it has been proposed that the iron sensor involved in hepcidin's regulation is a complex of HFE, holo-TfR2, and HJV (Gao et al., 2009; Andrews, 2008). Here, saturated Tf binds to TfR2 and mediates its association with HFE, a MHC Class I like molecule found to be responsible for the majority cases of hereditary hemochromatosis (Beutler, 2006). When HFE and TfR2 interact, a BMP-SMAD signaling cascade ensues, resulting in the transcription of Hepcidin mRNA (Ganz, 2008). This finding is supported by humans carrying loss of function mutations in TMPRSS6, a membrane protease that serves to cleave HJV, a coreceptor for SMAD signaling through BMP receptor which serves to suppress the HFE-TfR2 signal in iron deficiency (Ganz, 2008).

What is the relevance of FBXL5 in this setting? Recent preliminary findings suggest the HFE-TfR2 model of iron sensing is not important in mammals, since knockout mice for HFE and TfR2 can still mount an appropriate Hepcidin response to high systemic iron levels (Fleming et al., 2009; Ramos et al., 2009). Furthermore, recent work by the Ganz laboratory suggests that an

additional pathway involving an intracellular iron sensor may be responsible for Hepcidin upregulation in states of high iron (Ramos et al., 2009). Whether FBXL5 plays a role in this process and thus serves as a master regulator of cellular and systemic iron homeostasis will hopefully be answered by future work in our laboratory.

Our laboratory has held a long standing interest in cellular sensors, particularly oxygen and its control of Hypoxia Inducible Factor. With the findings that FBXL5 responds to both iron and oxygen levels, we find another example of the many levels of cross talk that occur between metabolic pathways in human physiology. The next section discusses the crosstalk between iron and oxygen homeostasis and the new role that FBXL5 plays in this process.

Section IVD - Cellular Iron and Oxygen homeostasis

Overview

Eukaryotic cells employ iron and oxygen in processes that are essential for life, including oxidative phosphorylation, synthesis of metabolites and cofactors, and posttranslational modifications (Ozer and Bruick, 2007; Rouault, 2006; Wallander et al., 2006). In contrast, excess amounts of iron and oxygen result in cytotoxic oxidative stress (Galaris and Pantopoulos, 2008), necessitating tight regulation of iron and oxygen availability. The Hypoxia Inducible Factors (HIF),

and the Iron Regulatory Proteins (IRPs) are key mediators of cellular oxygen and iron homeostasis, respectively. Because iron and oxygen are often intimately connected in their metabolism, it is not surprising that their levels are coordinately regulated in cells. Such crosstalk is achieved in part by cellular regulatory factors that sense and respond to both iron and oxygen and is reinforced by overlap in the gene targets regulated by each pathway.

Overview of Mammalian Cellular Oxygen Homeostasis

Appropriate responses to changes in cellular oxygen tension are largely mediated through transcriptional activation of genes by Hypoxic Inducible Factors (HIF) (Semenza, 2007). HIF is a dimer of basic helix-loop-helix (bHLH) and Per-Arnt-Sim (PAS) domain transcription factors, HIF-α and HIF-β (Ozer and Bruick, 2007). The HIF-β subunit, also known as Aryl-Hydrocarbon-Nuclear Transporter (ARNT), is a constitutively expressed partner for multiple bHLH-PAS transcription factors (Semenza, 2007). The HIF-α subunit, however, is regulated in response to changes in cellular oxygen availability.

Under normoxic conditions, HIF-α is ubiquitinated by an E3 ligase complex containing the product of the von Hippel Lindau tumor suppressor gene (VHL) and targeted for degradation by the proteasome (Figure IV-3) (Ivan et al., 2001; Jaakkola et al., 2001). A specific region in HIF-α, termed the Oxygen Degradation Domain (ODD) is necessary and sufficient for VHL recognition of

HIF-α. A family of three iron and 2-oxoglutarate dioxygenases hydroxylate proline residues in the ODD thereby recruiting HIF-α to the VHL E3 Ligase complex (Bruick and McKnight, 2001; Epstein et al., 2001; Ivan et al., 2002). These dioxygenases hydroxylate the HIF-α ODD under normoxic conditions but are inhibited in hypoxia, thus sparing HIF-α from VHL mediated degradation. The recruitment of transcriptional coactivators to HIF-α is also inhibited in an oxygen-dependent manner by hydroxylation of an asparagine residue in its C-terminal transactivation domain by another iron and 2-oxoglutarate dioxygenase, Factor Inhibiting HIF-1 (FIH-1) (Lando et al., 2002).

The biochemical properties of these dioxygenases allow them to serve as both iron and oxygen sensors in the cell. These enzymes require iron to activate dioxygen to hydroxylate residues on protein substrates as well as the cosubstrate 2-oxoglutarate (Figure IV-2). By virtue of their substrate requirements, these dioxygenases are believed to function as direct oxygen sensors in the pathway, with *in vitro* K_m values for oxygen that appear to correlate with relative *in vivo* sensitivities to oxygen (Ozer and Bruick, 2007). However, the relationship between dioxygenase activity and changes in oxygen availability is likely to be further modulated by other mechanisms such as feedback loops and mitochondria-derived signals (Ozer and Bruick, 2007). Because of their iron requirement, these enzymes may also function as iron sensors, as evidenced by low dioxygenase activity seen in cells deficient in iron (Peyssonnaux et al., 2008).

Induction of HIF-α results in transcription of genes that confer adaptation to hypoxia. For example, at the cellular level HIF induces the transcription of genes involved in glycolysis, promoting adaptation to anaerobic metabolism.(Semenza, 2007) HIF can also regulate systemic hypoxic responses, for example, by inducing erythropoietin (EPO) and Vasoendothelial Growth Factor (VEGF) gene expression to promote greater delivery of oxygen to tissues (Semenza, 2007).

Overview of Iron Homeostasis

In mammals, iron is absorbed from the diet in the form of insoluble ferric salts through the proximal part of the small intestine. Intestinal epithelial cells (IECs) absorb iron through the apical membrane protein Divalent Metal Transporter 1 (DMT1) and then export it into the bloodstream through the basolateral membrane protein, Ferroportin (FPN) (Hentze et al., 2004; Muckenthaler et al., 2008; Pantopoulos, 2004). Exported iron binds to its serum carrier, Transferrin (Tf), and is then transported throughout the body to be utilized by all cells, particularly erythroid precursors in the bone marrow (Wrighting and Andrews, 2008).

Since mammals have no active means to secrete excess iron from the body, iron levels are primarily regulated through control of dietary absorption in the intestine, mobilization of iron stores from the liver, and recycling in the

reticuloendothelial system (Wrighting and Andrews, 2008). A major effector hormone that regulates this systemic homeostasis is hepcidin (Peyssonnaux et al., 2008). In response to high iron concentrations, hepcidin is transcriptionally upregulated in the liver and secreted into the bloodstream, where it binds to its receptor, FPN, causing this iron exporter to be internalized and degraded (Nemeth et al., 2004). As a result, export of iron into the blood stream from the intestine and splenic macrophages decreases, and Tf bound iron levels decrease. In states of iron deficiency, hepcidin transcription is repressed, and FPN levels increase leading to greater iron availability in the body (Wrighting and Andrews, 2008).

At the cellular level, iron homeostasis occurs largely through coordinated regulation of iron import, utilization, and storage. Cells acquire iron mostly through receptor mediated endocytosis of Tf through Transferrin Receptor 1 and 2 (TfR 1 and 2).(Hentze et al., 2004) Cells utilize much of this iron by incorporation into enzyme prosthetic groups such as iron sulfur clusters or heme, while excess iron is sequestered by ferritin, an iron storage protein (Galaris and Pantopoulos, 2008; Wrighting and Andrews, 2008). These processes are coordinately regulated as a function of cellular iron bioavailability at the level of post-transcriptional regulation.

Post transcriptional regulation of iron metabolism was first described in ferritin mRNA, where in states of low iron, a *cis*-acting Iron Response Element (IRE)(Piccinelli and Samuelsson, 2007) in the 5' untranslated region (UTR)

promotes the binding of Iron Regulatory Proteins (IRP1 and 2) (Hentze et al., 2004; Rouault, 2006). IRP binding results in suppression of ribosome binding and decreases synthesis of the ferritin protein (Rouault, 2006). IREs alternatively function to stabilize mRNAs when they are located in the 3'UTR.(Hentze et al., 2004) In the case of Transferrin Receptor 1, IRP binding protects the mRNA from endonucleolytic degradation (Koeller et al., 1989). IREs have since been identified in other genes (Table IV-1) though functional roles have not been validated for all. Thus, in the low iron state, IRPs bind to IREs to increase bioavailable iron levels by upregulation of iron uptake and downregulation of iron utilization and storage. When cells have excess iron, IRPs fail to bind IREs, reducing bioavailable iron by a decrease in iron uptake, and an increase in utilization and storage (Figure IV-4).

Iron governs the IRP1 and 2 binding activity through distinct mechanisms (Figure IV-4). In states of high iron, IRP1 assembles an iron sulfur cluster, gaining aconitase activity but losing its ability to bind RNA in the process (Rouault, 2006). IRP2, despite being 59% identical to IRP1, cannot assemble an iron sulfur cluster. Instead, in the high iron state IRP2 is ubiquitinated and degraded by the proteasome, thus removing its RNA binding activity from cells (Pantopoulos, 2004).

Together, IRP1 and 2 are essential regulators of mammalian iron homeostasis, though they can largely compensate for one another, as deletion of

either gene results in viable and fertile mice (Meyron-Holtz et al., 2004a). IRP2 null mice do however display microcytic anemia and iron overload in the intestine and liver (LaVaute et al., 2001); (Smith et al., 2006) While global IRP deficiency results in misregulation of iron homeostasis, an inappropriate excess of IRP binding activity has also been shown to affect systemic iron management. For example, the *Shiraz* phenotype of microcytic anemia and iron overload is due to mutation in glutaredoxin 5, a critical component of iron sulfur cluster biogenesis (Wingert et al., 2005). In this setting, the IRE binding form of IRP1 is upregulated even in the iron replete state, resulting in repression of heme synthesis by inhibition of erythroid 5'aminolevulinic acid synthase (eALAS) (Wingert et al., 2005).

Cross-talk between Oxygen and Iron Homeostasis Regulatory Pathways

The bioavailability of iron affects the cellular hypoxic response in several ways. As noted in cell culture studies, manipulation of iron levels in the media alters HIF-α induction through affects on dioxygenase activity (Ozer and Bruick, 2007). As a result, it is proposed that dioxygenases may function as iron sensors though it remains to be seen whether these enzymes play an extensive role in physiological iron sensing. Iron's role in the hypoxic response pathway has been further underscored by the recent discovery of an IRE within the 5' UTR of HIF-2α (Sanchez et al., 2007). Consequently, HIF-2α translation is downregulated in

states of iron deficiency, and upregulated in iron excess (Sanchez et al., 2007). HIF-2α function can also be altered by small molecules that modulate the binding of IRP1 to IREs (Zimmer et al., 2008). The physiological importance of this additional layer of regulation remains to be studied though it could serve to limit hypoxia-induced erythropoiesis when body iron stores are limited (Sanchez et al., 2007).

Oxygen or iron deficiency can in turn, alter cellular iron homeostasis following HIF induction. HIF binds to HREs found within several genes involved in iron metabolism (Table IV-2), promoting iron uptake from serum, iron scavenging, and iron retention. HIF is also known to impact systemic iron homeostasis. For example, HIF-2α directly mediates dietary iron absorption through transcription of genes involved in IEC iron transport (Mastrogiannaki et al., 2009), underlying an observation made nearly 50 years ago that hypoxia increases dietary iron absorption through the intestine (Mendel, 1961). The hypoxia response pathway was also found to be crucial to the regulation of the systemic hormone, hepcidin (Peyssonnaux et al., 2007); (Nicolas et al., 2002). HIF-1 induction, resulting from hypoxia or reduced iron availability, represses hepcidin expression in the liver upon binding to HREs within the hepcidin promoter. Reduced hepcidin levels should in turn enhance absorption of dietary iron to compensate.

In addition to mediating HIF-dependent induction of genes involved in iron homeostasis, oxygen levels have also been known to directly influence cellular iron levels through the IRP pathway. Oxygen can influence IRP1 activity in cells by affecting the stability of its iron sulfur cluster (Meyron-Holtz et al., 2004b). With respect to IRP2, hypoxia promotes its RNA binding activity through increased stability, even under iron replete conditions that usually favor its degradation (Hanson et al., 2003). Though several models have been proposed to explain how cellular iron and oxygen levels are sensed and translated to changes in IRP2 regulation, the responsible mechanisms remain poorly understood (Pantopoulos, 2004) .

A Candidate Iron and Oxygen Sensor Governing IRP Stability

Our laboratory has recently identified an iron-regulated E3 ligase that mediates the iron dependent degradation of IRP2 (Salahudeen et al., Submitted). This E3 ligase, a member of the Skp-Cullin-F-box (SCF) complex class of E3 ligases, interacts with IRP2 and can catalyze its polyubiquitination *in vitro*. The F-box-containing subunit of this SCF complex, FBXL5, is regulated by iron at the level of its own protein stability: FBXL5 is stabilized under iron-replete conditions and degraded when cellular iron availability is low. Iron-dependent regulation is conferred by an iron- and dioxygen-binding domain located within FBXL5's N-terminus. In the presence of iron, this region folds into a hemerythrin

domain, previously only found in marine invertebrates and bacteria where they frequently serve as oxygen carriers (Stenkamp, 1994). Structurally, the hemerythrins form an alpha helical bundle, wherein they directly bind to two iron atoms through carboxylate and imidazole side chains of its amino acids (Figure IV-5). The two iron atoms form a μ-oxo diiron center contained within the hydrophobic core of the alpha helical bundle, and can reversibly bind dioxygen (Figure IV-5) (Stenkamp, 1994).

In the setting of iron sensing and IRP2 ubiquitination, FBXL5 may sense iron and oxygen concentrations through the stability of its hemerythrin domain. In the absence of iron and oxygen, the hemerythrin domain is unstable. Unfolding of the hemerythrin domain appears to unmask a degron for an as-yet unidentified E3 ligase to promote FBXL5 degradation. This decrease in FBXL5 protein accumulation results in a corresponding increase in IRP2 stability. Conversely, in settings of high iron and oxygen the hemerythrin domain is stabilized, concealing the FBXL5 degron. The ensuing increase in its stability allows FBXL5 to assemble into an SCF complex capable of catalyzing the polyubiquitination and degradation of IRP2 (Figure IV-5).

Summary

Coordinate regulation of iron and oxygen homeostasis facilitate appropriate responses to perturbations of either of these metabolites at the cellular level. In cells, the HIF and IRP pathways respond to changes in both iron and oxygen levels. We now know of enzymes in each pathway that are capable of directly sensing and signaling changes in cellular iron and oxygen levels: dioxygenases for HIF and the hemerythrin containing FBXL5 for IRPs (Figure IV-5). By binding both iron and oxygen, these sensors provide a basis for cross-talk between these pathways. Furthermore, cells exhibit cross-talk between the HIF and IRP pathway through overlapping control of gene expression. This cross-talk between iron and oxygen homeostasis pathways at the cellular level may also be extended to the systemic level. In addition, coordinate regulation of oxygen and iron homeostasis may be achieved indirectly through a variety of other mechanisms not discussed here (Hentze and Kuhn, 1996; Taylor, 2008). Together, these observations provide new insights and opportunities to address diseases stemming from misregulation of oxygen and iron homeostasis, including anemia, iron overload disorders, susceptibility to infection, ischemic damage, and cancer.

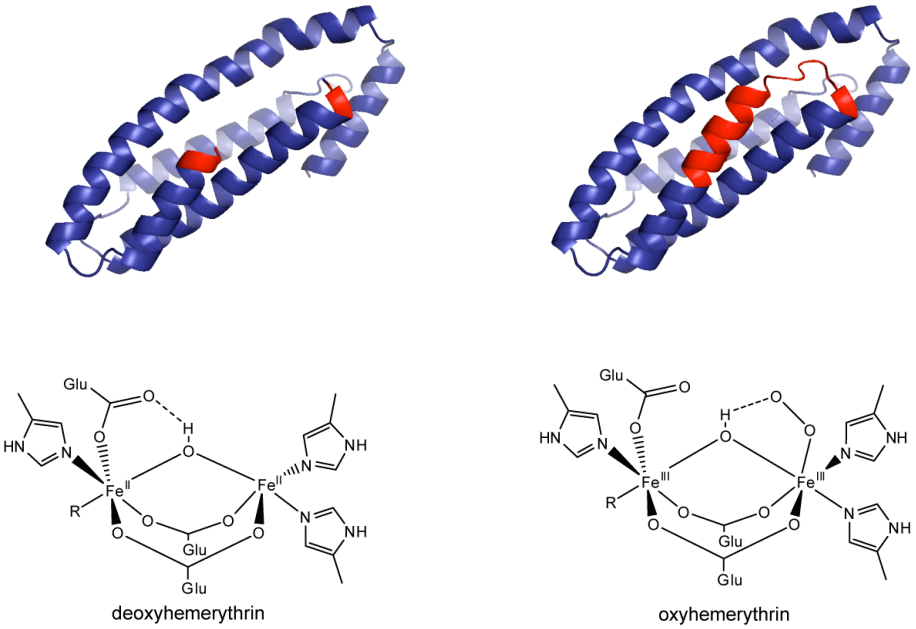

Figure IV-1.

FBXL5's proposed mechanism of oxygen sensing. In the absence of oxygen, a glutamate residue (E58) hydrogen bonds to the μ-hydroxo hydrogen. In the oxy state, the oxygen bound to the pentacoordinate iron competes with E58 to form a hydrogen bond with the μ-oxo hydrogen. This potential conformational change could result in alterations in the structure of the Hr domain, particularly the disordered third helix which encompasses a putative degron (Figure III-39). In this scenario, the third helix (delineated in red), moves from an unstructured to a structured state as a consequence of oxygen binding and displacing E58. As a result, the degron would be further masked from recognition by a separate E3 ligase. In the absence of oxygen, the third helix would be less ordered and the degron less sequestered. Therefore, the hemerythrin domain would be subjected to greater rates of ubiquitination and proteasomal degradation.

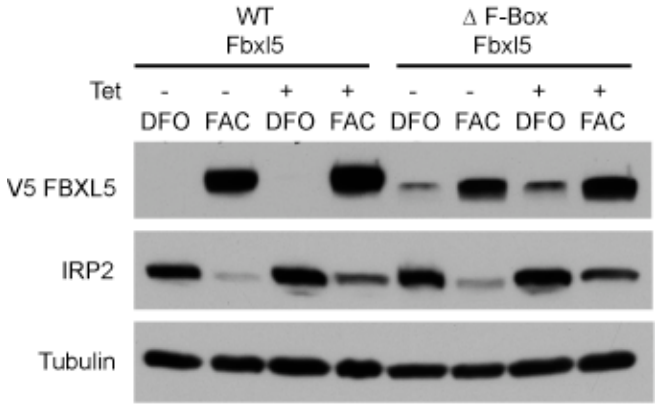

Figure IV-2.

Immunoblots of 293 TRex FBXL5 shRNA cells. Endogenous FBXL5 was suppressed (Tet +), and cells were transfected with wildtype FBXL5 or FBXL5 lacking its F-box domain.

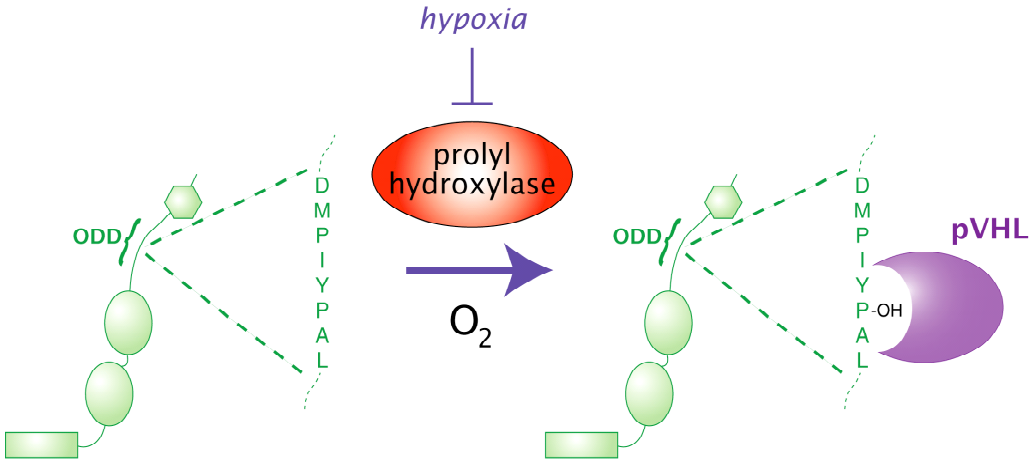

Figure IV-3.

HIF regulation by iron and oxygen levels. Under normoxic conditions, HIF-α is targeted for degradation by the VHL-containing E3 ubiquitin ligase complex. VHL recognizes HIF-α following hydroxylation of proline residues by Fe(II)- and 2-oxoglutarate-dependent dioxygenases (top). These enzymes utilize iron in their active sites (bottom) to activate dioxygen. Under conditions of low oxygen and/or iron, HIF-α cannot be hydroxylated and is spared from degradation.

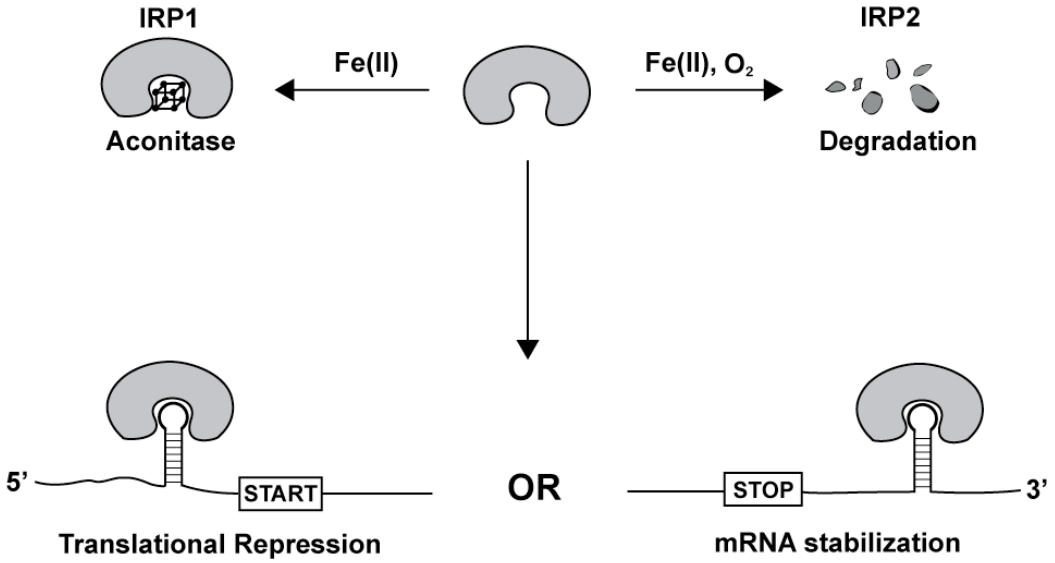

Figure IV-4.

Iron dependent regulation of the IRPs. In states of low iron, IRPs are capable of binding Iron Response Elements (IREs) in the 5' or 3' (UTR) in mRNAs of genes contributing to iron homeostasis. IRP binding in turn blocks translation initiation or mRNA degradation, respectively. In states of high iron, IRP1 loses its IRE binding activity following assembly of an iron sulfur cluster and conversion to a cytosolic aconitase. In contrast, IRP2 is polyubiquitinated and degraded by the proteasome under iron and oxygen replete conditions.

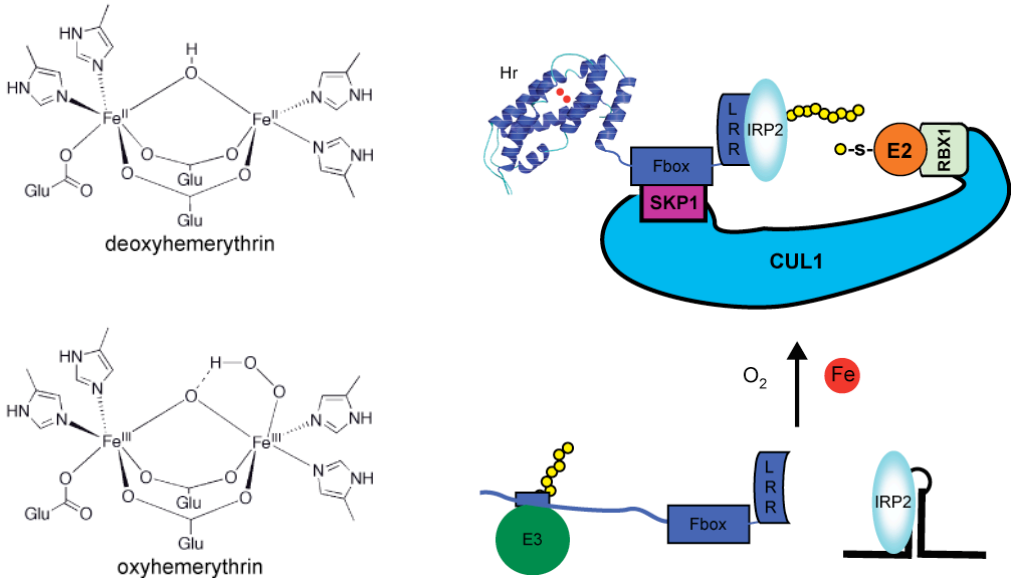

Figure IV-5.

Model of the hemerythrin iron and oxygen binding site. Imidazole and carboxylate residues from conserved amino acid side chains bind a diiron center connected by a bridging oxygen atom (μ-oxo). Oxygen can be reversibly bound onto the pentacoordinate iron and forms a peroxo radical species that is stabilized by protonation and coordination to the bridging oxygen atom.

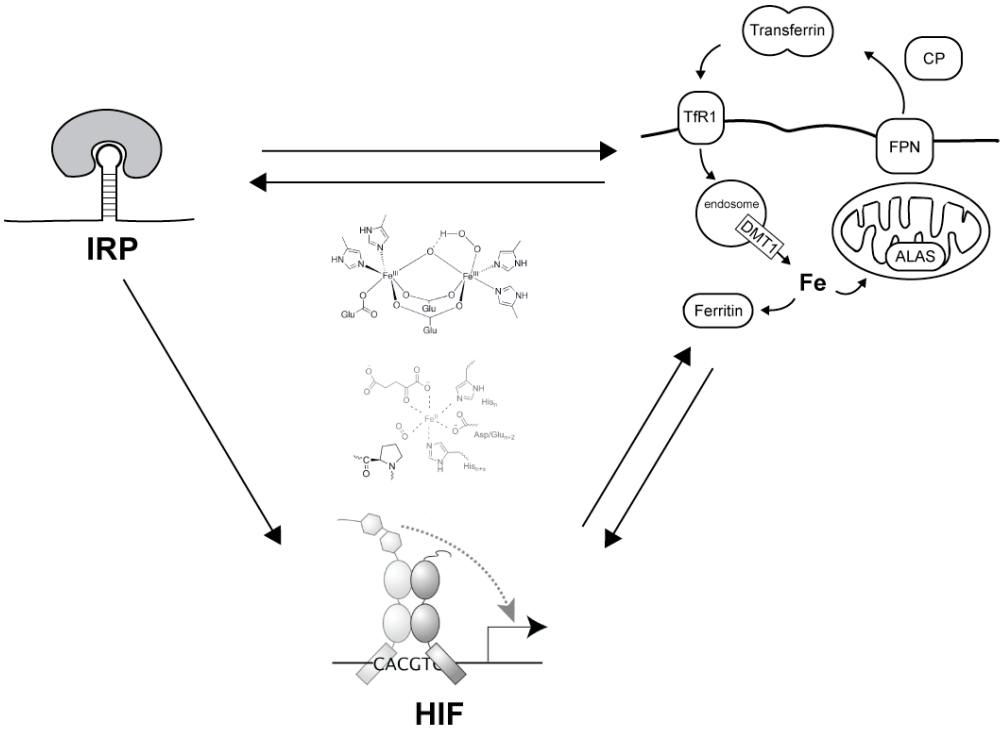

Figure IV-6.

Cross-talk between pathways mediating iron and oxygen homeostasis. At the cellular level, both iron and oxygen are sensed by dioxygenases and hemerythrin to regulate HIF-α and IRP2 stability, respectively. In addition, the HIF and IRP pathways are intertwined at the level of target gene expression, as the HIF-2α 5' UTR contains an IRE while both HIF and IRPs mediate expression of genes involved in cellular and systemic iron homeostasis.

TABLE IV-1. HIF Target genes involved in iron homeostasis.

Gene Symbol	Protein Name	Proposed Function
CP[a]	Ceruloplasmin	Iron oxidation in bloodstream
DMT1[b,c]	Divalent Metal Transporter 1	Intestinal iron import
HAMP[d,e]	Hepcidin	Systemic iron effector
HMOX1[f]	Heme Oxygenase-1	Heme catabolism
TFRC[a]	Transferrin Receptor	Cellular iron uptake
TF[f,g]	Transferrin	Serum iron transport

a. Peyssonnaux et al., 2008.
b. Shah et al., 2009.
c. Mastrogiannaki et al., 2009.
d. Peyssonnaux et al., 2007.
e. HIF represses transcription of Hepcidin.
f. Manalo, et al., 2005.
g. Xia et al., 2009.

APPENDIX

Protein Identification Results of Trypsin Digestion of FLAG-IRP2 Pulldown Samples (Section IIC)

Hit	Protein Name	GI No.	Score	MW (kDa)	Pep. No.	Peptide Sequence
1	Iron-responsive element-binding protein 2 (IRE-BP 2) (Iron regulatory protein 2) (IRP2)	gil1352477	4012	104.9 kDa	39	
2	iron-regulatory protein 2	gil897581	3808	104.0 kDa	37	
3	Skb1Hs [Homo sapiens]	gil2323410	1778	72.7 kDa	22	
4	heat shock 70kDa protein 1A variant [Homo sapiens]	gil62089222	1439	77.4 kDa	26	
6	unnamed protein product [Homo sapiens]	gil14042637	730	17.5 kDa	7	
7	kinesin family member 11 [Homo sapiens]	gil13699824	653	119.1 kDa	22	
8	WD repeat domain 77 [Homo sapiens]	gil13129110	549	36.7 kDa	9	
9	beta-spectrin	gil338443	518	274.5 kDa	22	
11	SPTAN1 protein [Homo sapiens]	gil31565122	440	282.1 kDa	17	
12	Chain A, Crystal Structure Of 3-Mbt Repeats Of Lethal (3) Malignant Brain Tumor (Seleno-Met) At 1.8	gil34810502	391	37.6 kDa	1	HLFVSQSHSPPPLGFQVGSKLEAVDR
14	RNA-binding protein 10 (RNA-binding motif protein 10) (G patch domain-containing protein 9)	gil12644371	344	103.4 kDa	11	
15	Eukaryotic translation initiation factor 4B [Homo sapiens]	gil49256408	329	69.1 kDa	4	
16	serine/threonine kinase 38 [Homo sapiens]	gil6005814	327	54.2 kDa	12	
17	beta actin variant [Homo sapiens]	gil62897625	306	41.7 kDa	9	
19	tubulin, beta, 2 [Homo sapiens]	gil5174735	267	49.8 kDa	11	
20	heat shock 70kDa protein 8 isoform 1 [Homo sapiens]	gil5729877	238	70.9 kDa	12	
21	hypothetical protein [Homo sapiens]	gil4914604	192	55.4 kDa	8	
22	Chain , The Solution Structure Of The Second Kunitz Domain Of Tissue Factor Pathway Inhibitor, Nm	gil2982026	176	8.4 kDa	3	
23	tubulin alpha 6 [Homo sapiens]	gil14389309	163	49.9 kDa	5	
24	hypothetical protein LOC144097 [Homo sapiens]	gil39930523	163	41.0 kDa	4	
25	gelsolin isoform a precursor [Homo sapiens]	gil4504165	162	85.6 kDa	6	
26	spindlin 1 [Homo sapiens]	gil11559844	161	27.1 kDa	6	
27	serologically defined breast cancer antigen NY-BR-99 [Homo sapiens]	gil12060857	148	30.9 kDa	6	
28	unnamed protein product [Homo sapiens]	gil32488	146	84.6 kDa	5	
29	alpha-actin	gil178027	146	42.1 kDa	6	
30	NS1-binding protein [Homo sapiens]	gil3851214	145	69.0 kDa	6	
31	[Human pre-mRNA splicing factor SF2p32, complete sequence.], gene product	gil338043	135	30.9 kDa	5	
32	chloride channel, nucleotide-sensitive, 1A [Homo sapiens]	gil4502891	131	26.2 kDa	3	
33	heterogeneous nuclear ribonucleoprotein H1 [Homo sapiens]	gil5031753	126	49.2 kDa	3	
34	poly A binding protein, cytoplasmic 4 [Homo sapiens]	gil4504715	123	70.7 kDa	5	
35	nucleolin	gil189306	123	76.3 kDa	4	
36	Chain L, Crystal Structure Of Fab Fragment Complexed With Gibberellin A4	gil24158782	123	23.7 kDa	2	
37	hnRNP U protein [Homo sapiens]	gil32358	120	88.9 kDa	5	
38	translation initiation factor [Homo sapiens]	gil496902	115	46.8 kDa	3	
39	uracil DNA glycosylase [Homo sapiens]	gil35053	115	35.5 kDa	4	
40	histone H2A.2 [Homo sapiens]	gil31979	113	13.9 kDa	1	AMGIMNSFVNDIFER
41	Chain A, Glutathione S-Transferase (E.C.2.5.1.18) (Class Pi)	gil494066	111	23.2 kDa	2	
42	Chain A, Human Transcriptional Coactivator Pc4 C-Terminal Domain	gil2981801	111	7.8 kDa	3	
43	eukaryotic translation initiation factor 3, subunit 5 epsilon, 47kDa [Homo sapiens]	gil4503519	105	37.5 kDa	1	IQDALSTVLQYAEDVLSGK
44	ribosomal protein P2 [Homo sapiens]	gil4506671	105	11.7 kDa	3	
45	90kDa heat shock protein	gil306891	104	83.2 kDa	5	
46	insulin-like growth factor 2 mRNA binding protein 3 [Homo sapiens]	gil30795212	103	63.7 kDa	4	
47	DNA-binding protein B	gil181486	103	40.0 kDa	3	
48	2-phosphopyruvate-hydratase alpha-enolase; carbonate dehydratase [Homo sapiens]	gil693933	102	47.1 kDa	6	
49	spliceosomal protein SAP 130 [Homo sapiens]	gil6006515	101	135.5 kDa	5	
50	anti-colorectal carcinoma heavy chain [Homo sapiens]	gil425518	101	50.6 kDa	4	
51	C protein	gil306875	100	31.9 kDa	3	
52	mitogen-activated protein kinase kinase kinase 7 interacting protein 1 isoform beta [Homo sapiens]	gil41281798	95	49.9 kDa	5	
53	beta-subunit (AA 1-312) [Homo sapiens]	gil28931	94	34.0 kDa	2	
54	protein phosphatase 1B isoform 2 [Homo sapiens]	gil29558022	94	42.7 kDa	6	
55	eukaryotic initiation factor 4AII [Homo sapiens]	gil485388	91	46.4 kDa	1	MFVLDEADEMLSR
56	cofilin 1 (non-muscle), isoform CRA_c [Homo sapiens]	gil119594857	90	15.6 kDa	2	
57	unnamed protein product [Homo sapiens]	gil28243	88	280.6 kDa	5	
58	CD68 antigen variant [Homo sapiens]	gil62088766	87	42.4 kDa	3	
59	eukaryotic translation initiation factor 4A isoform 1 [Homo sapiens]	gil4503529	86	46.1 kDa	4	
60	heterogeneous nuclear ribonucleoprotein F [Homo sapiens]	gil4826760	86	45.6 kDa	3	
61	unnamed protein product [Homo sapiens]	gil32111	83	14.2 kDa	2	
62	reticulocalbin 2, EF-hand calcium binding domain [Homo sapiens]	gil4506457	81	36.9 kDa	2	

63	ribosomal protein P1 isoform 1 [Homo sapiens]	gil4506669	81	11.5 kDa	1	AAGVNVEPFWPGLFAK
64	tyrosine 3/tryptophan 5 -monooxygenase activation protein, epsilon polypeptide [Homo sapiens]	gil5803225	81	29.2 kDa	2	
65	heterogeneous nuclear ribonucleoprotein A2/B1 isoform A2 [Homo sapiens]	gil4504447	77	36.0 kDa	1	LFIGGLSFETTEESLR
66	small nuclear ribonucleoprotein D1 polypeptide 16kDa [Homo sapiens]	gil5902102	77	13.3 kDa	1	YFILPDSLPLDTLLVDVEPK
67	Tyrosine-protein kinase JAK1 (Janus kinase 1) (JAK-1)	gil125060	77	131.9 kDa	3	
68	tyrosine 3/tryptophan 5 -monooxygenase activation protein, zeta polypeptide [Homo sapiens]	gil4507953	75	27.7 kDa	1	GIVDQSQQAYQEAFEISK
69	serine/threonine kinase 38 like [Homo sapiens]	gil24307971	75	54.0 kDa	8	
70	IGF2 mRNA-binding protein 1 isoform [Homo sapiens]	gil78523098	75	48.6 kDa	4	
71	Chain A, Solution Structure Of Calcium-Calmodulin N-Terminal	gil16974825	73	8.5 kDa	3	
72	Rig homolog [human, brain, Peptide Partial, 135 aa]	gil262391	72	15.8 kDa	2	
73	t-complex polypeptide 1 [Homo sapiens]	gil36796	72	60.4 kDa	3	
74	ribosomal protein L19 [Homo sapiens]	gil4506609	71	23.5 kDa	1	VWLDPNETNEIANANSR
75	6-phosphofructo-2-kinase/fructose-2,6-bisphosphatase [Homo sapiens]	gil2827312	69	59.5 kDa	2	
76	DnaJ protein homolog [Homo sapiens]	gil219588	68	44.8 kDa	2	
77	ribosomal protein L10 [Homo sapiens]	gil3164202	67	9.4 kDa	1	FNADEFEDMVAEK
78	78 kDa glucose-regulated protein precursor (GRP 78) (Heat shock 70 kDa protein 5) (Immunoglobulin h	gil2506545	67	72.4 kDa	4	
79	[Human mRNA, complete cds.], gene product	gil348239	65	54.2 kDa	2	
80	scar protein	gil337930	64	27.4 kDa	3	
81	14-3-3 gamma protein [Homo sapiens]	gil5726310	64	28.4 kDa	1	NVTELNEPLSNEER
82	BOLA2 protein [Homo sapiens]	gil38541696	62	6.8 kDa	1	DLEAEHVEVEDTTLNR
83	ribosomal protein L3	gil337580	62	45.4 kDa	3	
84	transgelin 2 [Homo sapiens]	gil4507357	61	22.4 kDa	1	YGINTTDIFQTVDLWEGK
86	Myosin-10 (Myosin heavy chain 10) (Myosin heavy chain, nonmuscle IIb) (Nonmuscle myosin heavy chain	gil1346640	61	228.8 kDa	3	
87	actin-like protein [Homo sapiens]	gil62420995	61	11.4 kDa	2	
88	chaperonin [Homo sapiens]	gil31542947	61	61.0 kDa	3	
89	hRlf beta subunit (p102 protein) [Homo sapiens]	gil1552242	60	90.9 kDa	1	TPMENIGLQDSLLSR
90	TTP1 [Homo sapiens]	gil15426038	60	20.1 kDa	1	EQPGDLFNEDWDSELK
91	PREDICTED: similar to cytoplasmic beta-actin [Homo sapiens]	gil88942898	60	17.1 kDa	2	
92	ribosomal protein S3a [Homo sapiens]	gil4506723	59	29.9 kDa	1	VFEVSLADLQNDEVAFR
93	eIF-3 p110 subunit [Homo sapiens]	gil1931584	58	105.3 kDa	2	
94	ornithine aminotransferase, OAT [human, gyrate atrophy of the choroid and retina (GACR) patient, Pe	gil1168056	58	48.5 kDa	1	AFYNNVLGEYEEYITK
95	phosphoribosyl pyrophosphate synthetase 2, isoform CRA_a [Homo sapiens]	gil119619211	58	25.7 kDa	1	FSNQETSVEIGESVR
96	unnamed protein product [Homo sapiens]	gil36102	57	34.1 kDa	1	LFIGGLSFETTDESLR
97	eukaryotic translation elongation factor 2 [Homo sapiens]	gil4503483	56	95.3 kDa	1	ALLELQLEPEELYQTFQR
98	cullin 1 [Homo sapiens]	gil21358757	56	30.5 kDa	2	
99	hypothetical protein [Homo sapiens]	gil6807907	55	47.5 kDa	3	
100	Sad1 unc-84 domain protein 2 [Homo sapiens]	gil6538749	55	49.2 kDa	2	
101	unnamed protein product [Homo sapiens]	gil37848	54	14.8 kDa	1	LLQDSVDFSLADAINTEFK
102	myosin	gil531143	54	9.7 kDa	1	GDPLGGVISNYLLEK
103	myosin regulatory light chain MRCL3 [Homo sapiens]	gil5453740	53	19.8 kDa	2	
104	tropomodulin 3 [Homo sapiens]	gil6934244	53	39.6 kDa	3	
105	Chain B, Core Of The Alu Domain Of The Mammalian Srp	gil11513833	52	12.1 kDa	1	VLLESEQFLTELTR
106	MHC class I antigen [Homo sapiens]	gil9187989	51	21.2 kDa	1	APWVEKEGPEYWDR
107	Chain , Thioredoxin (Reduced Form)	gil230939	51	11.7 kDa	1	TAFQEALDAAGDK
108	ribosomal protein S24 isoform c [Homo sapiens]	gil4506703	50	15.4 kDa	1	TTGFGMIYDSLDYAK
109	ribosomal protein L7a [Homo sapiens]	gil4506661	50	30.0 kDa	1	AGVNTVTTLVENK
110	ribosomal protein S8 [Homo sapiens]	gil4506743	50	24.2 kDa	2	
111	KIAA1470 protein [Homo sapiens]	gil7959201	49	60.4 kDa	1	DVACGANHTLVLDSQK
112	small nuclear ribonucleoprotein polypeptide D3 [Homo sapiens]	gil4759160	49	13.9 kDa	1	VLHEAEGHIVTCETNTGEVYR
113	immunoglobulin kappa light chain [Homo sapiens]	gil21311289	48	14.4 kDa	1	ASGVPDRISGSGSGTDFTLK
114	Srp20 [Mus musculus]	gil2125864	48	14.2 kDa	1	NPPGFAFVEFEDPR
115	elongation factor Tu	gil704416	47	49.5 kDa	1	TIGTGLVTNTLAMTEEEK
116	ribosomal protein L7 [Homo sapiens]	gil35903	47	29.2 kDa	1	YGIICMEDLIHEIYTVGK
117	RNF111 protein [Homo sapiens]	gil14714485	46	15.7 kDa	1	MVPDMAGYPHIR
118	S-adenosylmethionine decarboxylase proenzyme (EC 4.1.1.50) old gene name AMD	gil178518	46	38.3 kDa	1	DYSGFDSIQSFFYSR
119	smooth muscle myosin alkali light chain	gil467828	46	17.6 kDa	2	
120	Malate dehydrogenase, mitochondrial precursor	gil6648067	45	35.5 kDa	1	VAVLGASGGIGQPLSLLLK
121	unnamed protein product [Homo sapiens]	gil10437832	45	111.7 kDa	1	ILNLYTPLNEFEER

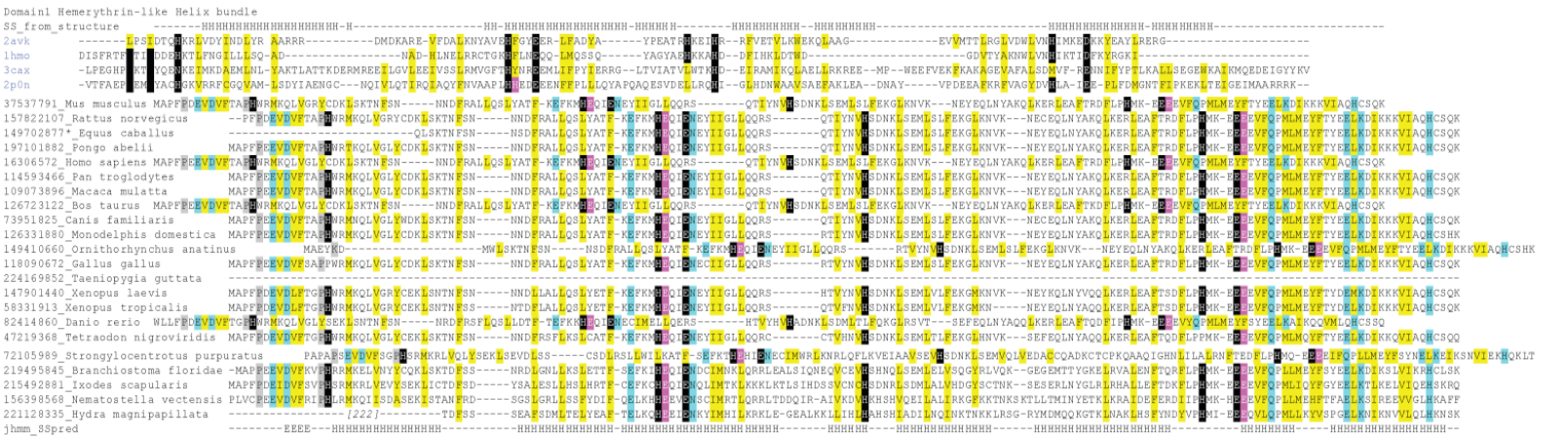

Multiple Sequence Alignment of FBXL5's Hemerythrin Domain

Crystallization of FBXL5's Hemerythrin Domain

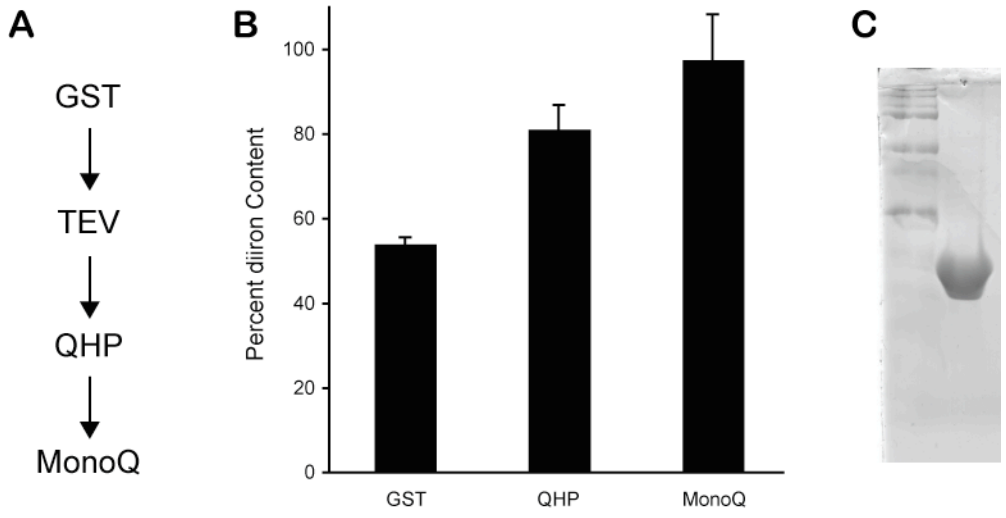

Purification of FBXL5's Hemerythrin domain. (A) Purification scheme of the hemerythrin domain (B) diiron content at each stage of the purification, (percentage of a 2:1 iron to protein molar stochiometry) measured by ferene and Bradford reagents. (C) Coomassie Brilliant Blue staining of the final purified domain.

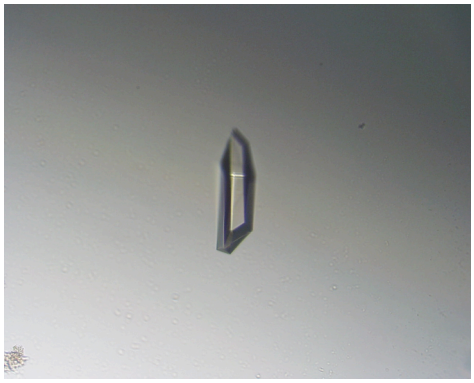
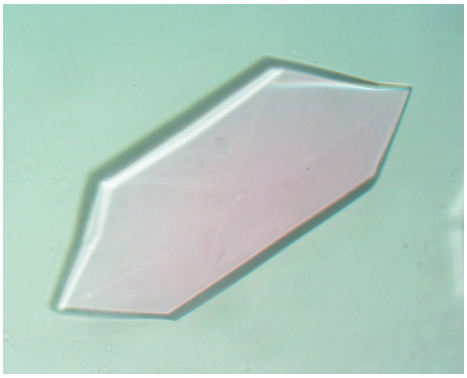
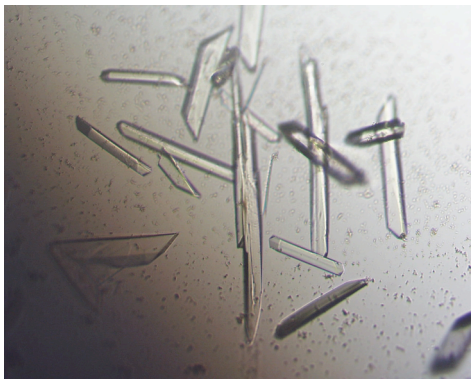
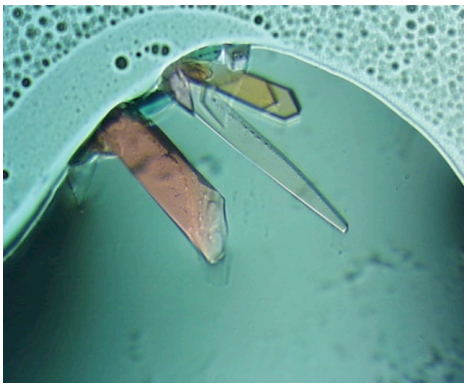
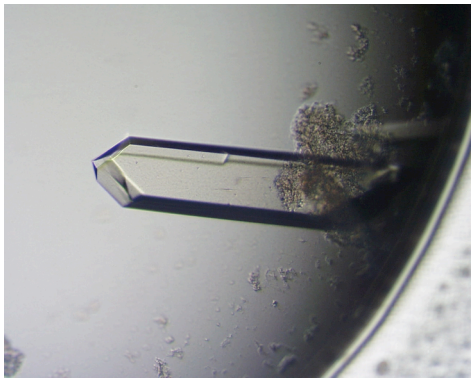

Microscopic images of FBXL5 hemerythrin domain crystals grown in 0.1M HEPES pH 6.5 (final pH 7.0), 10% PEG 6,000.

Data Collection, Phasing, and Refinement Statistics for FBXL5 Structure

Data collection			
Crystal	Native	Fe[a] *peak*	Fe[a] *inflection point*
Energy (eV)	12,559.6	7122.6	7118.8
Resolution range (Å)	44.7 – 1.84 (1.88-1.84)	44.7-2.50 (2.54-2.50)	44.7-2.50 (2.54-2.50)
Unique reflections	28,254 (1,433)	11,365 (564)	11,319 (574)
Multiplicity	5.0 (5.0)	4.9 (4.0)	4.9 (3.9)
Data completeness (%)	99.8 (100.0)	99.6 (98.9)	99.5 (99.0)
R_{merge} (%)[b]	4.7 (69.0)	5.5 (11.2)	4.8 (9.8)
I/σ(I)	29.2 (2.0)	55.6 (19.2)	53.6 (19.2)
Wilson B-value (Å^2)	29.8	50.3	
Phase determination			
Anomalous scatterers	iron, 4 out of 4 possible sites; sulfur, 2 sites[c]		
Figure of merit (44.7-2.50 Å)	0.59 (0.85 after density modification)		
Refinement statistics			
Resolution range (Å)	36.5 -1.84 (1.91-1.84)		
No. of reflections R_{work}/R_{free}	28,240/1,427 (2,549/129)		
Data completeness (%)	99.4 (95.0)		
Atoms (non-H protein/solvent/other)	2,350/81/4		
R_{work} (%)	23.2 (24.9)		
R_{free} (%)	26.8 (30.7)		
R.m.s.d. bond length (Å)	0.005		
R.m.s.d. bond angle (°)	0.812		

Mean B-value (Å^2) (protein/solvent)	34.6/40.3
Ramachandran plot (%) (favored/additional/disallowed)[d]	99.3/0.7/0.0
Maximum likelihood coordinate error	0.57
Missing residues	Chain A: 1-5, 72-84, 159-161. Chain B: 1-5, 67-84, 160-161.
Alternate conformations	None

Data for the outermost shell are given in parentheses.

[a]Bijvoet-pairs were kept separate for data processing

[b]$R_{\text{merge}} = 100\ \Sigma_h\Sigma_i|I_{h,\ i} - \langle I_h\rangle|/\Sigma_h\Sigma_i I_{h,\ i}$, where the outer sum (h) is over the unique reflections and the inner sum (i) is over the set of independent observations of each unique reflection.

[c]Two well-ordered methionine sulfur atoms were located in *SHELXD* and refined in *MLPHARE.*

[d]As defined by the validation suite MolProbity (Davis, I.W., Leaver-Fay, A., Chen, V.B., Block, J.N., Kapral, G.J., Wang, X., Murray, L.W., Arendall, W.B., Snoeyink, J., Richardson, J.S. and Richardson, D.C. (2007) MolProbity: all-atom contacts and structure validation for proteins and nucleic acids. Nucleic Acids Res. *35*, W375-W383.).

BIBLIOGRAPHY

Adams, P.D., Grosse-Kunstleve, R.W., Hung, L.-W., Ioerger, T.R., McCoy, A.J., Moriarty, N.W., Read, R.J., Sacchettini, J.C., Sauter, N.K. and Terwilliger, T.C. (2002) PHENIX: building new software for automated crystallographic structure determination. Acta Cryst. *D58*, 1948-1954.

Andrews, N.C. (2008). Forging a field: the golden age of iron biology. Blood *112*, 219-230.

Ardley, H.C., and Robinson, P.A. (2005). E3 ubiquitin ligases. Essays Biochem *41*, 15-30.

Beinert, H. (1978). Micro methods for the quantitative determination of iron and copper in biological material. Methods in Enzymology *54*, 435-445.

Beutler, E. (2006). Hemochromatosis: genetics and pathophysiology. Annu Rev Med *57*, 331-347.

Bourdon, E., Kang, D.K., Ghosh, M.C., Drake, S.K., Wey, J., Levine, R.L., and Rouault, T.A. (2003). The role of endogenous heme synthesis and degradation domain cysteines in cellular iron-dependent degradation of IRP2. Blood Cells Mol Dis *31*, 247-255.

Bruick, R.K., and McKnight, S.L. (2001). A conserved family of prolyl-4-hydroxylases that modify HIF. Science *294*, 1337-1340.

Caron, P.R., Watt, P., and Wang, J.C. (1994). The C-terminal domain of Saccharomyces cerevisiae DNA topoisomerase II. Mol Cell Biol *14*, 3197-3207.

Casey, J.L., Hentze, M.W., Koeller, D.M., Caughman, S.W., Rouault, T.A., Klausner, R.D., and Harford, J.B. (1988). Iron-responsive elements: regulatory RNA sequences that control mRNA levels and translation. Science *240*, 924-928.

Chen, D., Kon, N., Li, M., Zhang, W., Qin, J., and Gu, W. (2005). ARF-BP1/Mule is a critical mediator of the ARF tumor suppressor. Cell *121*, 1071-1083.

Clarke, S.L., Vasanthakumar, A., Anderson, S.A., Pondarre, C., Koh, C.M., Deck, K.M., Pitula, J.S., Epstein, C.J., Fleming, M.D., and Eisenstein, R.S. (2006). Iron-responsive degradation of iron-regulatory protein 1 does not require the Fe-S cluster. EMBO J *25*, 544-553.

Cowtan, K. and Main, P. (1998) Miscellaneous algorithms for density modification. Acta Cryst. *D54*, 487-493.

Crichton, R.R. (2009). Iron Metabolism: From Molecular Mechanisms to Clinical Consequences 3rd edn (Wiley).

Davis, I.W., Leaver-Fay, A., Chen, V.B., Block, J.N., Kapral, G.J., Wang, X., Murray, L.W., Arendall, W.B., Snoeyink, J., Richardson, J.S. and Richardson, D.C. (2007) MolProbity: all-atom contacts and structure validation for proteins and nucleic acids. Nucleic Acids Res. *35*, W375-W383.

De Domenico, I., Ward, D.M., Langelier, C., Vaughn, M.B., Nemeth, E., Sundquist, W.I., Ganz, T., Musci, G., and Kaplan, J. (2007). The molecular mechanism of hepcidin-mediated ferroportin down-regulation. Mol Biol Cell *18*, 2569-2578.

Dycke, C., Bougault, C., Gaillard, J., Andrieu, J.P., Pantopoulos, K., and Moulis, J.M. (2007). Human iron regulatory protein 2 is easily cleaved in its specific domain: consequences for the haem binding properties of the protein. Biochem J *408*, 429-439.

Epstein, A.C., Gleadle, J.M., McNeill, L.A., Hewitson, K.S., O'Rourke, J., Mole, D.R., Mukherji, M., Metzen, E., Wilson, M.I., Dhanda, A.*, et al.* (2001). C. elegans EGL-9 and mammalian homologs define a family of dioxygenases that regulate HIF by prolyl hydroxylation. Cell *107*, 43-54.

Fenton, H.J.H. (1894). Oxidation of tartaric acid in presence of iron. J Chem Soc, Trans *65*, 899-911.

Fishback, F.A.H., P.M.; Hoy, T.G. (1969). J Mol Biol *39*, 235.

Fleming, M.D., Romano, M.A., Su, M.A., Garrick, L.M., Garrick, M.D., and Andrews, N.C. (1998). Nramp2 is mutated in the anemic Belgrade (b) rat: evidence of a role for Nramp2 in endosomal iron transport. Proc Natl Acad Sci U S A *95*, 1148-1153.

Fleming, M.D., Trenor, C.C., 3rd, Su, M.A., Foernzler, D., Beier, D.R., Dietrich, W.F., and Andrews, N.C. (1997). Microcytic anaemia mice have a mutation in Nramp2, a candidate iron transporter gene. Nat Genet *16*, 383-386.

Fleming, R., Britton, R., Migas, M., Rozier, M., Waheed, A., Sly, W. Regulation of Hepcidin by Dietary Iron in Mice with Functional Loss of HFE and Transferrin Receptor 2. (2009). Third Congress of the International BioIron Society. June 7-11. Porto, Portugal.

Galaris, D., and Pantopoulos, K. (2008). Oxidative stress and iron homeostasis: mechanistic and health aspects. Crit Rev Clin Lab Sci *45*, 1-23.

Galy, B., Ferring-Appel, D., Kaden, S., Grone, H.J., and Hentze, M.W. (2008). Iron regulatory proteins are essential for intestinal function and control key iron absorption molecules in the duodenum. Cell Metab *7*, 79-85.

Ganz, T. (2005). Hepcidin--a regulator of intestinal iron absorption and iron recycling by macrophages. Best Pract Res Clin Haematol *18*, 171-182.

Gietz, R.D., and Woods, R.A. (2002). Transformation of yeast by lithium acetate/single-stranded carrier DNA/polyethylene glycol method. Methods Enzymol *350*, 87-96.

Guo, B., Phillips, J.D., Yu, Y., and Leibold, E.A. (1995). Iron regulates the intracellular degradation of iron regulatory protein 2 by the proteasome. J Biol Chem *270*, 21645-21651.

Hanson, E.S., Rawlins, M.L., and Leibold, E.A. (2003). Oxygen and iron regulation of iron regulatory protein 2. J Biol Chem *278*, 40337-40342.

Harlow, E., and Lane, D. (1988). Antibodies: A Laboratory Manual (Cold Spring Harbor Laboratory Press).

Harrison, P.M.H., R.J.; Hoy, T.G.; Macara, I.G. (1974). Iron in Biochemistry and Medicine (New York, Academic Press).

Hennessy, D.J., Reid, G.R., Smith, F.E., and Thompson, S.L. (1984). Ferene - a new spectrophotometric reagent for iron. Canadian Journal of Chemistry *62*, 721.

Hentze, M.W., Caughman, S.W., Rouault, T.A., Barriocanal, J.G., Dancis, A., Harford, J.B., and Klausner, R.D. (1987). Identification of the iron-responsive

element for the translational regulation of human ferritin mRNA. Science *238*, 1570-1573.

Hentze, M.W., and Kuhn, L.C. (1996). Molecular control of vertebrate iron metabolism: mRNA-based regulatory circuits operated by iron, nitric oxide, and oxidative stress. Proc Natl Acad Sci U S A *93*, 8175-8182.

Hentze, M.W., Muckenthaler, M.U., and Andrews, N.C. (2004). Balancing acts: molecular control of mammalian iron metabolism. Cell *117*, 285-297.

Hershko, A., and Ciechanover, A. (1998). The ubiquitin system. Annu Rev Biochem *67*, 425-479.

Ishikawa, H., Kato, M., Hori, H., Ishimori, K., Kirisako, T., Tokunaga, F., and Iwai, K. (2005). Involvement of heme regulatory motif in heme-mediated ubiquitination and degradation of IRP2. Mol Cell *19*, 171-181.

Ivan, M., Haberberger, T., Gervasi, D.C., Michelson, K.S., Gunzler, V., Kondo, K., Yang, H., Sorokina, I., Conaway, R.C., Conaway, J.W.*, et al.* (2002). Biochemical purification and pharmacological inhibition of a mammalian prolyl hydroxylase acting on hypoxia-inducible factor. Proc Natl Acad Sci U S A *99*, 13459-13464.

Ivan, M., Kondo, K., Yang, H., Kim, W., Valiando, J., Ohh, M., Salic, A., Asara, J.M., Lane, W.S., and Kaelin, W.G., Jr. (2001). HIFalpha targeted for VHL-mediated destruction by proline hydroxylation: implications for O2 sensing. Science *292*, 464-468.

Iwai, K., Drake, S.K., Wehr, N.B., Weissman, A.M., LaVaute, T., Minato, N., Klausner, R.D., Levine, R.L., and Rouault, T.A. (1998). Iron-dependent oxidation, ubiquitination, and degradation of iron regulatory protein 2: implications for degradation of oxidized proteins. Proc Natl Acad Sci U S A *95*, 4924-4928.

Iwai, K., Klausner, R.D., and Rouault, T.A. (1995). Requirements for iron-regulated degradation of the RNA binding protein, iron regulatory protein 2. EMBO J *14*, 5350-5357.

Jaakkola, P., Mole, D.R., Tian, Y.M., Wilson, M.I., Gielbert, J., Gaskell, S.J., Kriegsheim, A., Hebestreit, H.F., Mukherji, M., Schofield, C.J.*, et al.* (2001).

Targeting of HIF-alpha to the von Hippel-Lindau ubiquitylation complex by O2-regulated prolyl hydroxylation. Science *292*, 468-472.

Jones, T. A., Zou, J. Y., Cowan, S. W., and Kjeldgaard. (1991) Improved methods for building protein models in electron density maps and the location of errors in these models, Acta Cryst. *A47* 110-119.

Koeller, D.M., Casey, J.L., Hentze, M.W., Gerhardt, E.M., Chan, L.N., Klausner, R.D., and Harford, J.B. (1989). A cytosolic protein binds to structural elements within the iron regulatory region of the transferrin receptor mRNA. Proc Natl Acad Sci U S A *86*, 3574-3578.

Kurtz, D.M., Jr. (1990). Oxo- and hydroxo-bridged diiron complexes: a chemical perspective on a biological unit. *Chemical Reviews 90*, 585-606.

Lando, D., Peet, D.J., Gorman, J.J., Whelan, D.A., Whitelaw, M.L., and Bruick, R.K. (2002). FIH-1 is an asparaginyl hydroxylase enzyme that regulates the transcriptional activity of hypoxia-inducible factor. Genes Dev *16*, 1466-1471.

LaVaute, T., Smith, S., Cooperman, S., Iwai, K., Land, W., Meyron-Holtz, E., Drake, S.K., Miller, G., Abu-Asab, M., Tsokos, M.*, et al.* (2001). Targeted deletion of the gene encoding iron regulatory protein-2 causes misregulation of iron metabolism and neurodegenerative disease in mice. Nat Genet *27*, 209-214.

Leibold, E.A., and Munro, H.N. (1988). Cytoplasmic protein binds in vitro to a highly conserved sequence in the 5' untranslated region of ferritin heavy- and light-subunit mRNAs. Proc Natl Acad Sci U S A *85*, 2171-2175.

Li, W., Bengtson, M.H., Ulbrich, A., Matsuda, A., Reddy, V.A., Orth, A., Chanda, S.K., Batalov, S., and Joazeiro, C.A. (2008). Genome-wide and functional annotation of human E3 ubiquitin ligases identifies MULAN, a mitochondrial E3 that regulates the organelle's dynamics and signaling. PLoS ONE *3*, e1487.

Lynch, S.R. (2005). The impact of iron fortification on nutritional anaemia. Best Pract Res Clin Haematol *18*, 333-346.

Mastrogiannaki, M., Matak, P., Keith, B., Simon, M.C., Vaulont, S., and Peyssonnaux, C. (2009). HIF-2alpha, but not HIF-1alpha, promotes iron absorption in mice. J Clin Invest.

Mendel, G.A. (1961). Studies on iron absorption. I. The relationships between the rate of erythropoiesis, hypoxia and iron absorption. Blood *18*, 727-736.
Meyron-Holtz, E.G., Ghosh, M.C., Iwai, K., LaVaute, T., Brazzolotto, X., Berger, U.V., Land, W., Ollivierre-Wilson, H., Grinberg, A., Love, P.*, et al.* (2004a). Genetic ablations of iron regulatory proteins 1 and 2 reveal why iron regulatory protein 2 dominates iron homeostasis. EMBO J *23*, 386-395.

Meyron-Holtz, E.G., Ghosh, M.C., and Rouault, T.A. (2004b). Mammalian tissue oxygen levels modulate iron-regulatory protein activities in vivo. Science *306*, 2087-2090.

Minor, W., Cymborowski, M., Otwinowski, Z. and Chruszcza, M. (2006) HKL-3000: the integration of data reduction and structure solution – from diffraction images to an initial model in minutes. Acta Cryst. *D62*, 859–866.

Morris, R. J., Zwart, P. H., Cohen, S., Fernandez, F. J., Kakaris, M., Kirillova, O., Vonrhein, C., Perrakis, A., and Lamzin, V. S. (2004) Breaking good resolutions with ARP/wARP, J Synch. Rad. *11*, 56-59.

Muckenthaler, M.U., Galy, B., and Hentze, M.W. (2008). Systemic iron homeostasis and the iron-responsive element/iron-regulatory protein (IRE/IRP) regulatory network. Annu Rev Nutr *28*, 197-213.

Nemeth, E., Tuttle, M.S., Powelson, J., Vaughn, M.B., Donovan, A., Ward, D.M., Ganz, T., and Kaplan, J. (2004). Hepcidin regulates cellular iron efflux by binding to ferroportin and inducing its internalization. Science *306*, 2090-2093.

Nicolas, G., Chauvet, C., Viatte, L., Danan, J.L., Bigard, X., Devaux, I., Beaumont, C., Kahn, A., and Vaulont, S. (2002). The gene encoding the iron regulatory peptide hepcidin is regulated by anemia, hypoxia, and inflammation. J Clin Invest *110*, 1037-1044.

Nordlund, P., and Eklund, H. (1995). Di-iron-carboxylate proteins. Curr Opin Struct Biol *5*, 758-766.

Ohgami, R.S., Campagna, D.R., Greer, E.L., Antiochos, B., McDonald, A., Chen, J., Sharp, J.J., Fujiwara, Y., Barker, J.E., and Fleming, M.D. (2005). Identification of a ferrireductase required for efficient transferrin-dependent iron uptake in erythroid cells. Nat Genet *37*, 1264-1269.

Otwinowski, Z. (1991) Maximum likelihood refinement of heavy atom parameters. In Wolf, W. Evans, P.R. and Leslie, A.G.W. (eds), *Isomorphous Replacement and Anomalous Scattering*. Science & Engineering Research Council, Cambridge, UK, pp. 80-86.

Ozer, A., and Bruick, R.K. (2007). Non-heme dioxygenases: cellular sensors and regulators jelly rolled into one? Nat Chem Biol *3*, 144-153.
Pantopoulos, K. (2004). Iron metabolism and the IRE/IRP regulatory system: an update. Ann N Y Acad Sci *1012*, 1-13.

Peyssonnaux, C., Nizet, V., and Johnson, R.S. (2008). Role of the hypoxia inducible factors HIF in iron metabolism. Cell Cycle *7*, 28-32.

Peyssonnaux, C., Zinkernagel, A.S., Schuepbach, R.A., Rankin, E., Vaulont, S., Haase, V.H., Nizet, V., and Johnson, R.S. (2007). Regulation of iron homeostasis by the hypoxia-inducible transcription factors (HIFs). J Clin Invest *117*, 1926-1932.

Piccinelli, P., and Samuelsson, T. (2007). Evolution of the iron-responsive element. RNA *13*, 952-966.

Pigeon, C., Ilyin, G., Courselaud, B., Leroyer, P., Turlin, B., Brissot, P., and Loreal, O. (2001). A new mouse liver-specific gene, encoding a protein homologous to human antimicrobial peptide hepcidin, is overexpressed during iron overload. J Biol Chem *276*, 7811-7819.

Prousek, J. (2007). Fenton chemistry in biology and medicine. . Pure Appl Chem *79*, 2325-2338.

Qiu, A., Jansen, M., Sakaris, A., Min, S.H., Chattopadhyay, S., Tsai, E., Sandoval, C., Zhao, R., Akabas, M.H., and Goldman, I.D. (2006). Identification of an intestinal folate transporter and the molecular basis for hereditary folate malabsorption. Cell *127*, 917-928.

Ramos, E., Phung, Y., Gabayan, V., Ganz, T., and Nemeth, E. (2009). The Pathogenesis of Hereditary Hemochromatosis. Third Congress of the International BioIron Society. June 7-11. Porto, Portugal.

Rouault, T.A. (2006). The role of iron regulatory proteins in mammalian iron homeostasis and disease. Nat Chem Biol *2*, 406-414.

Rouault, T.A., Hentze, M.W., Haile, D.J., Harford, J.B., and Klausner, R.D. (1989). The iron-responsive element binding protein: a method for the affinity purification of a regulatory RNA-binding protein. Proc Natl Acad Sci U S A *86*, 5768-5772.

Salahudeen, A.A., Thompson, J.T., Ruiz, J.C., Ma, H., Li, Q., Kinch, L.N., Grishin, N.V., and Bruick, R.K. (2009) An E3 Ligase Possessing an Iron Responsive Hemerythrin Domain Is a Regulator of Iron Homeostasis. Science. PMID: 19762597

Samaniego, F., Chin, J., Iwai, K., Rouault, T.A., and Klausner, R.D. (1994). Molecular characterization of a second iron-responsive element binding protein, iron regulatory protein 2. Structure, function, and post-translational regulation. J Biol Chem *269*, 30904-30910.

Sanchez, M., Galy, B., Muckenthaler, M.U., and Hentze, M.W. (2007). Iron-regulatory proteins limit hypoxia-inducible factor-2alpha expression in iron deficiency. Nat Struct Mol Biol *14*, 420-426.

Schneider, T. R., and Sheldrick, G. M. (2002) Substructure solution with SHELXD, Acta Cryst. *D58*, 1772-1779.

Semenza, G.L. (2007). Hypoxia-inducible factor 1 (HIF-1) pathway. Sci STKE *2007*, cm8.

Sheffield, P., Garrard, S., and Derewenda, Z. (1999). Overcoming expression and purification problems of RhoGDI using a family of "parallel" expression vectors. Protein Expr Purif *15*, 34-39.

Smith, S.R., Ghosh, M.C., Ollivierre-Wilson, H., Hang Tong, W., and Rouault, T.A. (2006). Complete loss of iron regulatory proteins 1 and 2 prevents viability of murine zygotes beyond the blastocyst stage of embryonic development. Blood Cells Mol Dis *36*, 283-287.

Song, B.L., Sever, N., and DeBose-Boyd, R.A. (2005). Gp78, a membrane-anchored ubiquitin ligase, associates with Insig-1 and couples sterol-regulated ubiquitination to degradation of HMG CoA reductase. Mol Cell *19*, 829-840.

Stenkamp, R.E. (1994). Dioxygen and Hemerythrin. Chemical Reviews *94*, 715-726.

Taylor, C.T. (2008). Mitochondria and cellular oxygen sensing in the HIF pathway. Biochem J *409*, 19-26.

Tokunaga, F., Sakata, S., Saeki, Y., Satomi, Y., Kirisako, T., Kamei, K., Nakagawa, T., Kato, M., Murata, S., Yamaoka, S.*, et al.* (2009). Involvement of linear polyubiquitylation of NEMO in NF-kappaB activation. Nat Cell Biol *11*, 123-132.

Ullman, E.F., Kirakossian, H., Singh, S., Wu, Z.P., Irvin, B.R., Pease, J.S., Switchenko, A.C., Irvine, J.D., Dafforn, A., Skold, C.N.*, et al.* (1994). Luminescent oxygen channeling immunoassay: measurement of particle binding kinetics by chemiluminescence. Proc Natl Acad Sci U S A *91*, 5426-5430.

Walden, W.E., Selezneva, A.I., Dupuy, J., Volbeda, A., Fontecilla-Camps, J.C., Theil, E.C., and Volz, K. (2006). Structure of dual function iron regulatory protein 1 complexed with ferritin IRE-RNA. Science *314*, 1903-1908.

Wallander, M.L., Leibold, E.A., and Eisenstein, R.S. (2006). Molecular control of vertebrate iron homeostasis by iron regulatory proteins. Biochim Biophys Acta *1763*, 668-689.

Wang, J., Chen, G., Muckenthaler, M., Galy, B., Hentze, M.W., and Pantopoulos, K. (2004). Iron-mediated degradation of IRP2, an unexpected pathway involving a 2-oxoglutarate-dependent oxygenase activity. Mol Cell Biol *24*, 954-965.
Wang, J., Fillebeen, C., Chen, G., Biederbick, A., Lill, R., and Pantopoulos, K. (2007). Iron-dependent degradation of apo-IRP1 by the ubiquitin-proteasome pathway. Mol Cell Biol *27*, 2423-2430.

Willems, A.R., Schwab, M., and Tyers, M. (2004). A hitchhiker's guide to the cullin ubiquitin ligases: SCF and its kin. Biochim Biophys Acta *1695*, 133-170.

Wingert, R.A., Galloway, J.L., Barut, B., Foott, H., Fraenkel, P., Axe, J.L., Weber, G.J., Dooley, K., Davidson, A.J., Schmid, B.*, et al.* (2005). Deficiency of glutaredoxin 5 reveals Fe-S clusters are required for vertebrate haem synthesis. Nature *436*, 1035-1039.

Wrighting, D.M., and Andrews, N.C. (2008). Iron homeostasis and erythropoiesis. Curr Top Dev Biol *82*, 141-167.

Yamanaka, K., Ishikawa, H., Megumi, Y., Tokunaga, F., Kanie, M., Rouault, T.A., Morishima, I., Minato, N., Ishimori, K., and Iwai, K. (2003). Identification of the ubiquitin-protein ligase that recognizes oxidized IRP2. Nat Cell Biol *5*, 336-340.

Zhang, J.H., and Kurtz, D.M., Jr. (1992). Metal substitutions at the diiron sites of hemerythrin and myohemerythrin: contributions of divalent metals to stability of a four-helix bundle protein. Proc Natl Acad Sci U S A *89*, 7065-7069.

Zhang, J.H., Kurtz, D.M., Jr., Xia, Y.M., and Debrunner, P.G. (1991). Reconstitution of the diiron sites in hemerythrin and myohemerythrin. Biochemistry *30*, 583-589.

Zhang, N., Liu, J., Ding, X., Aikhionbare, F., Jin, C., and Yao, X. (2007). FBXL5 interacts with p150Glued and regulates its ubiquitination. Biochem Biophys Res Commun *359*, 34-39.

Zhang, P., Land, W., Lee, S., Juliani, J., Lefman, J., Smith, S.R., Germain, D., Kessel, M., Leapman, R., Rouault, T.A.*, et al.* (2005). Electron tomography of degenerating neurons in mice with abnormal regulation of iron metabolism. J Struct Biol *150*, 144-153.

Zimmer, M., Ebert, B.L., Neil, C., Brenner, K., Papaioannou, I., Melas, A., Tolliday, N., Lamb, J., Pantopoulos, K., Golub, T.*, et al.* (2008). Small-molecule inhibitors of HIF-2a translation link its 5'UTR iron-responsive element to oxygen sensing. Mol Cell *32*, 838-848.

Zumbrennen, K.B., Hanson, E.S., and Leibold, E.A. (2008). HOIL-1 is not required for iron-mediated IRP2 degradation in HEK293 cells. Biochim Biophys Acta *1783*, 246-252.